NTNU – Trondheim
Norwegian University of
Science and Technology

Wind-induced Dynamic Response of High Rise Buildings

Karl Hermann Mathias
Bjørnland

Civil and Environmental Engineering
Submission date: June 2013
Supervisor: Einar Norleif Strømmen, KT
Co-supervisor: Øystein Vagnildhaug, Norconsult AS

Norwegian University of Science and Technology
Department of Structural Engineering

Department of Structural Engineering
Faculty of Engineering Science and Technology
NTNU- Norwegian University of Science and Technology

ACCESSIBILITY

OPEN

MASTER THESIS 2013

SUBJECT AREA:	DATE:	NO. OF PAGES:
Structural Engineering	06.06.2013	20 + 108 + 36

TITLE:

Wind-induced Dynamic Response of High Rise Buildings

Vindindusert dynamisk respons av høyhus

BY:

Karl Hermann Bjørnland

SUMMARY:
This thesis aims to investigate the dynamic response of a high rise concrete structure. Calculations are performed for Lerkendal Hotel, a slender 75 meter high building located in Trondheim. Buffeting response has been the main focus in the calculations, and both displacements, accelerations and cross sectional forces have been obtained.
Initially, acceleration demands regarding human comfort in a structure subjected to wind induced vibrations were established using design codes. In addition, the expected structural damping of a high rise concrete structure was estimated using literature. To determine basic dynamic properties for the given structure, a modal FEM-analysis was conducted using SAP2000.
A theoretical study was performed to establish the basis needed for buffeting response calculations. The structure was treated as a cantilevered, line like beam. A MATLAB computer program was made to perform all calculations. Using given and estimated input values, single mode single component response calculations were conducted for the two first translational modes. In addition, accelerations and cross sectional forces were estimated using Eurocode 1: 1-4 to serve as a conservative basis for comparison.
The obtained cross sectional forces for wind excitation of the first mode were found to be considerably higher than the ones obtained from building design codes. It was found likely that the bending stiffness of the structure had been estimated too high, resulting in high resonant forces. For wind excitation of the second mode, theoretical forces proved to coincide well to results obtained from the Eurocode. The frequency weighted acceleration was found to be much higher than the perception limit for both modes. Estimates from design codes supported the high values. As a possible solution, it was proposed that tuned mass dampers could be installed in the structure to reduce the acceleration. It was also suggested that the perception limit used could be too strict for the given structure regarding human comfort.

RESPONSIBLE TEACHER: Einar N. Strømmen

SUPERVISOR(S): Einar N. Strømmen, Øystein Vagnildhaug

CARRIED OUT AT: Department of Structural Engineering (NTNU)

Institutt for konstruksjonsteknikk
FAKULTET FOR INGENIØRVITENSKAP OG TEKNOLOGI
NTNU – Norges teknisk-naturvitenskapelige universitet

MASTEROPPGAVE 2013

for

Karl Hermann Bjørnland

VINDINDUSERT DYNAMISK RESPONS AV HØYHUS

Wind-induced dynamic response of high rise building

Det skal bygges et 75 m høyt hotellbygg ved Lerkendal Stadion like syd for Trondheim sentrum. Bygget har ikke ubetydelig slankhet og det blir stående fritt i forholdsvis åpent terreng. Vindinduserte svingninger kan skape uakseptable forskyvninger og akselerasjoner i de øverste etasjene av bygget. Hensikten med denne oppgaven er å finne ut hvilke krav som må stilles til hendelser av dynamisk respons med hensyn til menneskelig komfort i denne typen bygninger, og å foreta en responsberegning av det aktuelle systemet for å finne ut om det må iverksettes spesielle tiltak for å tilfredsstille kravene. I den grad det er av vesentlig betydning skal asymmetri inkluderes i beregningene, men det kan antas at systemet med tilstrekkelig nøyaktighet kan modelleres som en utkraget linjekonstruksjon utsatt for turbulent vind i horisontalretningen.

Oppgaven skal gjennomføres i samarbeid rådgivende ingeniør (Norconsult AS), hvor Sivilingeniør Øystein Vagnildhaug er studentens kontaktperson. Oppgave forslås lagt opp etter følgende plan:

1. Det foretas et litteraturstudium med sikte på å kvantifisere de øvre grensene for menneskelig komfort med hensyn til akselerasjon i horisontalretningen.

2. Det foretas et litteraturstudium med sikte å bestemme hvilke dempningsegenskaper som kan forventes av et høyhus i betong.

3. Det utvikles et Matlabprogram for beregning av vindindusert dynamisk respons av en vertikalt utkraget bjelke med asymmetrisk tverrsnitt. Programmet skal i tillegg til forskyvninger også omfatte beregninger av relevante snittkrefter og akselerasjoner.

4. I samråd med veileder og kontaktperson skal studenten kvantifisere de nødvendige data som gjelder for det aktuelle hotellprosjektet ved Lerkendal Stadion. Det skal deretter foretas en dynamisk responsberegning, og en kontroll av forskyvninger og akselerasjoner.

5. I den grad tiden tillater det skal det utarbeides et Matlabprogram som simulerer vindfeltets horisontal komponent i variabel høyde over bakken, og som anvendes på en enkel elementmodell i Abaqus.

I løpet av arbeidet med oppgaven kan studenten selv velge hvilke problemstillinger han ønsker å legge vekt på.

NTNU, 2013-01-03 Einar Strømmen

Abstract

This thesis aims to investigate the dynamic response of a high rise concrete structure. Calculations are performed for Lerkendal Hotel, a slender 75 meter high building located in Trondheim. Buffeting response has been the main focus in the calculations, and both displacements, accelerations and cross sectional forces have been obtained.

Initially, acceleration demands regarding human comfort in a structure subjected to wind induced vibrations were established using design codes. In addition, the expected structural damping of a high rise concrete structure was estimated using literature. To determine basic dynamic properties for the given structure, a modal FEM-analysis was conducted using SAP2000.

A theoretical study was performed to establish the basis needed for buffeting response calculations. The structure was treated as a cantilevered, line like beam. A MATLAB computer program was made to perform all calculations. Using given and estimated input values, single mode single component response calculations were conducted for the two first translational modes. In addition, accelerations and cross sectional forces were estimated using Eurocode 1: 1-4 to serve as a conservative basis for comparison.

The obtained cross sectional forces for wind excitation of the first mode were found to be considerably higher than the forces obtained from building design codes. It was found likely that the bending stiffness of the structure had been estimated too high, resulting in high resonant forces. For wind excitation of the second mode, theoretical forces proved to coincide well to forces obtained from the Eurocode.

The frequency weighted acceleration was found to be much higher than the perception limit for both modes. Estimates from design codes supported the high values. As a possible solution, it was proposed that tuned mass dampers could be installed in the structure to reduce the acceleration. It was also suggested that the perception limit used could be too strict for the given structure regarding human comfort.

Sammendrag

Denne masteroppgaven undersøker den vindinduserte dynamiske responsen til et høyhus i betong. Beregninger har blitt utført for Lerkendal Hotell, et 75 meter høyt betongbygg med betydelig slankhet som oppføres i Trondheim. Buffeting-respons har vært oppgavens hovedfokus. Både forskyvninger, akselerasjoner og tverrsnittskrefter har blitt beregnet ved bruk av aerodynamisk teori.

Krav som stilles til menneskelig komfort i bygninger utsatt for vindinduserte vibrasjoner har blitt fastsatt. Ved hjelp av flere standarder ble det funnet grenseverdier for frekvensvektet akselerasjon i bygget. I tillegg ble dempingen som kan forventes i et høyt betongbygg bestemt. Metoder fra standarder og annen litteratur ble brukt for å estimere dempningsratene for byggets første svingemoder.

En elementmetodeanalyse ble utført i programmet SAP2000 for å bestemme de grunnleggende dynamiske egenskapene til den aktuelle bygningen. Modelleringen ble gjennomført i 3D for å bestemme de aktuelle egenfrekvensene og svingeformene.

Teorigrunnlaget for beregning av buffeting-respons har blitt funnet i litteraturen. Bygningen ble tilnærmet som en utkraget bjelke med rektangulært tverrsnitt. Et MATLAB-program ble utviklet for gjennomføring av beregninger. Enkeltkomponentrespons for de to første svingemodene har blitt beregnet ved hjelp av oppgitte og estimerte parametre. I tillegg har akselerasjoner og tverrsnittskrefter blitt beregnet ved hjelp av Eurokode 1: 1-4. Standarder gir som regel konservative verdier, og det var derfor forventet at estimatene fra Eurokoden skulle være høyere enn verdiene beregnet ved hjelp av aerodynamisk teori.

Kreftene beregnet for eksitasjon av den første moden var mye høyere enn Eurokodeestimatene. En gjennomgang av parametre viste at den mest sannsynlige årsaken var at den estimerte bøyestivheten var for høy. De beregnede tverrsnittskreftene for eksitasjon av den andre moden stemte relativt godt med kreftene estimert ved hjelp av Eurokoden.

Den frekvensvektede akselerasjonen viste seg å være mye høyere enn de gjeldende kravene for begge de beregnede svingemodene. Også estimater fra Eurokoden gav høye verdier for akselerasjon. Det ble argumentert for at akselerasjonskravene kunne være for strenge for det gjeldende bygget. En mulighet for å redusere akselerasjonen vil være å installere massedempere i bygget.

Preface

This master thesis was written for the Department of Structural Engineering at the Norwegian University of Science and Technology (NTNU) between the 16. of January and the 6. of June 2013. The theme of the thesis has been dynamic response of a high rise concrete structure subjected to turbulent wind loading. In addition, demands regarding human comfort has been established and checked. Procedures from design codes have also been investigated.

Calculations performed in this thesis have been conducted using MATLAB R2012a. In addition, basic dynamic properties have been estimated using the CSI-Berkeley developed software SAP2000 version 15. The program CrossX has also been used to obtain cross sectional data.

I would like to thank my supervisor Prof.Dr. Einar N. Strømmen for all the help, advice and feedback he has provided throughout the semester. He has given me great freedom, allowing me to focus on aspects that I found interesting. I would also like to thank Prof.emer. Kolbein Bell for useful input. Feedback from friends and fellow students has been rewarding and highly appreciated.

Finally, I would like to thank Norconsult for supplying the theme for this thesis. Especially Øystein Vagnildhaug, who has served as a co-supervisor, providing useful advice and input data whenever needed.

Trondheim, 6. June 2013

Karl Hermann Bjørnland

Contents

List of Parameters

Latin Letters

A	Area
A_{fr}	Friction area, Eurocode
a	Fourier amplitude
a_n	Acceleration
A_{ref}	Zone area, Eurocode
B	Structural depth parallel to main flow (L2 in MATLAB)
b	Structural width, Eurocode
B^2	Background pressure distribution factor, Eurocode
B_q	Buffeting load coefficient
C	Damping property
c	Amplitude factor
c_o	Terrain shape factor, Eurocode
C_D	Drag coefficient
c_f	Force factor, Eurocode
$c_{f,0}$	Base force factor, Eurocode
C_L	Lift coefficient
C_{nn}	Davenport decay constant
$\hat{Co}$	Co-spectral density
Cov	Covariance matrix
c_{pe}	External pressure coefficient, Eurocode
c_{pi}	Internal pressure coefficient, Eurocode
c_r	Roughness factor, Eurocode
$c_s c_d$	Structural factor, Eurocode
d	Structural depth, Eurocode
D	Structural width perpendicular to main flow (L1 in MATLAB)
E	Young's modulus
$E[\ ]$	Expected value, statistics
EI	Cross sectional bending stiffness
F	Cross sectional force
f	Frequency in Hz
f_L	Normalized frequency

f_s	Vortex shedding frequency
G	Shear modulus
GA	Cross sectional shear stiffness
$\hat{H}(\omega)$	Frequency response function
H, h	Height of structure
H_h, H_l, H_t	Weighting function parameters from ISO 2631-2
I_n	Turbulence intensity
I_y / I_z	2nd moment of inertia
$\hat{J}(\omega)$	Joint acceptance function
K	Stiffness property
$\mathbf{k}$	Structural stiffness matrix
k_i	Cross sectional shear constant
k_l	Turbulence factor, Eurocode
k_p	Peak factor for maximal response
k_r	Terrain roughness factor, Eurocode
L	Length (height) of Structure
L_{exp}	Wind-exposed length (height)
$L(z_s)$	Turbulence length scale, Eurocode
M	Cross sectional moment
$\mathbf{m}$	Structural mass matrix
M_i	Mass property
$\tilde{m}_i$	Distributed modal mass
$n_{1,x}$	Frequency estimate, Eurocode
P^*	Aerodynamic derivative
q	Wind loading
Q	Modal load
q_p	Peak velocity pressure, Eurocode
r	Response value
R^2	Resonance factor, Eurocode
S_n	Auto spectral density
S_{nn}	Cross-spectral density
St	Strouhal Number
$\mathbf{T}$	Stiffness property matrix
t	Time variable
T	Natural period of structure
$u(x,t)$	Turbulence component in main flow direction
V	Cross sectional shear force
$V(x), V$	Mean wind velocity

$v(x,t)$	Turbulence component perpendicular to main flow direction
v_b	Base wind velocity, Eurocode
$W(\omega)$	Frequency weighting function, ISO 2631-1
$w(x,t)$	Vertical turbulence component
w_e	External wind pressure, Eurocode
w_i	Internal wind pressure, Eurocode
x	Height coordinate
z_o	Roughness length, Eurocode
${}^{s}L_n$	Integral length scale (eddy size)
$z_{\min}$	Minimum reference height, Eurocode

- Factors from NS-EN 1991-1-4 used in Appendix 2 are not included.

Greek Letters

α	Angle between main wind flow and cross-sectional axis
α'	Lagomarsino damping estimate coefficient
$\boldsymbol{\beta}$	Modal shape derivative matrix
β	Angle of relative wind velocity
β'	Lagomarsino damping estimate coefficient
Δ	Step size
γ	Euler's constant
δ_j	Displacement from unit load method
$\delta_s, \delta_a, \delta_d$	Logarithmic decrement of damping, Eurocode
ζ	Damping ratio
η	Generalized coordinate
κ	Stiffness ratio
λ	Normalized wave length
μ	Aerodynamic mass ratio
μ_e	Mass per elevational area, Eurocode
ν	Zero-upcrossing frequency
ξ	Mode shape estimation constant, Eurocode
ρ	Air density
ρ_{nn}	Covariance coefficient
σ	Standard deviation
Φ	Mode shape estimate, Eurocode
ϕ	Modal shape vector
ψ_r	Corner reduction factor, Eurocode

ψ_λ	End effect factor, Eurocode
ω	Angular frequency in radians/second
ω_i	Natural frequency of structure

Superscripts

$\hat{o}$	Normalized quantity
o', o'', o'''	Derivatives with respect to height x
$\dot{o}, \ddot{o}, \dddot{o}$	Derivatives with respect to time t
$\overline{o}$	Average value
$\tilde{o}$	Modal property
$\lvert o \rvert$	Absolute value
o^T	Transposed quantity
o^*	Complex conjugated quantity

Subscripts

w	Frequency weighted
u, v	Turbulence or flow components
D, L	Drag, Lift
R, B	Resonant, background
i, j	Mode identity
ae	Aerodynamic property
x, y, z	Coordinate directions
r, a	Displacement, acceleration

Abbreviations

FRF	Frequency response function
JAF	Joint acceptance function
ULS	Ultimate limit state
SLS	Service limit state
RC	Reinforced Concrete
EC	Eurocode

1 Introduction

The influence of wind on structures is a complex subject. The wind field varies both in space and time, and thus a statistical approach is demanded to describe wind loading. For low and stiff structures, wind induces surface pressure and suction, which could be critical for facades and roofs. For bridges and tall buildings, the effects of wind are more complicated. Wind acting on tall and slender structures could result in several effects, among them buffeting and vortex shedding. These effects induces vibrations in the structure, which could lead to major displacements, accelerations and resulting forces.

In this thesis, the objective has been to gain knowledge and understanding of the effects that turbulent wind have on tall buildings. This includes both calculation methods, relevant parameters and demands regarding human comfort in buildings subjected to turbulent wind. The thesis has been formed in cooperation with Norconsult AS. They wanted focus on the theoretical approach to wind response calculations. Considerations made using building design codes would also be appreciated.

As foundation for this thesis, several sources of theoretical knowledge have been applied. The most important one has been Einar Strømmen's *Theory of Bridge Aerodynamics* [1]. This book contains all the theory needed to investigate the wind induced response of structures. Although the book is formulated for bridges, all considerations are applicable to buildings when some small alterations are introduced. As supplementary literature, *Wind Loads on Structures* by Claës Dyrbye and Svend O. Hansen [2] has been used frequently.

To acquire the knowledge and results desired in this thesis, goals in form of research questions have been defined. The following bullet points have been created with basis in the given assignment:

- Which dynamic response effect is dominating for the given structure, and how is the response calculated using aerodynamic theory?
- What demands regarding human comfort are given in building design codes, and are these demands fulfilled for the given structure?
- Does forces calculated by aerodynamic theory resemble estimates obtained from building design codes?
- How does key parameters affect the dynamic response?

To answer the research questions, acceleration demands regarding human occupancy have been investigated. Buffeting theory has been accounted for using the literature mentioned above. Relevant input parameters have been estimated, and then a MATLAB program has been developed to calculate the structural response. Finally, the obtained forces have been compared to values calculated using the Eurocode, and the obtained acceleration has been compared to the found demands. The influence of parameters has been tested and discussed.

2 Lerkendal Hotel

Lerkendal Hotel and Congress Centre (Figure 2.1) will be a landmark by Norwegian standards. With a height of 75 meters, it will be the third to highest conventional building in Norway. In Trondheim, it is only beaten by the spire of the Nidarosdomen cathedral (98 m), and the antenna on top of the Tyholt Tower (124 m) [3]. The slender structure has a cross section of approximately 45 times 15 meters.

Figure 2.1: Left: Architectural sketch of Lerkendal Hotel. Right: Building under construction 24.04.2013

The hotel tower is going to be part of a 35 000 m^2 complex (Figure 2.2) which will contain a congress centre and offices. The structure will be connected to the Lerkendal football stadium. The hotel will contain almost 400 rooms, with a capacity of nearly 2000 guests [4].

Figure 2.2: Lerkendal Hotel and Congress Centre, entire complex

2.1 Project Details

The complex is built by AB Invest, with HENT AS as a general contractor. The building is drawn by Voll Arkitekter. Ground was broken 12th of July 2012, and the planned opening takes place 30th of June 2014. The structure is built in concrete, with a total of twenty floors above ground level and two floors of underground parking.

The building is located at Lerkendal, approximately 3 kilometers outside of Trondheim city centre. The area is under development, and several office- and apartment buildings have been built nearby during the recent years. The surrounding terrain is relatively flat, and all the neighboring buildings are at least 50 meters lower than the Lerkendal Hotel. In other words, the structure will be visible for the entire city - and highly exposed to wind action. Figure 2.3 shows a panoramic view of the city centre of Trondheim, taken from the 16th floor.

Figure 2.3: Panoramic view of Trondheim taken from the 16th floor

The ground at the construction site consists mainly of clay. Test drilling was preformed down to 80 meters below ground level without reaching bedrock. As a result, the foundation is built upon concrete friction piles. A total of about 900 piles has been used beneath the entire complex. At 39 meters each, the total pile length is approximately 35 km [4].

2.2 Energy Pioneering

The Scandic Hotel chain states that Lerkendal Hotel aims to be the world's most energy efficient hotel [5]. Rambøll, who are responsible for building physics and energy advising, has a goal of achieving a maximal energy consumption of 50 kWh/m^2 each year [6]. For comparison, the Norwegian Water- and Energy department has defined Energy Class A for hotels as an energy demand of less than 135 kWh/m^2 per year [7]. Current building regulations demand a maximal energy consumption of 220 kWh/m^2 per year for hotels [8]. In other words, the energy goal for Lerkendal Hotel is far beyond the present standards.

To achieve this ambitious goal, several customized solutions are applied. The elevators are equipped with dynamos in order to charge while travelling downwards. Booking is done from the bottom floor and upwards, and floors with no occupancy are neither lit, heated or air conditioned. 350 m^2 solar collectors are installed at roof level in order to heat up the tap water. In addition, walls and windows are optimized to reduce energy demand. These energy saving measures and several other bright solutions has led to the project being sponsored 14 million NOK by ENOVA, a government organization which fronts environmental-friendly energy use [9].

3 Structural Behavior - SAP2000

To get a feeling of the dynamic behavior of Lerkendal Hotel, frequencies and mode shapes are calculated. The dynamic properties of a structure are accurately estimated by a FEM simulation. There are several options when it comes to FEM-software. The software chosen to estimate modes and frequencies for the building was SAP2000, version 15. SAP2000 was chosen as a result of availability, previous experience and relevance. SAP2000 is developed by Computers and Structures Inc., which is a company based in Berkeley, CA. It is specialized to calculate seismic action on structures, which makes it favorable for dynamic calculations.

3.1 Model of the Study Building

The building was modeled in 3D. To get as accurate results as possible, correct structural geometry was emphasized throughout the modeling process. Blueprints and floor plans served as basis for the modeling, see Appendices 8 and 9. The drawings given by Norconsult contained no information regarding materials or dimensions of the structural elements. Therefore, assumptions had to be made. Table 3.1 presents the structural elements used in the model.

Structural element	Material	Dimensions/profile
Concrete columns, 1st floor	B30, B500NC	500x500 mm
Concrete beams, foundation	B30, B500NC	500x250 mm
Steel beams, bracings	S355	HE200A
Concrete columns, top floor	B30, B500NC	250x250 mm
Concrete walls (structural)	B30, B500NC	250 mm
Concrete slabs	B30, B500NC	200 mm

Table 3.1: Structural elements used in SAP2000 model

3.1.1 Simplifications

Although the modeling aimed to represent the structural geometry as accurately as possible, some simplifications had to be made. The adjacent structures have been neglected, resulting in a cantilevered tower structure. Foundation properties have been assumed as fixed to the ground. To simplify the modeling, only structurally significant elements has been modeled. This excludes curtain walls and partitions, resulting in a somewhat smaller mass than the real structure. SAP2000 calculates modes and frequencies by solving the eigen value problem, given by Chopra [10] as

$$\left[\mathbf{k} - \omega_n^2 \cdot \mathbf{m}\right]\phi_n = 0 \tag{3.1}$$

k is the structural stiffness matrix, **m** is the structural mass matrix, ω_n is the eigen frequency of mode n, and ϕ_n is the modal shape of mode n. Eigen frequencies are found by solving the determinant equation

$$\det\left[\mathbf{k} - \omega_n^2 \cdot \mathbf{m}\right] = 0 \tag{3.2}$$

Mode shapes are found by substituting ω_n back into equation (3.1). As the equations above demonstrates, the two only properties that affects the structural behavior is mass and stiffness. The latter has been addressed by modeling all structurally significant elements. As mentioned above, neglecting structurally insignificant elements reduces the total structural mass. In addition, live load has been neglected in the calculations. Live load would have contributed to a higher mass, which would have resulted in lower eigen frequencies.

3.1.2 Structural Model

The model is shown in Figure 3.1. The width is set to 15 m, and the total height is 75 m. The angle of the mid bend is 35°. As mentioned in Section 2, there are 20 floors above ground level. The floor height is 3.4 meters. The first two floors are modeled as an aula reaching two floor heights, with the roof above carried by columns. The sky bar at the top also reaches over two floor heights. In total, this corresponds to 22 floor heights of 3,4 meters.

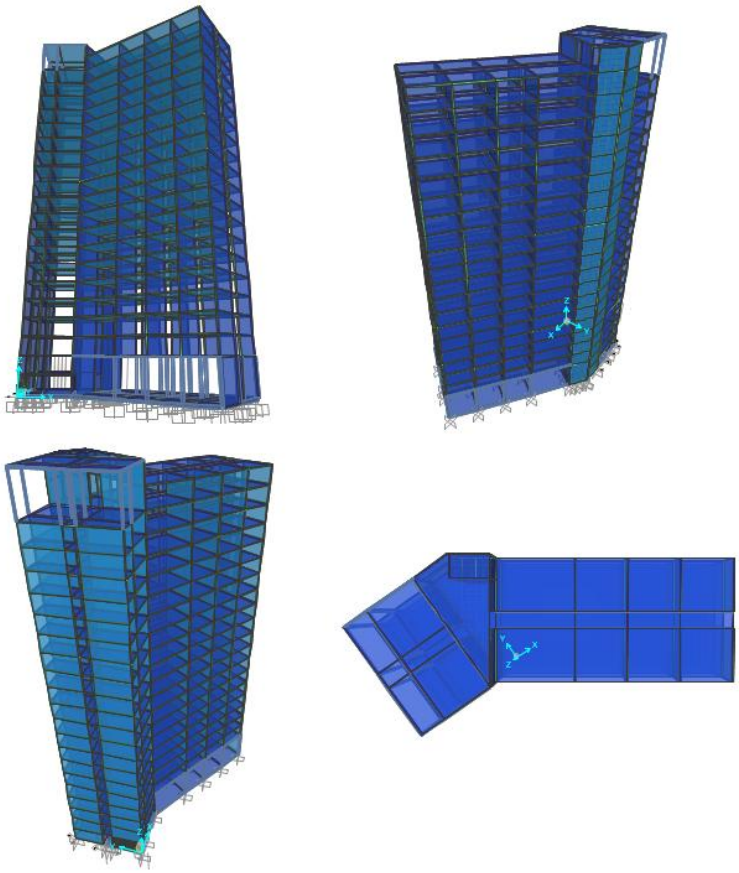

Figure 3.1: Structural model from SAP2000

3.2 Natural Frequencies and Mode Shapes

Although a limited amount of modes and frequencies are needed for further calculations, modes 1 through 10 are calculated in SAP. This is done both to investigate the structural behavior, and because local mode shapes for modes 5 and higher could reveal modeling errors. Table 3.2 shows frequencies and natural periods for modes 1-5.

Mode #	Frequency [Hz]	Angular Frequency [rad/s]	Period [s]
1	0.596	3.745	1.677
2	1.067	6.709	0.937
3	1.220	7.674	0.819
4	2.452	15.410	0.408
5	4.647	29.196	0.215

Table 3.2: Natural frequencies and periods, modes 1 - 5

As the table shows, the period is almost halved from the first to the second mode. The same applies to the difference between modes 3 , 4 and 5. Figure 3.2 shows the displacement pattern of the first three mode shapes.

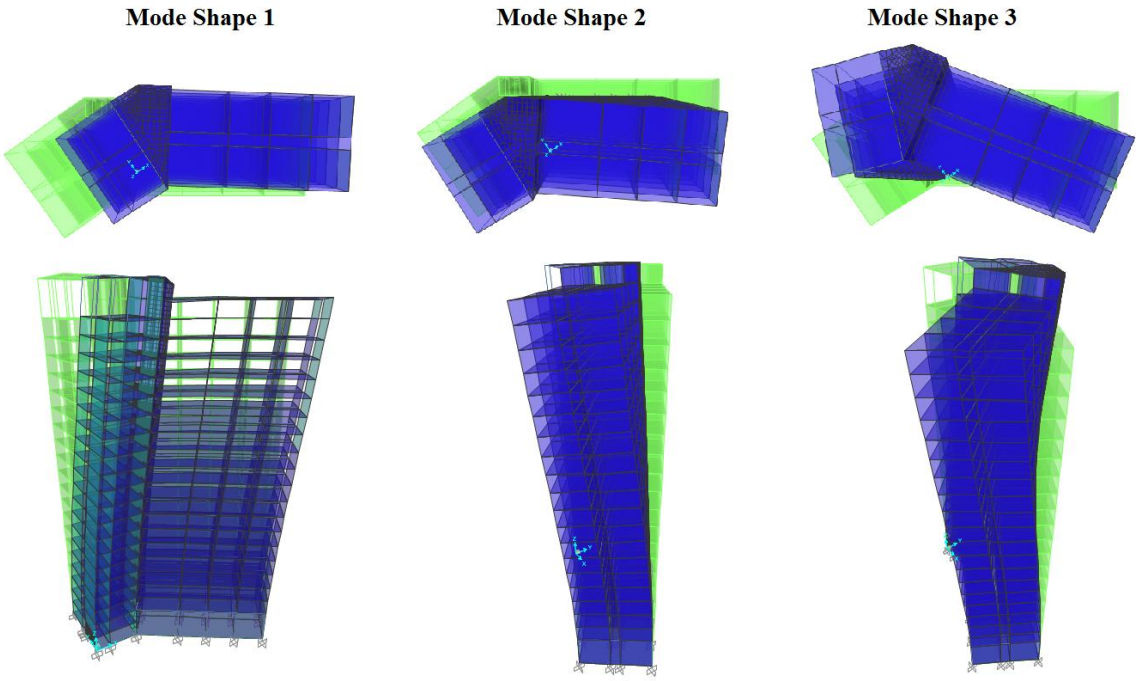

Figure 3.2: Graphical illustration of mode shapes 1, 2 and 3

The behavior displayed in Figure 3.2 is similar to what one could expect for a cantilevered beam. Mode 1 contains displacement in the longitudinal direction of the structure. Most of the

walls within the structure are parallel to the short edge, making the structure stiffer perpendicular to the longitudinal direction. The second mode contains displacement in the transverse direction, while the third mode is a torsional mode. Although the cross-section is asymmetrical and the stiffness- and mass properties are unevenly distributed, mode shapes are relatively pure. 2nd order modal shapes are also represented. Figure 3.3 shows modes 4 and 5.

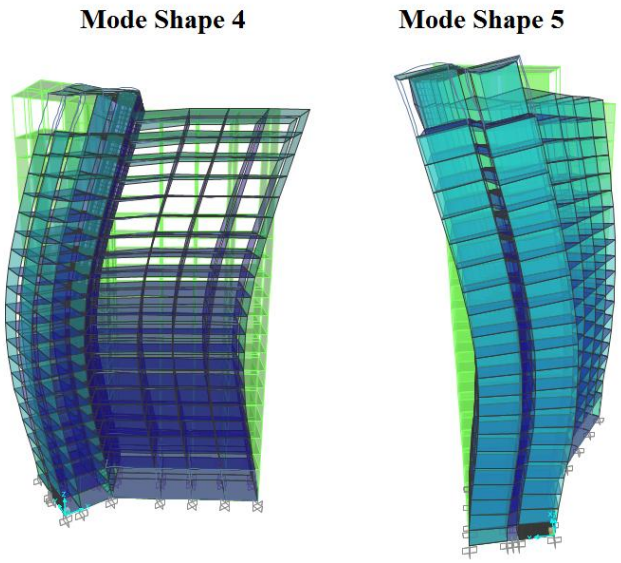

Figure 3.3: Mode shapes 4 and 5, 2nd order displacements

Both modes consists of second order displacements, as one could expect from beam theory.

3.2.1 Displacement patterns

Modal shapes could be represented more exact by the displacements at each floor. For simplicity, a node at one corner of each floor has been chosen to represent the displacements. Figure 3.4 presents the shapes of mode 1 and 2. Numerical values are given in Appendix 1.

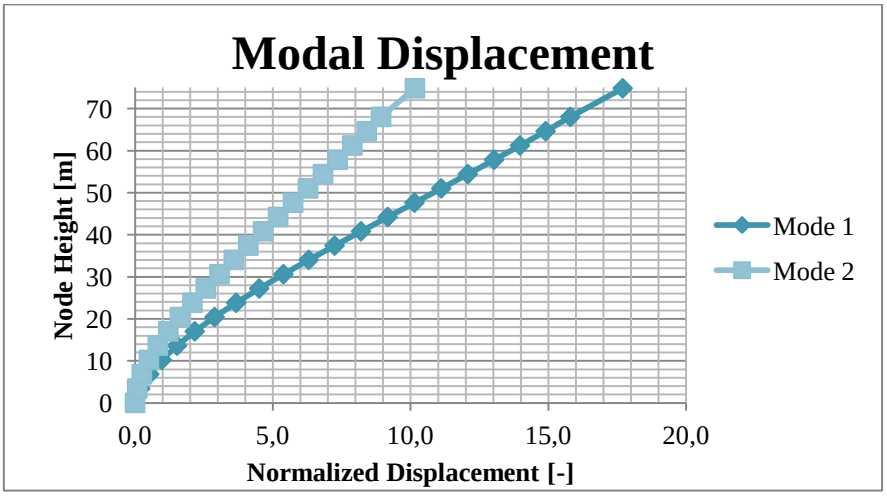

Figure 3.4: Modal displacements from SAP2000, modes 1 and 2

It should be mentioned that the units of the displacement values are useless. Modal calculations are performed without loading, making the displacement values hard to interpret. To use the values, they should be normalized, preferably by assuming that the displacement at the top floor is equal to unity. The normalized values will then represent the shape only.

To set the obtained modal shapes into perspective, the normalized Mode 1 (normalized with respect to displacement at the top) is plotted together with the NS-EN 1991-1-4 Appendix F, §F.3(1) suggestions for slowest mode shape [11]:

$$\Phi_1(z) = \left(\frac{z}{h}\right)^{\xi} \tag{3.3}$$

z represents the current height, while h is the total building height. Two alternatives correspond fairly well to the study building, namely

- Estimate 1: "Structures with a central core plus peripheral columns or larger columns plus shear bracings" - $\xi = 1,0$
- Estimate 2: "Slender cantilever buildings and buildings supported by central reinforced concrete cores" - $\xi = 1,5$

Figure 3.5 shows the resulting shapes as function of height z.

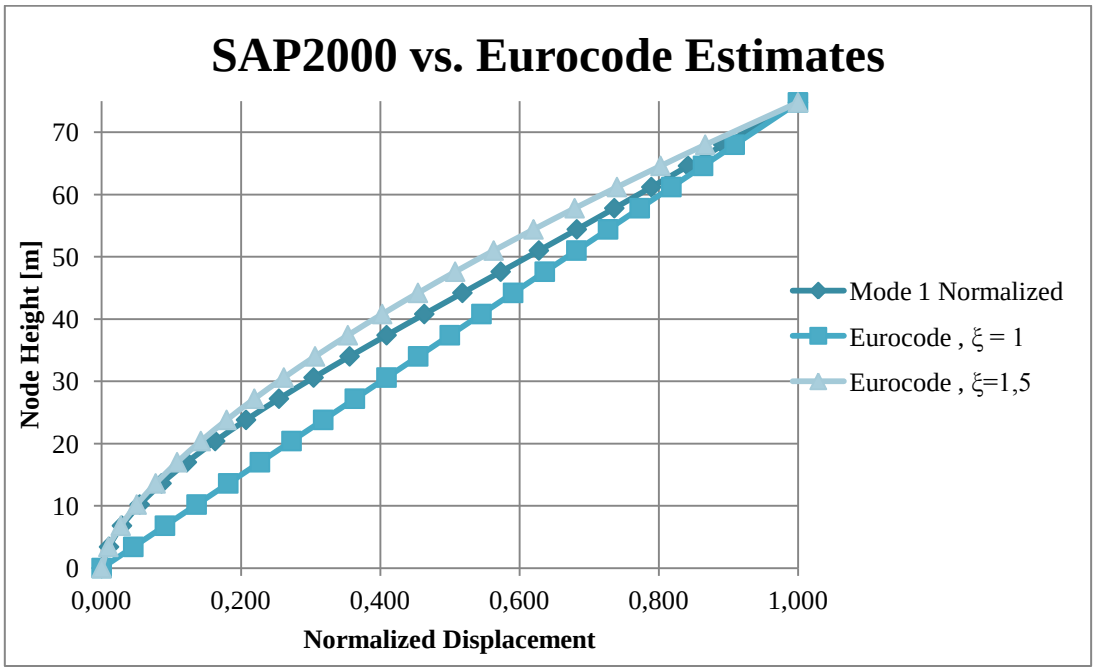

Figure 3.5: Mode 1 from SAP2000 compared to NS-EN 1991-1-4 estimates

It is seen that the Eurocode estimates and the calculated first mode corresponds well. The shape of Mode 1 obtained from SAP2000 is similar to estimate 2. Values corresponds best to estimate 2 for the lower floors, and then gradually approaches estimate 1 for higher floors.

3.3 Eigen Frequencies and Periods in Literature

To set the frequency-values from SAP2000 into context, it is useful to compare them to estimates found in the literature. Since the structural behavior is important in design for wind loading, estimates of the first eigen frequency is included in NS-EN 1991-1-4, in appendix F, § F.2. For multistory buildings taller than 50 meters, one estimate is given. This estimate is based on the work of Ellis [12]. Ellis states that simple prediction model provides sufficient accuracy (at that time formulated as "the most accurate" compared to computer based predictions). Based on data from 163 buildings, Ellis found that the first fundamental frequency could be predicted by $f_1 = 46/H$, where H is the building height. Similarly, the orthogonal translational mode could be predicted by $f_2 = 58/H$, while the first torsional mode could be predicted by $f_3 = 72/H$.

Lagomarsino [13] also developed formulas for predicting the natural periods of structures. Like Ellis, the formulas developed depended on building height only. The first period for reinforced concrete (RC) structures is given b $T_1 = H/55$, while the second transversal period is given by $T_2 = T_1 \cdot 0.266$. The third period (corresponding to a torsional mode) is given by $T_3 = H/78$. Looking at the Lagomarsino estimates compared to the estimates of Ellis, it is seen that the first eigen frequency is estimated somewhat higher by Lagomarsino (utilizing that $T_1 = 1/f_1$). The formula for the second period corresponds to $f_1 = 207/H$, which is significantly higher than what Ellis predicted. The torsional mode is estimated higher by Lagomarsino than Ellis.

Table 3.3 presents the natural frequencies and periods calculated by SAP2000 together with the estimates by Ellis and Lagomarsino (a building height H of 75 m has been used).

Estimate	Parameter	Mode 1 (transversal)	Mode 2 (transversal)	Mode 3 (torsional)
Ellis (NS-EN)	Frequency [Hz]	f_1 = 46/H = 0.613	f_2 = 58/H = 0.773	f_3 = 72/H = 0.960
	Period [s]	T_1 = 1.63 s	T_2 = 1.29 s	T_3 = 1.04 s
Lagomarsino	Frequency [Hz]	f_1 = 55/H = 0.733	f_2 = f_1/0.266 = 2.757	f_3 = 78/H = 1.04
	Period [s]	T_1 = 1.36	T_2 = 0.36	T_3 = 0.96
SAP2000	Frequency [Hz]	f_1 = 0.596	f_2 = 1.067	f_3 = 1.220
	Period [s]	T_1 = 1.68	T_2 = 0.94	T_3 = 0.82

Table 3.3: Frequency and period estimates from literature

There are several interesting aspects to the data presented in Table 3.3. The first natural frequency is estimated fairly similar by Ellis and SAP2000, with a difference of only 2.9 %. Lagomarsino's frequency estimate is somewhat higher. For the second mode, the results are scattered. The Ellis-estimate is diverging almost 30 % from the value calculated by SAP2000. One explanation for the divergence could be that the basis for Ellis' formulas was rectangular buildings only, while the study building is asymmetric. Lagomarsino's Mode 2 estimate is not even remotely close to the other two. It is even higher than the Lagomarsino estimate for Mode 3, which is highly illogical. Examining the results from SAP2000, it is seen that the Lagomarsino Mode 2 frequency correspond fairly well to the SAP2000 frequency of mode 4, which is 2nd order displacement in the transversal direction. It is possible that Lagomarsino estimates higher order frequencies in the same direction as the first frequency, however this is not clearly explained in the article.

For the third mode, which is torsional, the three estimates correspond better. SAP2000 provides a frequency which is higher than the values predicted by both Ellis and Lagomarsino. The difference is about 17 % for Lagomarsino and 27 % for Ellis.

Although the Lagomarsino predictions seems to deviate the most on average, it is important to note that Lagomarsino developed prediction models for RC buildings separately, while the prediction model suggested by Ellis does not distinguish between types of buildings. Neglecting the Lagomarsino estimate of the 2nd frequency, it seems that the different estimates supports the values obtained from the SAP2000 calculations.

4 Acceleration Demands

Acceleration demands are often crucial for design of tall buildings, and must therefore be checked to ensure that accelerations in a structure subjected to vibrations is not uncomfortable for the occupants. In this section, comfort and perception demands regarding acceleration in buildings are investigated.

4.1 Demands from Standards

Design demands are given by building codes. To find the current demands, several codes and standards have been checked, and the most appropriate limits and methods have been chosen. The relevant findings are summarized below.

4.1.1 NS-EN 1990 and NS-EN 1991-1-4

NS-EN 1990 [14] is basis for all structural design. It gives the first hint of what needs to be taken into account when a structure is exposed to dynamic loading. §A1.4.4 states that comfort of the occupants needs to be considered to ensure satisfying behavior regarding structural vibrations during use. It is recommended that the natural frequencies of a structure is kept higher than threshold values determined by the purpose of the building and the source of structural vibration. The standard refers to NS-EN 1991-1-1 and 1-4, and to ISO 10137.

NS-EN 1991-1-4 [11] concerns wind actions on structures. The majority of the standard describes how to calculate wind pressure and forces for given structural shapes and terrain types. It also provides two methods for calculating the peak acceleration of a structure induced by wind. However, these peak accelerations are not accompanied by design limits or threshold values.

4.1.2 ISO 10137

ISO 10137 [15] deals with serviceability of structures and walkways against vibrations. Annex C §C.1 provides information about vibration criteria for human occupancy. It states that the experience of acceleration depends strongly on the frequency. Hence, frequency filters are given by ISO-2631-1 and -2.

Annex D (Guidance for human response to wind-induced motions in buildings), provides a hands-on method for testing whether an acceleration value is acceptable. Acceleration limits are drawn into a diagram with user input peak acceleration (A, [m/s^2]) and first natural frequency (f_0, [Hz]), see Figure 4.1. The 2-curve represents residential areas, which includes hotels. The curves are developed by evaluation of empirical data from existing buildings. The return period of the peak acceleration is recommended to be one year.

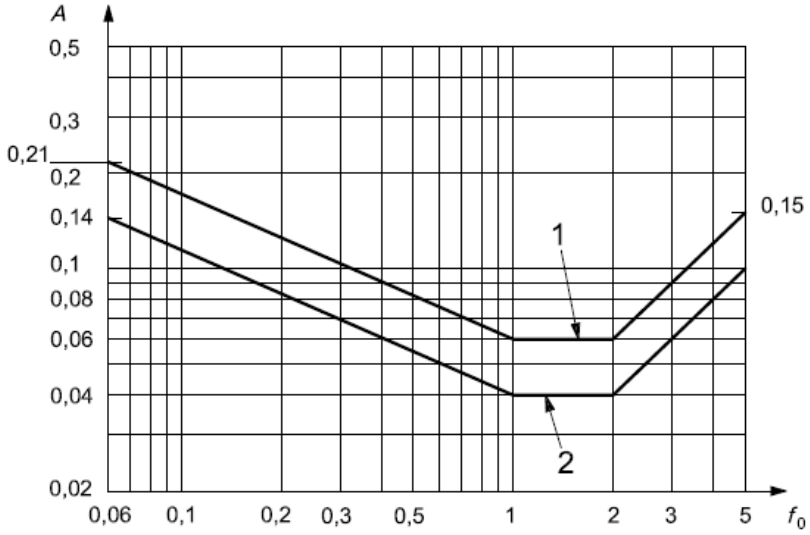

Figure 4.1: Peak acceleration vs. frequency from ISO 10137. Curve 1 represents offices, curve 2 represents residential buildings and hotels

As Figure 4.1 clearly shows, frequencies between 1 and 2 Hz are the least favorable for human comfort. ISO 10137 recommends that the peak acceleration A is calculated using ISO 4354, which is a standard similar to NS-EN 1991-1-4 described in Section 4.1.1. In this thesis, NS-EN 1991-1-4 has been used instead of ISO 4354, because the former contains a National Annex which provides parameters suitable for Norwegian conditions.

4.1.3 ISO 2631-1 and -2

The two parts of ISO 2631 [16] concerns evaluation of human exposure to whole-body vibration. According to ISO-2631-1 Annex C.2 and 3, perception of vibrations is highly individual and differs with respect to situation. According to Annex C.3, experience data has shown that occupants of residential buildings are likely to complain if frequency weighted vibration magnitudes exceed a given perception limit, which has a mean value of 0.015 m/s^2 (expected between 0.01 and 0.02 m/s^2). Comparing the demands from ISO 10137 and ISO 2631, it is seen that the perception limit given by ISO 2631-1 is way stricter than the figure found in ISO 10137. This is mainly because of the difference between perception and comfort. An acceleration that is barely noticeable would not give great discomfort. ISO 2631-1 also provides acceleration values defining different comfort levels. However, these values are valid for public transport, and therefore not applicable here.

According to §6.4.2, the frequency weighted acceleration is given by

$$a_w = \left[\sum (a_{i,rms} \cdot W_i)^2\right]^{1/2} \tag{4.1}$$

a_w represent the frequency weighted acceleration, while $a_{i,rms}$ and W_i are the root mean square acceleration and weighting function respectively. The index i refers to a 1/3 octave band, which is a way of dividing the frequency domain. The weighting function applicable to

buildings is given by ISO 2631-2, Appendix A. It is a function of the frequency f in Hz, and is calculated as follows.

$$
\begin{aligned}
W_i(f) &= |H_h(f)| \cdot |H_l(f)| \cdot |H_t(f)| \\
|H_h(f)| &= \sqrt{\frac{f^4}{f^4 + f_1^4}} \\
|H_l(f)| &= \sqrt{\frac{f_2^5}{f^4 + f_2^4}} \\
|H_t(f)| &= \sqrt{\frac{f_3^2}{f^2 + f_3^2}}
\end{aligned}
\tag{4.2}
$$

f_1, f_2 and f_3 are constants given in the standard. The idea of the procedure is to weigh every acceleration contribution with respect to its frequency. This will account for the fact that certain frequencies are easier to perceive, like illustrated by Figure 4.1. The weighting function will be shown in detail in Section 10.2.

4.2 Acceleration Estimate by the Eurocode

As mentioned above, NS-EN 1991-1-4 provides two different methods for calculating the peak acceleration of a building subjected to wind loading. To obtain an indication of what acceleration could be expected at the top of the study building, the two methods are used to calculate acceleration in both principle directions (corresponding to excitation of modes 1 and 2 found in Section 3.2). The obtained accelerations will also be useful for comparison later in this thesis.

The two calculation methods are given in Appendix B and C in the standard. According to the National Annex, neither of the methods are preferred over the other. In other words, choice of method is left to the engineer. Both methods calculates the standard deviation of acceleration, which then is weighted by a top factor. The input values needed for the methods are mainly geometry and mass data, together with wind field specifications. Remaining data is found by standard estimates, mainly by using Appendix F in NS-EN 1991-1-4.

The performed calculations are relatively complex, and will not be shown here. The full procedure including values is given in Appendix 2. Both the given methods (from now on named method B and C) were calculated to look for differences between the two. It is noted that Appendix F only gives one estimate for natural frequency, and thus both directions are calculated using the same frequency. The obtained accelerations are shown in Table 4.1.

	Wind against the short side	**Wind against the long side**
Method B	0.029 m/s^2	0.084 m/s^2
Method C	0.037 m/s^2	0.104 m/s^2

Table 4.1: Acceleration estimates from NS-EN 1991-1-4 Appendix B and C

As the table shows, higher accelerations are obtained for wind loading against the long side of the structure. At first glance, the values seem high compared to the demands presented earlier. However, the calculated values are not directly comparable to neither of the demands. The perception limit from ISO 2631-1 is valid for frequency weighted accelerations. When it comes to the limits from ISO 10137, the problem at hand is return period. While the given limits are given for a 1 year return period, the wind velocities used in methods B and C are based on a 50 year return period wind.

To match the figure from ISO 10137, the basic wind velocity was reduced to 1 year return period using Equation 4.2 from NS-EN 1991-1-4, and methods B and C were recalculated. However, using the reduced velocity, none of the acceleration values were able to make the chart (the highest value was 0.0036 m/s^2). The reduction formula is extremely sensitive for low return periods. For example, a return period of 1 year reduces the wind velocity by more than 72 %, while a return period of 2 years reduces the velocity by only 7 %. It is clear that a reduction of 72 % (which gives a new mean wind velocity of about 8 m/s) could not be used for design, simply because it would be exceeded too often.

4.3 Acceleration Demands in this Thesis

In light of the argumentation above, the procedures from ISO 2631 has been chosen to check acceleration demands in this thesis. The reason for this is mainly the tricky return period of the ISO 10137 demands. The procedure for calculating frequency weighted acceleration will be described further in Section 6.2.3. The obtained acceleration will be compared to the upper perception limit given in ISO 2631-1.

5 Damping of the Structure

Damping has significant influence on the dynamic response of a structure. There are many different factors that influence the damping value. As an example, damping tend to increase when the displacement amplitude increases. Since wind results in relatively small displacements (e.g. compared to seismic excitation), the damping values for wind loads on structures are correspondingly small.

Damping could be approached as classical or nonclassical. According to Chopra [10], nonclassical damping is required if damping properties are unevenly distributed throughout a structure. Correspondingly, damping should be calculated separately for each structural part. If damping properties are evenly distributed, the same damping value could be used for the entire structure. The latter is known as classical damping, and will be adopted in this thesis. It should be mentioned that each mode of the structure has different damping ratios. The damping ratio is usually highest for the first mode, and then decays for higher modes.

5.1 Damping in literature

Lagomarsino [13] and Satake et. al. [17] have both performed studies on the expected damping in high-rise buildings. According to Lagomarsino, there are five factors that contributes to damping in a building:

- Damping in the structural materials
- Damping due to friction in structural joints and between structural and non-structural elements
- Energy dissipation in foundation soil
- Aerodynamic damping
- Passive and active dissipative systems

For the structure relevant in this thesis, three of these points are of special interest. There are no extra damping systems in the structure, neither active or passive. Damping effects caused by SSI (Soil-Structure Interaction) have been neglected. The two first bullet points are recognized as structural damping, and will be treated in this section.

According to Lagomarsino, damping in RC buildings has two "threshold values". The first threshold is activated by small vibrations, while the second is reached for high stresses only. The first threshold is caused by slipping between structural and non-structural elements. The second threshold of damping is caused by activation of micro sidings within the structural material.

Lagomarsino presents an estimate for the first damping threshold (slipping in structural joints), by introducing

$$\xi_i = \alpha' \cdot T_i + \beta' / T_i \tag{5.1}$$

where α' and β' are constants depending on type of building, and T_i is the natural period of the mode for which damping is estimated . For RC structures $\alpha' = 0.7238$ and $\beta' = 0.7026$. The estimation is shown in the article to correspond well with the estimates provided by the former Eurocode 1. As mentioned above, the second threshold is reached for relatively high stresses. Wind excitation will lead to limited response in a structure. Therefore, the first threshold value given in equation (5.1) is used as estimate for the total structural damping in this thesis.

Satake et. al. has gathered data from more than 200 buildings in Japan to study damping effects. The article investigates the effects on damping from building height, natural period, foundation conditions and building use. Like Lagomarsino, Satake concludes that material damping is of great significance for the total damping. Using empirical data for RC buildings, Satake proposes the following expression for damping ratio

$$\xi_1 = 0.014 \cdot f_1 \tag{5.2}$$

For higher modes, the damping ratio is given by

$$\xi_n = 1.4 \cdot \xi_{n-1} \tag{5.3}$$

Chopra [10] provides several options regarding damping calculations for structures. Since there obviously cannot be performed any measurements on buildings in the design face, Chopra states that damping assessments should be based upon empirical knowledge. A lot of data has been gathered from existing structures, and the preferable solution is to estimate damping based on known values from similar structures. Although Copra's approach to damping is based on seismic excitation, the values suggested are presented for various stress levels, where the lowest one could serve as an approximation for damping of wind-induced oscillations. For well-reinforced concrete structures at stresses of about half the yield point, Chopra states that a damping ratio of 2-3 % could be expected.

5.2 Aerodynamic Damping

The aerodynamic damping is caused by interaction between motion of a structure and motion of the air around it. It is a function of structural properties and the given wind field. The aerodynamic damping is accounted for in section 6.2.2.4.

5.3 NS-EN 1991-1-4 on Damping

Appendix F.5 in the standard provides an expression for the logarithmic decrement of damping, δ. It is divided into three parts:

- δ_s, which is the structural part
- δ_a, which is the aerodynamic part
- δ_d, which represents added damping devices

The standard provides tabulated values for the logarithmic decrement of structural damping δ_s for a wide range of structures. For RC structures $\delta_s = 0.1$.

The logarithmic decrement of the aerodynamic damping is found in § F.5(3), calculated as

$$\delta_a = \frac{c_f \cdot \rho \cdot V_m(z_s)}{2 \cdot n_{1,x} \cdot \mu_e} \tag{5.4}$$

One of the factors worth mentioning here is the equivalent mass per elevational area, μ_e, which has to be estimated for the structure at hand. Under certain criteria , μ_e could be replaced by the equivalent mass per area, m_e. According to § F.4(2), m_e could be represented by the average mass per meter over the top third of the structure. n_1 represents the frequency of the lowest eigen mode, which could be estimated by §F.2(2).

The final factor, δ_d, should according to § F.5(5) be calculated separately if there are external or internal damping devices present, which in this case it is not. In total, the expression for the logarithmic decrement of damping could be written as

$$\delta_{tot} = \delta_s + \frac{c_f \cdot b \cdot \rho \cdot V_m(z_s)}{2 \cdot n_1 \cdot m_e} \tag{5.5}$$

The logarithmic decrement of damping is not directly applicable in theoretical dynamics. According to Chopra [10], the logarithmic decrement is defines as the logarithm of the ratio between two successive peaks of damped free vibrations, in other words

$$\delta = \ln\left(\frac{u(t)}{u(t+T_D)}\right) \tag{5.6}$$

Chopra shows that, by assuming free vibration, the following expression for the logarithmic decrement of damping could be obtained:

$$\delta = \frac{2 \cdot \pi \cdot \zeta}{\sqrt{1-\zeta^2}} \tag{5.7}$$

Since the damping ratio tends to be small for wind loading, the square root in equation (5.7) takes a value close to one, which results in the approximate equation $\delta \simeq 2 \cdot \pi \cdot \zeta$, from which the damping ratio ζ could be found easily. Figure 5.1 shows equation (5.7) together with the simplified expression given above. It is seen that the two expressions correspond well for a damping ratio of 0.3 and lower. In this thesis, damping ratios are expected lower than that, and thus the simplified expression for δ could be used.

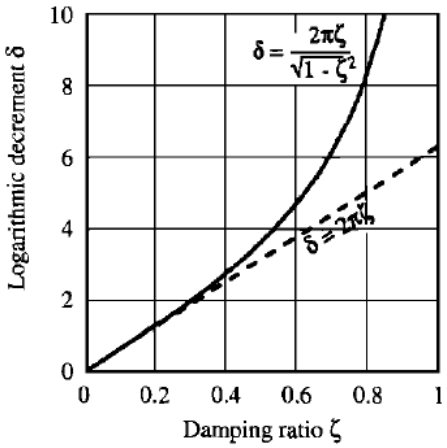

Figure 5.1: Damping from logarithmic decrement, Chopra sec. 2.2

5.4 Estimated Damping for Lerkendal Hotel

In the following, the damping ratio for the first three modes of the building has been estimated using both the logarithmic decrement-method in NS-EN 1991-1-4, §F.5, and the estimation formulas developed by Lagomarsino and Satake.

For all the three estimation alternatives, natural frequencies (or periods) are needed to calculate the damping ratios ζ. These quantities have already been estimated in Section 3.2. Calculations of ζ has been performed for all frequency estimations. Referring to Section 3.2, the Lagomarsino prediction of the second natural frequency of the structure deviates from other data, and has therefore been neglected in the damping calculations. Appendix F.5 in NS-EN 1991-1-4 only defines the logarithmic decrement of damping for the first mode shape in the wind-direction, hence damping ratios from the Eurocode has only been calculated for Mode 1. Figure 2.1 shows the damping ratios estimated for modes 1,2 and 3. Calculations and values are shown in Appendix 3.

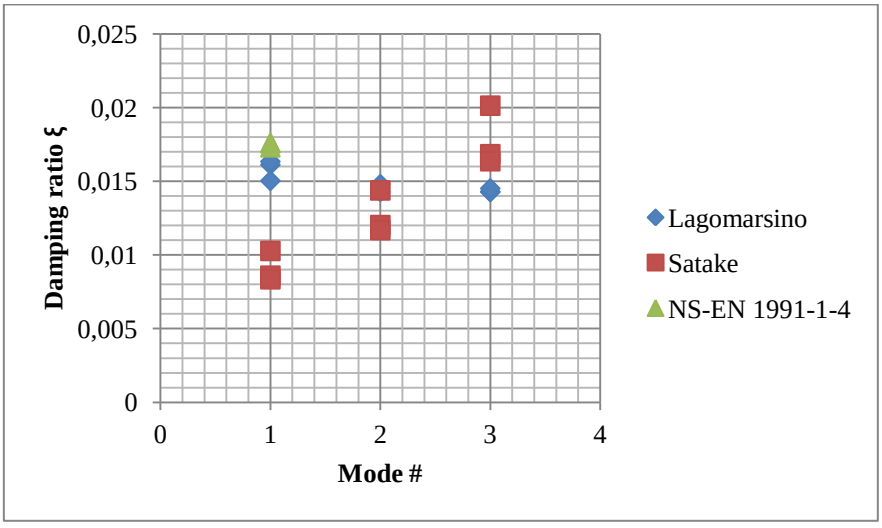

Figure 5.2: Damping estimates from literature, modes 1, 2 and 3

Figure 5.2 shows some clear trends. The damping ratios predicted by Satake increases for higher modes, while the values predicted by Lagomarsino have a slightly decreasing tendency. According to Kareem [18], the Lagomarsino prediction is one of a few estimates of damping that increases with increasing period. Generally, estimates of damping ratio in literature tend to decrease with increasing period.

For Mode 1, the Lagomarsino prediction (average ζ of 1.58 %) and the Eurocode estimation (average ζ of 1.75 %) correspond well, The Satake prediction is significantly lower, with an average ζ of 0.91 %.

The Satake and Lagomarsino prediction methods seem to correspond best for Mode 2. The average damping ratios are 1.45 % and 1.27 % for Lagomarsino and Satake respectively. Evaluating equations (5.1), (5.2) and (5.3) it is found that the two prediction formulas will correspond for periods of about 0.98 s. Looking at Table 3.2, it is seen that the natural period of Mode 2 is approximately 0.94 seconds, which confirms the correspondence between the two estimation models.

The damping ratio of Mode 3 has been included to visualize trends for the different estimation models. Looking at the values, the Satake prediction provides the highest damping ratios for Mode 3, with an average at 1.8 %. The average Lagomarsino prediction value is 1.4 %.

5.5 Choosing Damping Values

After consulting Einar Strømmen [19], it was decided that the Satake prediction was the most realistic damping estimate. The reason for this was the fact that the damping is higher for higher modes, which is logical because higher modes often are damped out in dynamic systems. In addition, Satake provides the lowest values for modes 1 and 2, which will result in the most conservative displacements and forces in the structure.

The damping ratios obtained using frequency estimates from SAP2000 are chosen to reassure correspondence between modal shapes and damping ratios used in the calculations. The damping ratios used in this thesis are shown in Table 5.1.

Mode Number	Damping Ratio (Satake)
Mode 1	0.008
Mode 2	0.012

Table 5.1: Structural damping for modes 1 and 2, estimated from Satake

6 Theory Section

The dynamic response of the study building is calculated from aerodynamic theory. The response parameters that will be calculated are peak acceleration and peak displacement at the top of the tower, and the base reactions (in form of base shear and base moment). In the following, the necessary theory is accounted for.

The governing assumption of the calculations is that a single mode single component approach can be used. This implies that only one structural mode is considered at a time, and that the resulting response only has one component - in the same direction as the modal displacement. The main basis for the theoretical derivations is *Theory of Bridge Aerodynamics* by Einar Strømmen [1]. All the relevant theory is presented in this book. *Wind Loads on Structures* by Claës Dyrbye and Svend O. Hansen [2] has been used as supplementary literature where extra clarifications were needed. These books are referred to throughout this section.

Theory of Bridge Aerodynamics is formulated to fit calculations for horizontal, line like bridges. To make the theory applicable to a tower structure, some small alterations and assumptions has been made. One of the most important ones is how the structure is considered. For bridges, the main wind flow acts on one side of the bridge deck cross section. For a tower structure, however, the main flow could come from any direction. The maximal response from a single mode excitation will occur when the main flow acts in the same direction as the modal displacement. As a result of the above, main flow has been assumed to act in the same direction as the modal displacements for all modes.

Single mode single component calculations are performed for the transversal modes 1 and 2 found in Section 3.2. The rotational Mode 3 has not been calculated. The reason for this is that calculation procedures are fairly similar for transversal and rotational modes. Thus, the learning outcome from calculating the rotational mode would not outweigh the extra workload.

6.1 Vortex Shedding

Vortex shedding is a phenomenon that needs to be considered for wind response calculations. Figure 6.1 shows the principle of vortex shedding for a square body. Vortices are shed alternately from opposite sides of the cross section. The phenomenon results in a fluctuating load perpendicular to the flow direction, with corresponding response. Dyrbye & Hansen explains the phenomenon by the fact that the wind velocity will be higher on the opposite side of where the vortex is formed. When velocity increases, the pressure decreases, resulting in a force which pulls the structure away from the side where the vortex is formed.

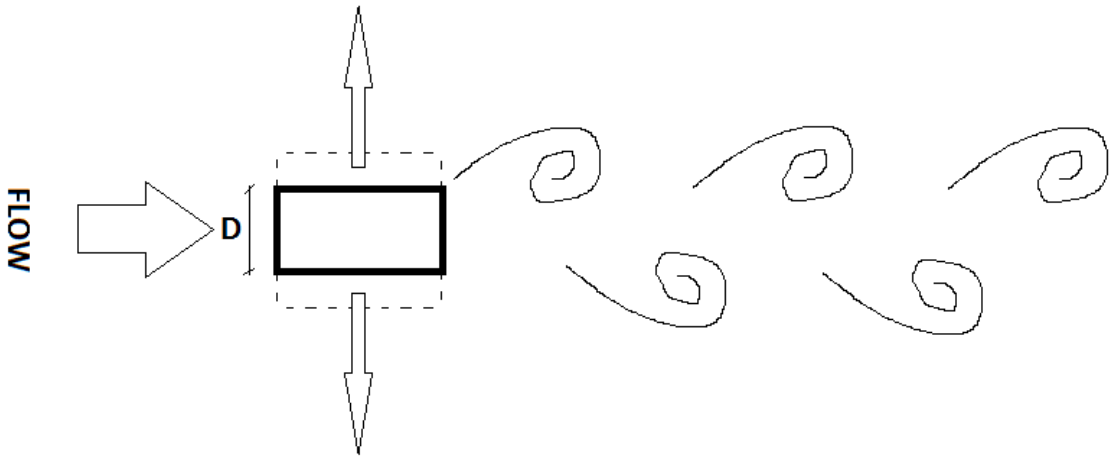

Figure 6.1: Principle of Vortex Shedding

6.1.1 Shedding Frequency

According to Dyrbye & Hansen, the vortices are shed with a frequency of

$$f_s = St \cdot \frac{V}{D} \tag{6.1}$$

Vortex shedding could result in great structural response if the shedding frequency f_s equals a natural frequency f_n of the structure corresponding to a structural mode perpendicular to the flow direction. As equation (6.1) shows, the shedding frequency depends on three factors. The cross sectional width D perpendicular to flow, the mean wind velocity V, and the Strouhal number St. Resonance will occur when the shedding frequency equals the mentioned natural frequency, which happens for a critical wind velocity defined by

$$V_{crit} = \frac{1}{St} \cdot f_n \cdot D \tag{6.2}$$

To determine whether vortex induced response will be a problem for the study building, the critical velocity should be determined.

6.1.2 Strouhal Number

While the cross sectional width is known, and the natural frequencies of the structure has been determined in Section 3.2, the Strouhal number St from equation (6.2) still needs to be determined. Again referring to Dyrbye & Hansen, the Strouhal number depend on surface structure, cross sectional shape and wind turbulence. To determine St for the study building, the relations of NS-EN 1991-1-4 Figure E.1 [11] has been adopted. For sharp-edged, rectangular cross sections, the relation between St and ratio between cross sectional depth and with, d/b is given by Figure 6.2.

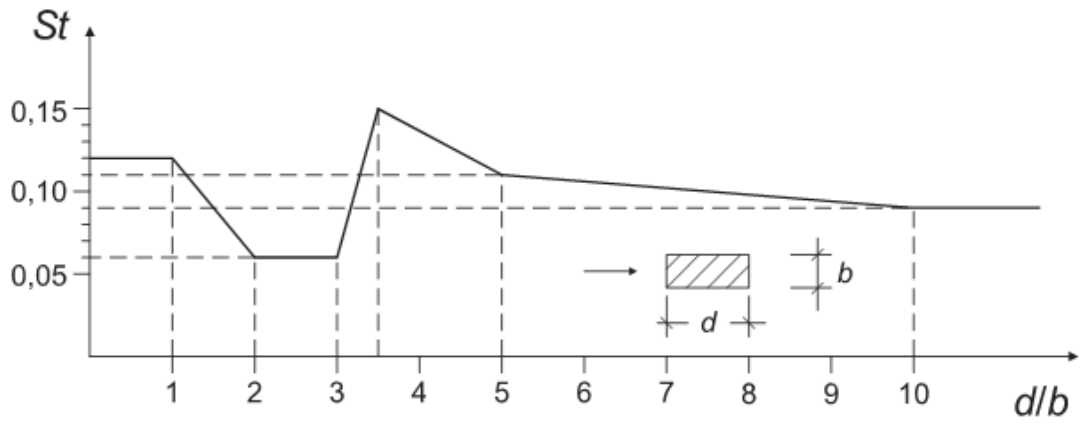

Figure 6.2: Strouhal number calculation from NS-EN 1991-1-4 Appendix E

The cross section of the structure is assumed to be a rectangular body measuring 45 times 15 meters. Depending on flow direction, the depth to with ratio is either $45/15 = 3$ wind against the short side, or $15/45 = 0.33$ for wind against the long side. This corresponds to Strouhal numbers of St = 0.06 and 0.12 respectively.

6.1.3 Critical Velocity

Using equation (6.2), the critical velocity V_{crit} for both directions are calculated. By using the frequencies from Section 3.2, it is found that

Wind against the short side:

$$V_{crit} = \frac{1}{0.06} \cdot 0.59597 Hz \cdot 15m = 149\ m/s \tag{6.3}$$

Wind against the long side:

$$V_{crit} = \frac{1}{0.12} \cdot 1.0677 Hz \cdot 45m = 400\ m/s \tag{6.4}$$

It is clear that the obtained values of V_{crit} are vast compared to the wind velocities that could be expected to occur. In fact, both the V_{crit} values are higher than any wind gust ever registered [20]. Although the estimated size and shape of the cross section entails some uncertainty, the effect of vortex induced response could be neglected for the study building.

6.2 Buffeting Response

In this section, the necessary theory for calculating the buffeting response of the structure is accounted for. Buffeting could be described as pressure fluctuations in the wind field caused by turbulence. These pressure fluctuations induces structural response. The theory presented here is crucial for understanding how the response is calculated, which variables and parameters are included, and how the calculation procedure is conducted.

To start with, it is assumed that the structure at hand is linear elastic, and that there is a linear relation between wind flow and loading. Furthermore, the flow is assumed Gaussian, stationary and homogenous. This allows for the maximal response to be divided into a flow induced and a turbulence induced part, which corresponds to the mean value and probability density distribution respectively. Mathematically, this is expressed as

$$r_{\max}(x_r) = \bar{r}(x_r) + k_p \sigma_r(x_r) \tag{6.5}$$

where x_r refers to height above ground. The turbulence induced part of the response is given by a peak-factor k_p multiplied by the standard deviation σ_r at the given height for a given time interval (normally 10 minutes). Obtaining the standard deviation is a complicated process, which will be shown in detail later.

6.2.1 Static Response

The static displacements could be estimated either by a FEM-approach, or by using basic beam theory. Considering the structure as a cantilevered beam exposed to horizontal wind loading, the static displacements are easily calculated using the unit-load method.

The static load in the y-direction is given by Strømmen as

$$\bar{q}_y(z) = \frac{\rho V(x)^2 D}{2} \cdot \bar{C}_D \tag{6.6}$$

D represents the width of the cross section perpendicular to the main flow. $\bar{C}_D$ is the drag coefficient for the relevant direction, while ρ is the density of air. The variation of mean wind velocity $V(x)$ is given in Section 8.2. According to Irgens [21], the unit-load method is based on the principle of virtual work. Using the moment diagram M given by the actual static loading, and the moment diagram $\tilde{M}$ given by a unit load $\tilde{F} = 1$ at the location and in the direction that the displacement δ should be calculated, the following expression is established

$$1 \cdot \delta_{j,M} = \int_L \tilde{M}_i \frac{M_i}{EI_j} dx \tag{6.7}$$

The moment diagrams $\tilde{M}$ and M are integrated over the height of the structure. EI is the relevant bending stiffness. The direction considered is given by $i, j = y, z$ and vice versa. In the same manner, the displacement given by shear strain energy is given by

$$1 \cdot \delta_{j,V} = \int_L \tilde{V}_i \cdot k_i \cdot \frac{V_i}{GA_j} dx \tag{6.8}$$

where V represents the shear force diagrams, GA is the shear stiffness (shear modulus times area), and k is the shear constant, which describes the distribution of share stresses over the cross section.

6.2.2 Standard Deviation of Displacement

The derivation that follows covers single mode, single component response calculations. It is presupposed that eigen frequencies are well separated and that coupling effects are negligible. As mentioned earlier, only one modal shape is included in the calculation at a time, and the resulting response has one component. Theory prior to the starting point is assumed known.

6.2.2.1 Spectral Density of Displacement

The standard deviation of displacement is given by integrating the spectral density of displacement S_r over the entire frequency domain. To obtain the spectral density of displacement, it is convenient to start with the equation of motion on modal form, given by

$$\tilde{M}_i \cdot \ddot{\eta}_i(t) + \tilde{C}_i \cdot \dot{\eta}_i(t) + \tilde{K}_i \cdot \eta_i(t) = \tilde{Q}_i(t) + \tilde{Q}_{ae_i}(t, \eta, \dot{\eta}, \ddot{\eta}) \tag{6.9}$$

Here, $\tilde{M}_i$ is the modal mass, $\tilde{C}_i$ is the modal damping, and $\tilde{K}_i$ is the modal stiffness for mode i. η, $\dot{\eta}$ and $\ddot{\eta}$ are the general coordinates derived by time. $\tilde{Q}_i(t)$ represents the flow induced loading on the structure, while $\tilde{Q}_{ae_i}(t, \eta, \dot{\eta}, \ddot{\eta})$ represents the load given by interaction between structural motion and air flow. Taking the Fourier Transform, the following is obtained.

$$\left(\tilde{M}_i \omega^2 + \tilde{C}_i i\omega + \tilde{K}_i\right) \cdot a_{\eta_i} = a_{\tilde{Q}_i}(\omega) + a_{\tilde{Q}_{ae_i}}(\omega, \eta, \dot{\eta}, \ddot{\eta}) \tag{6.10}$$

The a-factors are the fourier amplitudes of the general coordinates and modal load components. The fourier amplitude of the aerodynamic load term could be rewritten into a sum of cross sectional properties

$$\left(\tilde{M}_{ae_i} \omega^2 + \tilde{C}_{ae_i} i\omega + \tilde{K}_{ae_i}\right) \cdot a_{\eta_i} = a_{\tilde{Q}_{ae_i}}(\omega) \tag{6.11}$$

Equation (6.11) demands the assumption that the fourier amplitude contains all three cross sectional properties, which are proportional to and in phase with structural displacement, velocity and acceleration. Now using basic dynamic identities, inserting equation (6.11) into (6.10), moving $a_{\tilde{Q}_{ae_i}}$ to the left hand side, and dividing by $\tilde{K}_i = \omega_i^2 \tilde{M}_i$ it is obtained that

$$\left(1-\frac{\tilde{K}_{ae_i}}{\omega_i^2\tilde{M}_i}-\left(1-\frac{\tilde{M}_{ae_i}}{\tilde{M}_i}\right)\cdot\left(\frac{\omega}{\omega_i}\right)^2+2i\left(\zeta_i-\frac{\tilde{C}_{ae_i}}{2\omega_i\tilde{M}_i}\right)\frac{\omega}{\omega_i}\right)\cdot a_{\eta_i}(\omega)=\frac{a_{\tilde{Q}_i}(\omega)}{\tilde{K}_i} \tag{6.12}$$

(6.12) could be rewritten into the following expression

$$a_{\eta_i}(\omega)=\frac{\hat{H}_i(\omega)}{\tilde{K}_i}\cdot a_{\tilde{Q}_i}(\omega) \tag{6.13}$$

$\hat{H}_i(\omega)$ is the frequency response function of the system. Introducing that $\mu_{ae_i}=\tilde{M}_{ae_i}/\tilde{M}_i$, $\kappa_{ae_i}=\tilde{K}_{ae_i}/\omega_i^2\tilde{M}_i$ and $\zeta_{ae_i}=\tilde{C}_{ae_i}/2\omega_i\tilde{M}_i$, the frequency response function takes the form

$$\hat{H}(\omega)=\left[1-\kappa_{ae_i}-\left(1-\mu_{ae_i}\right)\cdot\left(\frac{\omega}{\omega_i}\right)^2+2i\left(\zeta_i-\zeta_{ae_i}\right)\frac{\omega}{\omega_i}\right]^{-1} \tag{6.14}$$

$\hat{H}_i(\omega)$ contains all the aerodynamic cross-sectional properties. The spectral density of η is found by using equation (6.13). The index * means complex conjugate.

$$\begin{aligned} S_{\eta_i}(\omega)&=\lim_{T\to\infty}\frac{1}{\pi T}\cdot(a_{\eta_i}^*\cdot a_{\eta_i})=\frac{\left|\hat{H}_i(\omega)\right|^2}{\tilde{K}_i^{\,2}}\cdot\lim_{T\to\infty}\frac{1}{\pi T}(a_{\tilde{Q}_i}^*\cdot a_{\tilde{Q}_i}) \\ \Rightarrow S_{\eta_i}(\omega)&=\frac{\left|\hat{H}_i(\omega)\right|^2}{\tilde{K}_i^{\,2}}\cdot S_{\tilde{Q}_i}(\omega) \end{aligned} \tag{6.15}$$

$S_{\tilde{Q}_i}(\omega)$ in equation (6.15) is the spectral density of loading. The fact that $\hat{\mathrm{H}}_i^*\cdot\hat{\mathrm{H}}_i=\left|\hat{H}_i^{\,2}\right|$ is easily shown by performing the multiplication. To get from general coordinates to the real response, the definition of general coordinates $r_i(z,t)=\phi_i(z)\cdot\eta_i(t)$ implies that $a_{r_i}=\phi_i\cdot a_{\eta_i}$. The spectral density of displacement, or response spectrum, is then given by

$$S_{r_i}(\omega)=\frac{\phi_i^2(z_r)}{\tilde{K}_i^{\,2}}\cdot\left|\hat{H}_i(\omega)\right|^2\cdot S_{\tilde{Q}_i}(\omega) \tag{6.16}$$

Strømmen shows how a discretization of a response spectrum could be used to peforme a time domain simulation of response. A spectral density could be discretized by

$$S_x(\omega_k)=\frac{c_k^2}{2\cdot\Delta\omega_k} \tag{6.17}$$

for each frequency interval k. The amplitude parameter c_k could be obtained by

$$c_k=\left(2\cdot S_x(\omega_k)\cdot\Delta\omega_k\right) \tag{6.18}$$

The time series simulation is then given by

$$x(t) = \sum_{k=1}^{N} c_k \cdot \cos(\omega_k t + \psi_k) \tag{6.19}$$

where ψ_k is a random phase angel between 0 and 2π. Such a simulation will be performed both for displacement and acceleration when results are obtained.

6.2.2.2 Spectral Density of Loading

To determine an expression for the spectral density of loading, the expression for the load itself has to be established. The displacements and rotations of a cross-section because of static and turbulence induced loading are shown in Figure 6.3.

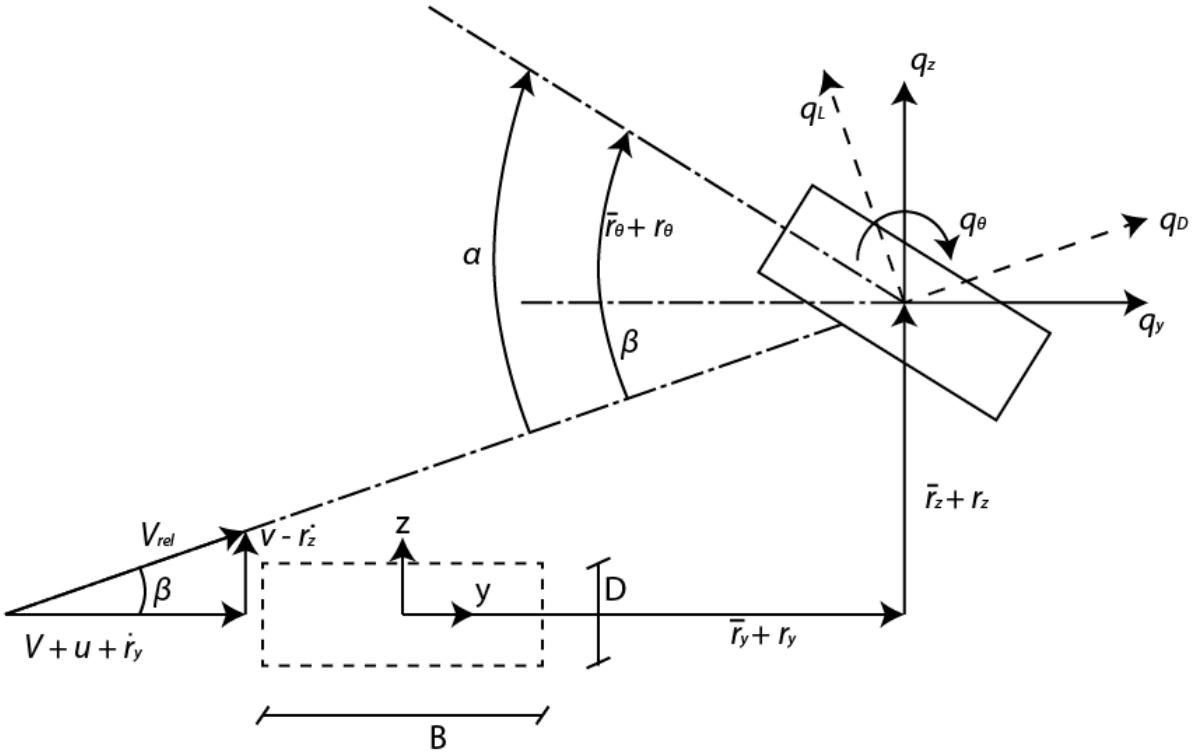

Figure 6.3: Flow, displacements and forces for wind loading

The x-coordinate is defined as the height axis of the tower. $\bar{r}_y(x)$, $\bar{r}_z(x)$ and $\bar{r}_\theta(x)$ are the static displacements given by the mean vind velocity V(x), while $r_y(x,t)$, $r_z(x,t)$ and $r_\theta(x,t)$ are the additional fluctuating responses induced by turbulence. Wind velocity in the displaced configuration is $V + u(x,t)$ in the along-wind direction and $v(x,t)$ in the direction perpendicular to main flow.

Forces on the structure in form of drag, lift and moment in the displaced position are defined by

$$\begin{bmatrix} q_D(x,t) \\ q_L(x,t) \\ q_M(x,t) \end{bmatrix} = \frac{1}{2} \cdot \rho \cdot V_{rel}^2 \cdot \begin{bmatrix} D \cdot C_D(\alpha) \\ B \cdot C_L(\alpha) \\ B^2 \cdot C_M(\alpha) \end{bmatrix} \tag{6.20}$$

V_{rel} is the instantaneous relative velocity at height x, α is the angel of flow compared to the cross-sectional axis at the same instance. The C-factors are load coefficients. Using Figure 6.3 above, these forces could be related to the structural coordinate system by

$$\mathbf{q}_{tot}(x,t) = \begin{bmatrix} q_y \\ q_z \\ q_\theta \end{bmatrix}_{tot} = \begin{bmatrix} \cos\beta & -\sin\beta & 0 \\ \sin\beta & \cos\beta & 0 \\ 0 & 0 & 1 \end{bmatrix} \cdot \begin{bmatrix} q_D \\ q_L \\ q_M \end{bmatrix} \tag{6.21}$$

The β-angle could be found from the Figure 6.3 as $\beta = \tan^{-1}\left(\frac{v - \dot{r}_z}{V + u - \dot{r}_y}\right)$. It is now assumed that the turbulence components u and v are small compared to the mean wind velocity V, and that the cross-sectional displacements r_i, where i equals y, z or θ, are small. Using these assumptions it could easily be shown that the following linearization applies

$$\begin{aligned} V_{rel}^2 &\approx V^2 + 2Vu - 2V\dot{r}_y \\ \alpha &\approx \bar{r}_\theta + r_\theta + \frac{v}{V} - \frac{\dot{r}_z}{V} \end{aligned} \tag{6.22}$$

According to Strømmen, the drag, lift and moment coefficients from equation (6.20) depend nonlinearly on the angle α. Considering α as two parts $\bar{\alpha} = \bar{r}_\theta$ and $\alpha_f = r_\theta + v/V - \dot{r}_z/V$ induced by the mean wind velocity and the fluctuations respectively, the load coefficients C could be divided into

$$\begin{bmatrix} C_D(\alpha) \\ C_L(\alpha) \\ C_M(\alpha) \end{bmatrix} = \begin{bmatrix} C_D(\bar{\alpha}) \\ C_L(\bar{\alpha}) \\ C_M(\bar{\alpha}) \end{bmatrix} + \alpha_f \begin{bmatrix} C_D'(\bar{\alpha}) \\ C_L'(\bar{\alpha}) \\ C_M'(\bar{\alpha}) \end{bmatrix} \tag{6.23}$$

which from now on are referred to as $\bar{C}_i$ and C_i', where $i = D, L, M$. Using the results obtained in (6.21), (6.22) and (6.23), the following load expression is obtained

$$\begin{bmatrix} q_y \\ q_z \\ q_\theta \end{bmatrix} = \rho V\left(\frac{V}{2}+u-\dot{r}_y\right)\left[\begin{bmatrix} \bar{C}_D D \\ \bar{C}_L B \\ \bar{C}_M B^2 \end{bmatrix} + \left(r_\theta + \frac{v-\dot{r}_z}{V}\right)\begin{bmatrix} C'_D D \\ C'_L B \\ C'_M B^2 \end{bmatrix}\right.$$
$$\left. -\frac{v-\dot{r}_z}{V}\begin{bmatrix} \bar{C}_L B \\ -\bar{C}_D D \\ 0 \end{bmatrix} - \left(\frac{v-\dot{r}_z}{V}\right)\left(r_\theta + \frac{v-\dot{r}_z}{V}\right)\begin{bmatrix} C'_L B \\ C'_D D \\ 0 \end{bmatrix}\right] \tag{6.24}$$

Since all cross-sectional displacements and turbulence components are assumed small, the last term of equation (6.24) contains higher order values only and could therefore be neglected. Focusing on the y-direction only, equation (6.24) could be rewritten into

$$q_{y,tot}(x,t) = \bar{q}_y(x) + q_y(x,t) = \bar{q}_y + \mathbf{B_{q,y}}\cdot\mathbf{v} + \mathbf{C_{ae,y}}\cdot\dot{\mathbf{r}} + \mathbf{K_{ae,y}}\cdot\mathbf{r} \tag{6.25}$$

The terms in equation (6.25) are given in detail below. Products of quantities that have been assumed small are neglected.

$$\mathbf{v}(x,t) = \begin{bmatrix} u & v \end{bmatrix}^T \tag{6.26}$$

$$\mathbf{r}(x,t) = \begin{bmatrix} r_y & r_z & r_\theta \end{bmatrix}^T \tag{6.27}$$

$$\bar{q}_y = \frac{\rho V(x)^2 B}{2}\cdot\left(\frac{D}{B}\right)\bar{C}_D \tag{6.28}$$

$$\mathbf{B}_{q,y}(x) = \frac{\rho V(x) B}{2}\begin{bmatrix} 2\frac{D}{B}\bar{C}_D & \left(\frac{D}{B}\right)\cdot C'_D - \bar{C}_L \end{bmatrix} \tag{6.29}$$

$$\mathbf{C}_{ae,y} = -\frac{\rho V(x) B}{2}\begin{bmatrix} 2\frac{D}{B}\bar{C}_D & \left(\frac{D}{B}\right)\cdot C'_D - \bar{C}_L & 0 \end{bmatrix} \tag{6.30}$$

$$\mathbf{K}_{ae,y} = \frac{\rho V(x)^2 B}{2}\begin{bmatrix} 0 & 0 & \frac{D}{B}\bar{C}_D \end{bmatrix} \tag{6.31}$$

As mentioned, the terms given in equations (6.28) to (6.31) represent y-direction only. The equation system could easily be expanded to include the z- and θ-direction as well, by writing out the rest of equation (6.24).

A further look at the aerodynamic properties should be included. $\mathbf{C}_{ae,y}$ and $\mathbf{K}_{ae,y}$ could be normalized and expressed by aerodynamic derivatives. For the y-direction properties this would, according to Strømmen, give

$$\mathbf{C}_{ae,y} = \frac{\rho B^2}{2}\cdot\omega_i(V)\cdot\hat{\mathbf{C}}_{ae,y} = \frac{\rho B^2}{2}\cdot\omega_i(V)\cdot\begin{bmatrix} P_1^* & P_5^* & BP_2^* \end{bmatrix} \tag{6.32}$$

The non dimensional P-factors are called aerodynamic derivatives. They could be determined by looking at equation (6.30)

$$\begin{bmatrix} P_1^* \\ P_5^* \\ BP_2^* \end{bmatrix} = \begin{bmatrix} -2\bar{C}_D \dfrac{D}{B} \dfrac{V(x)}{B\omega_i(V)} \\ -\left(\dfrac{D}{B} C_D' - \bar{C}_L\right)\left(\dfrac{V(x)}{B\omega_i(V)}\right) \\ 0 \end{bmatrix} \tag{6.33}$$

The derivatives are expressed as functions of the eigen frequency for Mode i, which in reality is a function of wind velocity. This effect is neglected here, i.e. the frequencies are assumed constant.

A similar expression as equation (6.32) could be established for $\mathbf{K}_{ae,y}$, but then normalized by $\mathbf{K}_{ae,y} = \dfrac{\rho B^2}{2} \cdot \left[\omega_i(V)\right]^2 \cdot \hat{\mathbf{K}}_{ae,y}$. The $\left[\omega_i(V)\right]^2$ term is not cancelled out by the P*-factors, which results in a demand for iteration if $\mathbf{K}_{ae,y}$ should be included in the calculations. This is relevant for mean wind velocities approaching instability limits, which is not the case here. Therefore, $\mathbf{C}_{ae,y}$ contains the relevant derivatives in this case.

From equation (6.25) the modal load is obtained by multiplying by the y-direction modal vector

$$\tilde{Q}_{y,tot}(t) = \int_{L_{\exp}} \phi_y(x) \cdot q_{y,tot}(x,t) dx \tag{6.34}$$

The total load $q_{y,tot}(x,t)$ could by equation (6.25) be separated into a flow induced and an aerodynamic part, like shown for the modal load in equation (6.9). All aerodynamic properties are moved to the left hand side of the equation system, and included in the frequency response function, equation (6.14), like shown in Section 6.2.2.1.

With the aerodynamic properties out of the picture, the load terms left are

$$q_y(x,t) = \bar{q}_y(x) + \mathbf{B}_q \cdot \mathbf{v}(x,t) \tag{6.35}$$

Only the flow induced contribution $\mathbf{B}_q \cdot \mathbf{v}$ will be considered in the following, while the static loading $\bar{q}_y$ has been assessed in Section 6.2.1. Combining equations (6.26), (6.29) and (6.34), the modal loading induced by flow is

$$Q_y(t) = \frac{\rho V(x) B}{2} \int_{L_{\exp}} \phi_y(x) \cdot \left[\frac{2D\bar{C}_D}{B} \cdot u(x,t) + \left(\frac{DC_D'}{B} - \bar{C}_L \right) v(x,t) \right] dx \tag{6.36}$$

Fourier transform of (6.36) gives

$$a_{\tilde{Q}_y}(\omega) = \frac{\rho V(x) B}{2} \int_{L_{\exp}} \phi_y(x) \cdot \left[\frac{2D\bar{C}_D}{B} \cdot a_u(x,\omega) + \left(\frac{DC'_D}{B} - \bar{C}_L \right) a_v(x,\omega) \right] dx \tag{6.37}$$

The spectral density of loading is then given by

$$\begin{aligned} S_{\tilde{Q}_y}(\omega) &= \lim_{T\to\infty} \frac{1}{\pi T} a^*_{\tilde{Q}_y} a_{\tilde{Q}_y} = \left(\frac{\rho V(x) B}{2} \right)^2 \cdot \lim_{T\to\infty} \frac{1}{\pi T} \\ &\cdot \left\{ \int_{L_{\exp}} \phi_y(x) \cdot \left[\frac{2D\bar{C}_D}{B} \cdot a^*_u(x,\omega) + \left(\frac{DC'_D}{B} - \bar{C}_L \right) a^*_v(x,\omega) \right] dx \right\} \\ &\cdot \left\{ \int_{L_{\exp}} \phi_y(x) \cdot \left[\frac{2D\bar{C}_D}{B} \cdot a_u(x,\omega) + \left(\frac{DC'_D}{B} - \bar{C}_L \right) a_v(x,\omega) \right] dx \right\} \end{aligned} \tag{6.38}$$

6.2.2.3 Joint Acceptance Function

The load spectral density from equation (6.38) contains cross spectral densities between turbulence components u and v. These cross spectral densities are usually small, and are therefore neglected. Rewriting equation (6.38) gives

$$\begin{aligned} S_{\tilde{Q}_y}(\omega) &= \iint_{L\exp} \phi_y(x_1) \cdot \phi_y(x_2) \cdot \left(\frac{\rho V(x) B}{2} \right)^2 \\ &\left[\left(\left(\frac{2D\bar{C}_D}{B} \right)^2 \cdot \lim_{T\to\infty} \frac{1}{\pi T} a^*_u(x_1,\omega) \cdot a_u(x_2,\omega) \right) \right. \\ &\left. + \left(\left(\frac{DC'_D}{B} - \bar{C}_L \right)^2 \lim_{T\to\infty} \frac{1}{\pi T} a^*_v(x_1,\omega) \cdot a_v(x_2,\omega) \right) \right] dx_1 dx_2 \end{aligned} \tag{6.39}$$

The introduction of integration variables x_1 and x_2 is necessary to transform the integral product from equation (6.38) into a double integral. To proceed the following definitions are introduced

$$\begin{aligned} S_{nn}(\Delta x,\omega) &= \lim_{T\to\infty} \frac{1}{\pi T} \left[a^*_n(x_1,\omega) \cdot a_n(x_2,\omega) \right] \\ I_n(x) &= \frac{\sigma_n(x)}{V(x)} \end{aligned} \tag{6.40}$$

$I_n(z)$ is the turbulence intensity, while $S_{nn}(x)$ is the cross spectral density. The turbulence intensity is equal to the ratio between standard deviation of the turbulent component and the mean wind velocity. According to Strømmen, the turbulence intensity perpendicular to main

flow is equal to $3/4$ of the turbulence intensity in the main flow direction. Using equations (6.40) and expanding equation (6.39) by $\frac{V(x)^2}{V(x)^2}$, it is obtained from equation (6.39) that

$$S_{\tilde{Q}_y}(\omega) = \left[\frac{\rho B}{2} \cdot J_y(\omega)\right]^2 \tag{6.41}$$

where the joint acceptance function $J_y(\omega)$ is given by

$$J_y^2(\omega) = \iint_{L_{\exp}} \phi_y(x_1) \cdot \phi_y(x_2) \cdot \left(V(x_1)^2 \cdot V(x_2)^2\right) \left\{ \begin{array}{l} A(x_1) \cdot A(x_2) \cdot \frac{S_{uu}(\Delta x, \omega)}{\sigma_u^2} \\ +B(x_1) \cdot B(x_2) \cdot \frac{S_{vv}(\Delta x, \omega)}{\sigma_v^2} \end{array} \right\} dx_1 dx_2 \tag{6.42}$$

where

$$\left. \begin{array}{l} A(x_i) = \left(\frac{2D\bar{C}_D}{B} I_u(x_i)\right) \\ B(x_i) = \left(\left(\frac{DC'_D}{B} - \bar{C}_L\right) I_v(x_i)\right) \end{array} \right\} i = 1, 2 \tag{6.43}$$

The Joint Acceptance Function describes how the structural mode shapes interact with the loading (and therefore the frequency and spatial properties of the air flow). It should be mentioned that the function calculated is not actually the JAF. For practical reasons, the wind velocity is included in the integral. This is not done in the JAF shown by Strømmen because the wind velocity is constant for bridge decks at constant heights. For the given case however, the wind velocity varies over the height of the structure. Including the velocity terms in the JAF is both convenient and saves computation time.

The cross spectral density functions $S_{nn}(\Delta x, \omega)$ within $J_y^2(\omega)$ describes the density of fluctuations in the n-direction with a given frequency for two points located a distance $\Delta x = |x_1 - x_2|$ from each other. It could, by using the definition of Co-spectrums, be written as the product of the normalized Co-spectrum and the spectral density of the relevant turbulence component, i.e.

$$\frac{S_{nn}(\Delta x, \omega)}{\sigma_n^2} = \frac{S_n(\omega)}{\sigma_n^2} \cdot \hat{Co}_{nn}(\Delta x, \omega) \tag{6.44}$$

The spectral density $\frac{S_n(\omega)}{\sigma_n^2}$ is a probabilistic way of describing the amount of turbulence fluctuations over the frequency spectrum. In other words, it describes if turbulence fluctuations of a given frequency are common or not. Kaimal et. al. [22] proposed an

expression that has been frequently used, and has been adopted by the Eurocode. Looking to Dyrbye & Hansen, the following version of the Kaimal spectral density is given

$$\frac{S_n(\omega)}{\sigma_n^2} = \frac{6.8 f_L}{\omega \cdot (1+10.2 f_L)^{5/3}} \tag{6.45}$$

The term f_L is given by $f_L = \frac{\omega \cdot {}^{s}L_n}{2\pi \cdot V(x)}$. ${}^{s}L_n$ is an integral length scale, and could according to Dyrbye & Hansen be interpreted as the average size of a gust in a given direction s. For a tower structure, the relevant direction is the same as the main flow, which here is denoted as y. The two considered turbulence components are u and v. Strømmen states that these eddy sizes should be obtained from full scale measurements. As an approximation, the following could be adopted

$$\begin{aligned} {}^{y}L_u &= 100 \cdot \left(\frac{x_f}{10}\right)^{0,3}, \quad \begin{cases} x_f = 10 & \text{for} \quad x \le 10m \\ x_f = x & \text{for} \quad x > 10m \end{cases} \\ {}^{y}L_v &= \frac{{}^{y}L_u}{4} \end{aligned} \tag{6.46}$$

Normalized Co-spectrums represent the spatial properties of the wind turbulence, and are often encountered in literature. As shown in equation (6.47), $\hat{Co}$ depends on the spacing between two considered points, Δx. If two points are located far from each other, the wind fields experienced at the two points could not be expected equal, and thus the cross spectral density is scaled down by $\hat{Co}_{nn}$. If the two points are closely spaced, they will experience similar wind fields, and thus the cross spectral density will not be reduced.

One of the most commonly used expressions for $\hat{Co}_{nn}$ was developed by Davenport [23]. Using empirical results from line like structures in flat terrain, the following expression was established for the Co-spectrum

$$\hat{Co}_{nn}(\Delta x, \omega) = e^{-C_{nm}\frac{\Delta x \cdot \omega}{2\pi \cdot V(x)}}, \quad \text{n = u,v} \quad \text{m = x,y,z} \tag{6.47}$$

C_{mn} is a decay constant that describes the spatial extent of turbulence correlation. It was conservatively estimated by Davenport to the value $C_{uz} = 7$. This value displays great variations. Dyrbye & Hansen suggests $C_{uz} = 10$, while Strømmen suggests $C_{uz} \approx 9$. The latter is adopted in this thesis.

The term $\frac{S_{nn}(\Delta x, \omega)}{\sigma_n^2}$ from equation (6.42) could, by using equations (6.44), (6.45) and (6.47) be written as

$$\frac{S_{nn}(\Delta x,\omega)}{\sigma_n^2}=\frac{6.8\left(\frac{{}^{y}L_n}{2\pi\cdot V(x)}\right)}{\left(1+10.2\left(\frac{\omega\cdot {}^{y}L_n}{2\pi\cdot V(x)}\right)\right)^{5/3}}\cdot e^{-C_{nm}\frac{\Delta x\cdot\omega}{2\pi\cdot V(x)}} \tag{6.48}$$

Expression (6.48) is clearly dependent on the mean wind velocity $V(x)$. Since the expression is not squared in equation (6.42), there is no way to include both variables x_1 and x_2 in $V(x)$. To cope with this problem, an engineering assessment has to be made. Since the objective of the calculations is to obtain the response at the top of the building, it is assumed that $V(x)$ in equation (6.48) equals the mean wind velocity at the top of the building, $V(x_r=75m)$. The same goes for the integral length scales ${}^{s}L_n$. Their height dependence is not straight forward to include in the calculations, and thus they are assumed evaluated at the tower top, x_f = 75 meters. With ${}^{s}L_n$ and $V(x)$ assumed constant, the double integral in equation (6.42) could easily be calculated.

6.2.2.4 Frequency Response Function & Aerodynamic Damping

Before the expression for the standard deviation of displacement is established, a look at the Frequency Response Function is required. The total function is given in equation (6.14). As mentioned in Section 6.2.2.2 below equation (6.34), all aerodynamic properties are included in the frequency response function. The stiffness term will only be significant for wind velocities close to instability limits, and could therefore be neglected. It was assumed in the derivation of wind loading that turbulence components and structural displacements were small. It is therefore reasonable to assume that also the structural accelerations are small, which allows for the mass-term to be neglected as well. The resulting frequency response function is then

$$\hat{H}_i(\omega)=\left[1-\left(\frac{\omega}{\omega_i}\right)^2+2i\left(\zeta_i-\zeta_{ae_i}\right)\frac{\omega}{\omega_i}\right]^{-1} \tag{6.49}$$

The only unknown term is the aerodynamic damping ratio, ζ_{ae_i}. It has already been introduced in Section 6.2.2.1 as $\zeta_{ae_i}=\tilde{C}_{ae_i}/2\omega_i\tilde{M}_i$. Using equations (6.32), (6.33) and known identities, it is found that

$$\begin{aligned}\zeta_{ae_y}&=\frac{\tilde{C}_{ae_y}}{2\omega_y\tilde{M}_y}=\frac{C_{ae_y}\cdot\int_{L_{\exp}}\phi_y^2dx}{2\omega_y\tilde{m}_y\cdot\int_{L}\phi_y^2dx}\\&=\frac{\rho B^2}{4\tilde{m}_y}\cdot P_1^*\cdot\frac{\int_{L_{\exp}}\phi_y^2dx}{\int_{L}\phi_y^2dx}=\frac{\rho B^2}{4\tilde{m}_y}\cdot\left(-2\bar{C}_D\frac{D}{B^2\omega_y}\right)\cdot\frac{\int_{L_{\exp}}\phi_y^2\cdot V(x)dx}{\int_{L}\phi_y^2dx}\end{aligned} \tag{6.50}$$

where any velocity-dependence of ω_y for simplicity has been neglected.

6.2.2.5 Standard Deviation of Buffeting Response

The standard deviation of displacement is found by integrating the displacement response spectrum over the entire frequency domain

$$\sigma_{r_y}^2(x) = \int_0^\infty S_{r_y}(x,\omega)d\omega \tag{6.51}$$

Using equation (6.16), inserting the spectral density of loading from equation (6.41) and replacing $\tilde{K}_i$ by $\omega_y^2\tilde{M}_y = \omega_y^2 \cdot \tilde{m}_y \int_L \phi_y^2 dx$, the standard deviation of displacement is obtained by

$$\sigma_{r_y}(x) = \left|\phi_y(z_r)\right| \cdot \frac{\rho B^3}{2\tilde{m}_y} \cdot \left(\frac{1}{B\omega_y}\right)^2 \cdot \left[\int_0^\infty \left|\hat{H}_y(\omega)\right|^2 \cdot \hat{J}_y^2(\omega)d\omega\right]^{1/2} \tag{6.52}$$

where the normalized Joint Acceptance Function is given by

$$\hat{J}_y^2(\omega) = J_y^2(\omega) / \left(\int_L \phi_y^2 dx\right)^2 \tag{6.53}$$

6.2.3 Acceleration

In the previous section the displacements were divided into a static and a fluctuating dynamic part. It is obvious that the static displacements does not induce any accelerations, i.e. it is the fluctuating part of the response that needs to be considered. Acceleration is usually found as the displacement derived twice with respect to time, $a_n(t) = \ddot{r}_n(t)$. To proceed, it is assumed that the structure oscillates like a cosine function

$$r_n(t) = c \cdot \cos(\omega_n t) \tag{6.54}$$

The parameter c describes the amplitude. Now $u(t)$ is derived twice by time

$$\begin{aligned} \dot{r}_n(t) &= -\omega_n \cdot c \cdot \sin(\omega_n t) \\ \ddot{r}_n(t) &= -\omega_n^2 \cdot c \cdot \cos(\omega_n t) \end{aligned} \tag{6.55}$$

which demonstrates that

$$a(t) = -\omega_n^2 \cdot u(t) \tag{6.56}$$

Taking the Fourier Transform of equation (6.56), it is obtained that

$$a_{a_n}(\omega) = -\omega_n^2 \cdot a_{r_n}(\omega) \tag{6.57}$$

The spectral density of acceleration is then given by

$$S_{a_n}(\omega) = \lim_{T\to\infty} \frac{1}{\pi T} a_{a_n}^* \cdot a_{a_n} = \omega_n^4 \cdot \lim_{T\to\infty} \frac{1}{\pi T} a_{r_n}^* \cdot a_{r_n} = \omega_n^4 \cdot S_{r_n}(\omega) \tag{6.58}$$

Now using the same procedures as shown in equation (6.51), it is found that

$$\sigma_{a_n}^2 = \int_0^\infty S_{a_n}(\omega) d\omega = \omega_n^4 \cdot \int_0^\infty S_{r_n}(\omega) d\omega \tag{6.59}$$

The peak acceleration of the structure is then obtained by multiplying the standard deviation by the peak factor.

As mentioned in Section 4.3, the acceleration needs to be weighted with respect to frequency before it is compared to the chosen design demands. As shown in equation (4.1), it is the root-mean-square-acceleration that is supposed to be frequency weighted. The RMS acceleration is an amplitude quantity, while the available acceleration is found from a spectral density. The frequency weighting function W is given to match an amplitude spectrum. To match it to a spectral density, W is squared before it is multiplied by the spectral density of acceleration, $S_{a_n}(\omega)$.

As understood from the above, the spectral density of acceleration is needed. Like shown in equation (6.58), S_{a_n} is found by multiplying the spectral density of displacement by the frequency in the fourth power. The spectral density of displacement is described by equation (6.16), and corresponds to the square of equation (6.52) without taking the integral of the FRF and the JAF. The height variation is neglected because only the acceleration at the tower top is of interest. In total, the spectral density of acceleration, $S_{a_n}(\omega)$, is obtained as

$$S_{a_n}(\omega) = \omega^4 \cdot \left(\frac{\rho B}{2\tilde{m}_y \omega_y^2} \right)^2 \cdot \left[\left| \hat{H}_y(\omega) \right|^2 \cdot \hat{J}_y^2(\omega) \right] \tag{6.60}$$

The total frequency weighted acceleration at the tower top is then obtained by

$$a_w = k_p \cdot \int_0^\infty S_{a_n}(\omega) \cdot \left(W(\omega) \right)^2 d\omega \tag{6.61}$$

6.3 Cross Sectional Forces

Calculation of cross sectional forces follows the same pattern as displacement response. The maximum cross sectional force at height x_r is given by

$$F_{\max}(x_r) = \bar{F}(x_r) + k_p \cdot \sqrt{\sigma_{F_B}^2(x_r) + \sigma_{F_R}^2(x_r)} \tag{6.62}$$

All terms of expression (6.62) are described below.

6.3.1 Static Forces

Since the structure is considered to be line-like and cantilevered, calculating the static forces is quite basic. Given the static loading from equation (6.6) the static base shear and base moment is found by integrating the force times the static influence function (equal to unity for the shear force and the lever-arm x for the base moment) over the height of the structure.

$$\begin{aligned} \bar{M} &= \int_{L_{\exp}} x \cdot \bar{q}(x)dx = \frac{\rho \bar{C}_D D}{2} \int_{L_{\exp}} x \cdot V(x)^2 dx \\ \bar{V} &= \int_{L_{\exp}} \bar{q}(x)dx = \frac{\rho \bar{C}_D D}{2} \int_{L_{\exp}} V(x)^2 dx \end{aligned} \tag{6.63}$$

6.3.2 Background Part of Cross Sectional Forces

As shown in equation (6.62), the dynamic cross sectional forces are split into a background part and a resonance part. The background part accounts for low-frequency oscillations in the cross sectional forces. Since the frequency is low, inertia effects are negligible, and there is no effect from motion induced loading. As shown in Section 6.2.2.2, the loading is given by

$$q(x,t) = B_{q,y} \cdot \mathbf{v} = \frac{\rho V(x) B}{2} \left[2\frac{D}{B}\bar{C}_D \quad \left(\frac{D}{B}\right) \cdot C_D' - \bar{C}_L \right] \cdot \begin{bmatrix} u(x,t) \\ v(x,t) \end{bmatrix} \tag{6.64}$$

The moment (and shear) at a given section of the building will be given by an expression similar to the one presented in (6.63), with the influence functions being the same as in equation (6.63). Now turning to basic statistics, it is known that variance of a quantity is given as the expectation value of the squared quantity, which provides the following

$$\begin{aligned} \sigma_{M_{z_B}}^2 &= E\left[\left\{ M_{z_B}(x_r,t) \right\}^2 \right] = E\left[\left\{ \int_{L_{\exp}} x \cdot q_y(x,t)dx \right\}^2 \right] \\ &= \iint_{L_{\exp}} x_1 \cdot x_2 \cdot E\left[q_y(x_1,t) \cdot q_y(x_2,t) \right] dx_1 dx_2 \end{aligned} \tag{6.65}$$

The double integral is introduced by using two integration variables x_1 and x_2. The influence function for shear force is 1, which gives the following expression

$$\sigma_{V_{yB}}^2 = \iint_{L_{\exp}} E\left[q_y(x_1,t)\cdot q_y(x_2,t)\right]dx_1dx_2 \tag{6.66}$$

The expectation value is common for both moment and shear force. Inserting expression (6.64) for $q_y(x,t)$ the expectation value takes the form

$$\begin{aligned} E\left[q_y(x_1,t)\cdot q_y(x_2,t)\right] &= \left(\frac{\rho V(x)B}{2}\right)^2 \\ \cdot E\left[\left[2\frac{D}{B}\bar{C}_D\cdot u(x_1,t)+\left(\left(\frac{D}{B}\right)\cdot C_D' - \bar{C}_L\right)v(x_1,t)\right]\right. & \\ \left.\cdot\left[2\frac{D}{B}\bar{C}_D\cdot u(x_2,t)+\left(\left(\frac{D}{B}\right)\cdot C_D' - \bar{C}_L\right)v(x_2,t)\right]\right] & \end{aligned} \tag{6.67}$$

The product above contains cross-covariances, namely $E\left[u(x_1,t)\cdot v(x_2,t)\right]$ and vice versa. According to Strømmen these quantities are usually neglected in wind engineering. The covariances that remain, $Cov_{nn}(\Delta x,t) = E\left[n(x_1,t)\cdot n(x_2,t)\right]$, n equals u or v, could be expressed by the variance and a covariance coefficient

$$Cov_{nn}(\Delta x) = \sigma_n^2\cdot\rho_{nn}(\Delta x) \tag{6.68}$$

The covariance coefficient is a complicated parameter which is influenced by the up-wind terrain, and should preferably be determined by full-scale measures at the construction site. However, by assuming homogenous conditions, it could according to Strømmen be approximated by

$$\rho_{nn}(\Delta x) \approx e^{\frac{-\Delta x}{{}^xL_n}} \tag{6.69}$$

The integral length scale ${}^xL_n$ could, like explained in Section 6.2.2.3, be interpreted as the size of the vortices. It equals $1/3$ and $1/4$ of ${}^yL_u$ for u and v turbulence respectively.

The procedure from here is similar to the one shown in Section 6.2.2.3. Using equations (6.64), (6.65), (6.67), (6.68) and (6.69), and expanding by $\frac{V(x)^2}{V(x)^2}$ (which allows substituting $\frac{\sigma_n^2}{V(x)^2}$ by I_n^2), it is obtained that

$$\sigma_{M_{B,z}}^2 = \left(\frac{\rho B}{2}\right)^2 \iint_{L_{\exp}} x_1\cdot x_2\cdot V(x_1)^2\cdot V(x_2)^2\cdot\left\{\left(A(x_1)\cdot A(x_2)\cdot e^{\frac{-\Delta x}{{}^xL_u}}\right)+\left(B(x_1)\cdot B(x_2)\cdot e^{\frac{-\Delta x}{{}^xL_v}}\right)\right\}dx_1dx_2 \tag{6.70}$$

where

$$\left.\begin{aligned} A(x_i) &= \left(\frac{2D\bar{C}_D}{B} I_u(x_i) \right) \\ B(x_i) &= \left(\left(\frac{DC'_D}{B} - \bar{C}_L \right) I_v(x_i) \right) \end{aligned} \right\} i = 1,2 \tag{6.71}$$

The expression for $\sigma^2_{V_{B,y}}$ is obtained by neglecting the $x_1 \cdot x_2$-term in equation (6.70).

6.3.3 Resonant Part of Cross Sectional Forces

The resonant part of the cross-sectional forces accounts for effects induced by structural motion. According to Strømmen these effects are important for structures that are soft enough to interact with the turbulent wind, which typically corresponds to eigen frequencies lower than 5 Hz. The study building has eigen frequencies far below the critical limit, and thus resonant effects need to be assessed. Like in Section 6.2.2.4, the aerodynamic mass- and stiffness properties are neglected, leaving only the aerodynamic damping to contribute. Moment and shear force for a section of the building are expressed by elementary beam theory as

$$\begin{aligned} V_y &= -EI_z r'''_y(x,t) \\ M_z &= EI_z r''_y(x,t) \end{aligned} \tag{6.72}$$

where r is the displacement of the structure, and EI_z describes bending stiffness about the z-axis. Introducing modal coordinates, a matrix $\mathbf{T}$ which holds the stiffness properties, and a matrix $\boldsymbol{\beta}$ which contains the derived modal shapes, cross sectional forces could be described as

$$\mathbf{F} = \begin{bmatrix} V_y \\ M_z \end{bmatrix} = \mathbf{T}\boldsymbol{\beta}\eta = \begin{bmatrix} -EI_z & 0 \\ 0 & EI_z \end{bmatrix} \begin{Bmatrix} \phi'''_y(x,t) \\ \phi''_y(x,t) \end{Bmatrix} \cdot \eta \tag{6.73}$$

The spectral density of the cross-sectional force vector is then given by

$$\mathbf{S}_F = \lim_{T\to\infty} \frac{1}{\pi T} [\mathbf{T}\boldsymbol{\beta} a^*_\eta] \cdot [\mathbf{T}\boldsymbol{\beta} a_\eta]^T = \mathbf{T}\boldsymbol{\beta} S_\eta \boldsymbol{\beta}^T \mathbf{T}^T \tag{6.74}$$

S_η in equation (6.74) contains both background and resonant response. According to Strømmen, the resonant part could be extracted by the following expression

$$S_{\eta_R} = \hat{H}^*_\eta(\omega) \cdot S_{\hat{Q}_R} \cdot \hat{H}^T_\eta(\omega) \tag{6.75}$$

The Frequency Response Function was described in Section 6.2.2.4, while

$$S_{\hat{Q}_R} = \frac{\iint_{L_{\exp}} \phi^T_y(x_1) \cdot S_q(\Delta x, \omega_y) \cdot \phi_y(x_2) dx_1 dx_2}{(\omega^2_y \tilde{M}_y)^2} \tag{6.76}$$

The numerator of equation (6.76) equals the expression found in equation (6.39), with

$$S_q = \left(\frac{\rho V(x) B}{2}\right)^2 \left[\left(\left(\frac{2D\bar{C}_D}{B}\right)^2 S_{uu}(\Delta x, \omega_i)\right) + \left(\left(\frac{DC'_D}{B} - \bar{C}_L\right)^2 S_{vv}(\Delta x, \omega_i)\right)\right] \tag{6.77}$$

By inserting equation (6.77) into equation (6.76), substituting $\tilde{M}_y = \tilde{m}_y \int_L \phi_y^2 dx$, and using the procedure defining the joint acceptance function in Section 6.2.2.3 plus the normalization in equation (6.53), it is found that

$$S_{\hat{Q}_R} = \frac{1}{\left(\omega_y^2 \tilde{m}_y\right)^2} \cdot \left(\frac{\rho B}{2}\right)^2 \cdot \hat{J}_y^2(\omega_y) \tag{6.78}$$

$\hat{J}_y^2(\omega_y)$ is the normalized Joint Acceptance Function evaluated at the respective eigen frequency $\omega = \omega_y$. Now combining equations (6.74), (6.75) and (6.78) the following expression for the spectral density $\mathbf{S}_F$ of the cross sectional forces is obtained

$$\mathbf{S}_F = \left(\left|\hat{H}_y(\omega)\right|^2 \cdot S_{\hat{Q}_R}\right) \cdot \left[\mathbf{T}\boldsymbol{\beta}\boldsymbol{\beta}^T\mathbf{T}^T\right] \tag{6.79}$$

The matrix product $\mathbf{T}\boldsymbol{\beta}\boldsymbol{\beta}^T\mathbf{T}^T$ results in a 2 by 2 matrix. The variance $\sigma_{F_R}^2$ is obtained through the covariance matrix, given by

$$\mathbf{Cov}_F = \int_0^\infty \mathbf{S}_F d\omega = \left[\mathbf{T}\boldsymbol{\beta}\boldsymbol{\beta}^T\mathbf{T}^T\right] \cdot S_{\hat{Q}_R} \cdot \int_0^\infty \left|\hat{H}_y(\omega)\right|^2 d\omega \tag{6.80}$$

Variances are given by the diagonal terms of $\mathbf{Cov}_F$, and by taking the square root of the diagonal terms it is obtained from (6.78), (6.79) and (6.80) that

$$\begin{bmatrix} \sigma_{V_R} \\ \sigma_{M_R} \end{bmatrix} = \frac{1}{\left(\omega_y^2 \tilde{m}_y\right)} \cdot \left(\frac{\rho B}{2}\right) \cdot \hat{J}_y(\omega_y) \cdot \left[\int_0^\infty \left|\hat{H}_i(\omega)\right|^2 d\omega\right]^{1/2} \begin{bmatrix} \left|\phi_y''' EI_z\right| \\ \left|\phi_y'' EI_z\right| \end{bmatrix} \tag{6.81}$$

The frequency response function is given in Section 6.2.2.4. According to Strømmen, integrating $\hat{H}_y(\omega)$ over the entire frequency domain gives

$$\int_0^\infty \left|\hat{H}_y(\omega)\right|^2 d\omega = \frac{\pi \omega_y}{4(\zeta - \zeta_{ae})} \tag{6.82}$$

Substituting (6.82) into (6.81) and rewriting some of the terms, it is found that

$$\begin{bmatrix} \sigma_{V_R} \\ \sigma_{M_R} \end{bmatrix} = \frac{\rho B}{4\tilde{m}_y \omega_y^2} \cdot \hat{J}_y(\omega_y) \cdot \left(\frac{\pi \omega_y}{(\zeta - \zeta_{ae})} \right)^{1/2} \cdot \begin{bmatrix} \left| \phi_y''' EI_z \right| \\ \left| \phi_y'' EI_z \right| \end{bmatrix} \tag{6.83}$$

7 Force Estimation by NS-EN 1991-1-4

The wind action standard [11] provides a method suitable for calculation of cross sectional forces, namely design by force coefficients. In the following, the design procedure has been used to calculate base shear and base moment for a structure similar to Lerkendal Hotel; a 75 meter high tower with a 45 times 15 meter cross section. The calculated quantities are of little use in a design situation. However, the main purpose of the calculations is to compare the values obtained by design codes to the ones obtained using aerodynamic theory.

When using design codes, load combinations from NS-EN 1990 [14] has to be utilized. Loads are calculated for the ultimate limit state. In the calculations, wind action is the dominating variable load. According to §6.4.3.2 and Table NA.A1.3.1 the wind load should be multiplied by 1.5 when cross sectional forces are obtained.

7.1 Design by Force Coefficients

The force coefficient method is given by §5.3 in the standard. In the following, the procedure will be summarized. Calculations are done in Excel, and details are given in Appendix 4. The force on a structure induced by wind is given by §5.3(2) in the standard as the sum of forces acting on all structural parts.

$$F_w = c_s c_d \cdot \sum_{parts} c_f \cdot q_p\left(z_e\right) \cdot A_{ref} \tag{7.1}$$

Calculations are performed for wind loading acting on both the short and the long side of the building, like shown in Figure 7.1. The Structural Factor $c_s c_d$ is calculated for the entire structure, while the other quantities are calculated for each structural part.

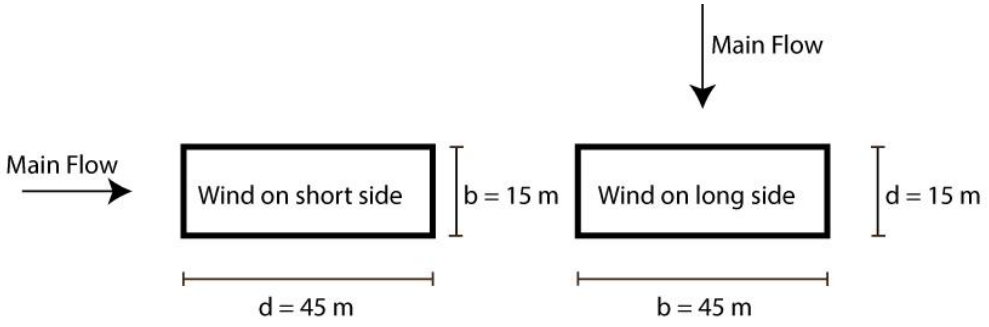

Figure 7.1: Wind load scenarios used in Eurocode calculations

7.1.1 Structural Factor $c_s c_d$

The structural factor is given by §6.1(1). It is calculated for a reference height, and contains information regarding the turbulence intensity of the wind field, pressure variation on the

structural surface, and resonance between wind turbulence and structural motion. Equation 6.1 from the standard gives

$$c_s c_d = \frac{1+2\cdot k_p \cdot I_v(z_s)\cdot\sqrt{B^2+R^2}}{1+7\cdot I_v(z_s)} \tag{7.2}$$

The turbulence intensity I_v and the resonance factor R^2 have been found in Appendix 2. The reference height z_s is $H\cdot 0.6 = 45\,m$ given by Figure 6.1 in the standard. The peak factor k_p is calculated from Appendix B in the standard. Further details on k_p are given in Section 8.3. The background factor B^2 is calculated by the method given by Appendix B, §B.1:

$$B^2 = \frac{1}{1+0.9\cdot\left(\frac{b+h}{L(z_s)}\right)^{0.63}} \tag{7.3}$$

The $L(z_s)$ factor has been calculated in Appendix 2. The eigen frequency estimate obtained from appendix F in the standard is used for both directions when calculating k_p. The obtained quantities and the structural factors are shown in Table 7.1.

Parameter	**Wind load on Long side**	**Wind Load on Short Side**
$I_v(z_s)$	0.199	0.199
R^2	0.083	0.202
B^2	0.527	0.572
k_p	3.32	3.42
$c_s c_d$	**0.849**	**0.918**

Table 7.1: Structural factors and relevant calculation parameters

7.1.2 The Force Coefficient c_f

c_f for sharp edged structures is given by §7.7 in the standard as the product of the rectangular force coefficient $c_{f,0}$ and an end-effect factor ψ_λ. It is calculated for each structural part. The factors $c_{f,0}$ and ψ_λ are found graphically using §7.6(1) and §7.13(2) respectively. Procedures are described in detail in Section 8.4.1.

7.1.3 Peak Velocity Pressure $q_p(z_e)$

The peak velocity pressure is given by §4.5. It is a function of the turbulence intensity and the mean wind velocity, and is calculated for a height z_e by

$$q_p\left(z_e\right)=\left[1+7\cdot I_v\left(z_e\right)\right]\cdot\frac{1}{2}\cdot\rho\cdot V_m^2\left(z_e\right) \tag{7.4}$$

As could be understood from equation (7.1), q_p has to be calculated for several heights z_e to obtain an accurate representation of the wind loading. The distribution of q_p is determined by §7.2.2 in the standard, and the relevant cases are shown in Figure 7.2 below.

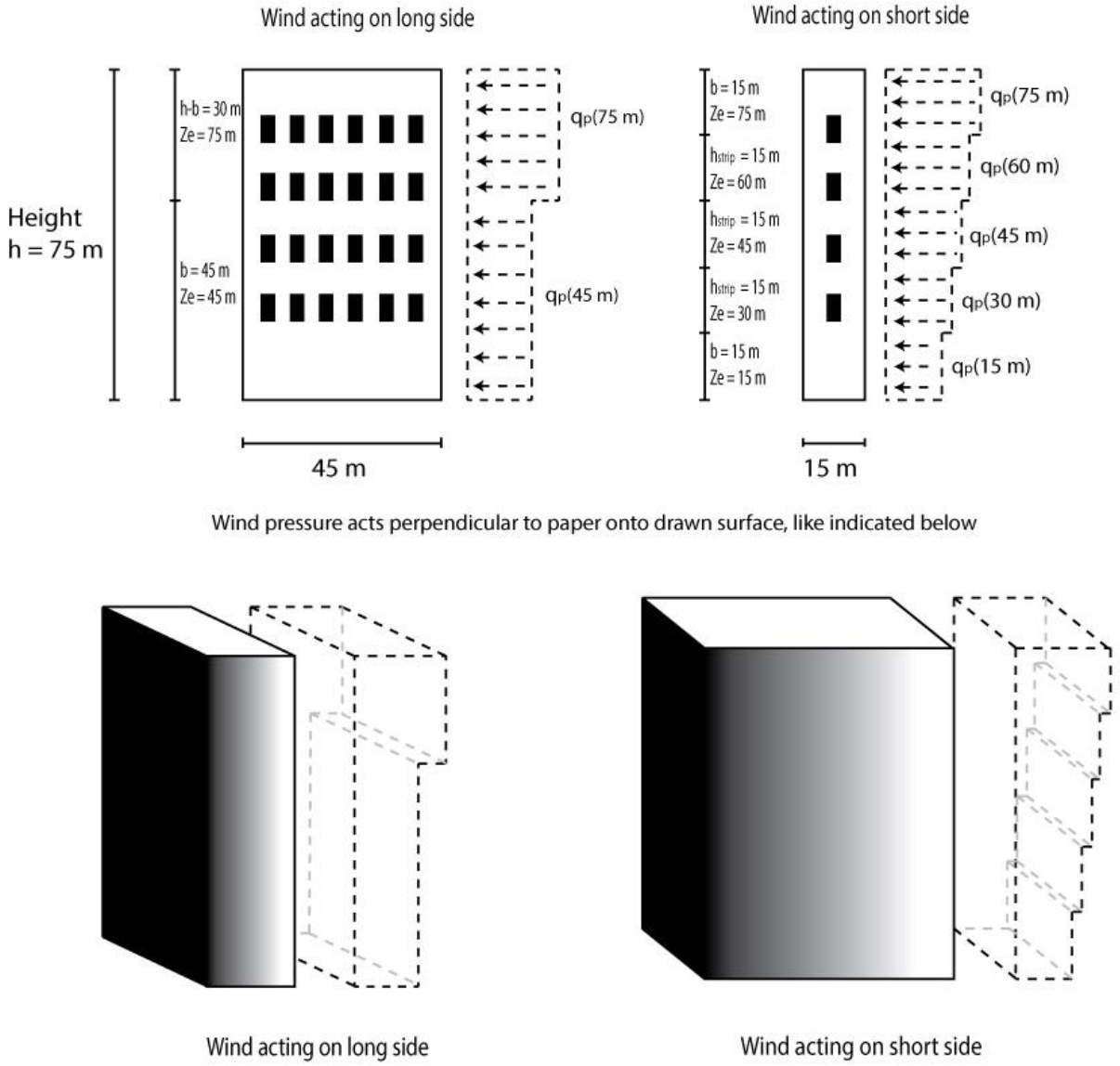

Figure 7.2: Velocity pressure distributions used in calculations

The discretization of the peak velocity pressure used for wind against the short side is chosen randomly, since §7.2.2 does not give any specifications regarding the size of h_{strip}.

7.1.4 Forces Obtained by the Force Coefficient Method

As mentioned above, calculations are performed in Excel, using formulas (7.1), (7.4) and methods accounted for above. Cross sectional forces are found by basic mechanics. Details are shown in Appendix 4. Table 7.2 quickly summarizes forces acting on each structural part, together with the resulting base shear and base moment for each wind direction.

Wind acting on long side		
	Force F_w [kN]	**Moment Contribution [kNm]**
$z_e = 45m$	4 130	92 980
$z_e = 75m$	3 110	186 810
Base Shear | Base Moment	**7 250**	**279 790**
Wind acting on short side		
	Force F_w [kN]	**Moment Contribution [kNm]**
$z_e = 15m$	222	1 660
$z_e = 30m$	277	6 240
$z_e = 45m$	312	11 710
$z_e = 60m$	338	17 750
$z_e = 75m$	359	24 220
Base Shear | Base Moment	**1 508**	**61 580**

Table 7.2: Forces, base shear and base moment obtained by the Force coefficient method

As could be seen from Table 7.2, wind acting on the long side of the building generates cross sectional forces almost 5 times higher than wind acting on the short side. One should expect a linear relation between loaded area and cross sectional load, which is not the case here. Referring to Appendix 4, the effect is caused by the force coefficient c_f, which is about 40 % higher for loading on the long side. The difference in c_f has to do with the shape of the structure. In addition, the average peak velocity pressure on the lower 45 meters of the building is about 15 % higher for loading on the long side. This effect is caused by the discretization from §7.2.2.

8 MATLAB Input Parameters

Before the MATLAB calculations are preformed, several input parameters needs to be determined. Natural frequencies, modal shapes and damping have already been accounted for in Sections 3.2 and 5.5. This section explains other vital input parameters, and how they are obtained.

8.1 Frequency Spectrum and Height Coordinate

Starting with the frequency spectrum, it is seen from equation (6.51) that obtaining σ_{r_y} demands integration over the entire frequency spectrum. Thus, the frequency vector should cover the interval $|0,\infty\rangle$. However, the integrand contains the Joint Acceptance Function and the Frequency Response Function. Both of these functions decays as the frequency gets high. An interval of $\omega = [0.001 \rightarrow 4\pi]$ rad/s includes both of the considered natural frequencies, and has been found sufficient to obtain the majority of response. The start value has been set to 0.001 to avoid dividing by zero. It goes without saying that the x interval contains the whole height of the tower, $x = [0 \rightarrow 75]$ m

To ensure accurate numerical integration, the frequency and x-vectors needs to contain enough points. The x and ω intervals are divided into 551 points. There are no specific reasons for this choice of subdivision. Calculations has been performed for various numbers of points between 200 and 2000 with fairly similar results, and 551 points was a result of weighting accuracy against computation time. Using the intervals mentioned above results in step sizes of $\Delta\omega \simeq 0.02$ rad/sec and $\Delta x \simeq 0.14$ m for frequency and tower height coordinate respectively.

For the simplicity of programming, the modal shape vectors are adjusted to have the same number of points as the x-and ω vectors. This is done by linear partition of the modal vectors from SAP2000, which originally contained 22 points. The lower 21 values are collected from nodes separated by intervals of 3.4 meters (which equals the floor height). Because the skybar at the top of the building reaches over two floors, the upper interval is twice as long. To get the same spacing in x-direction for all points, the 20 lowest intervals are divided into 25, while the upper interval is divided into 50. The result is modal vectors containing 551 points instead of 22.

8.2 Wind Velocity and Turbulence Intensity

The mean wind velocity $V(x)$ depends upon location, surrounding terrain and height above ground. It is also dependant on return period, with 50 years being the default period from Eurocode. NS-EN 1991-1-4 [11] Table NA.4(901.1) in the standard provides base wind velocities for all municipalities in Norway. For Trondheim the base value is $v_b = 26$ m/s. §4.2 and §4.3 accounts for seasonal, directional and terrain dependant variations. Both seasonal

and directional coefficients are set to 1.0. The mentioned paragraphs combined then gives the following expression for the mean wind velocity as a function of height x

$$V_m(x) = 0.19 \cdot \left(\frac{z_0}{z_{0,II}} \right)^{0.07} \cdot \ln\left(\frac{z}{z_0} \right) \cdot c_0(z) \cdot v_b \begin{cases} z = z_{\min} \text{ for } z \le z_{\min} \\ z = x \text{ for } z > z_{\min} \end{cases} \tag{8.1}$$

$c_0(z)$ is a terrain dependent factor. It is set to 1.0 because the terrain surrounding the construction site is relatively flat. The remaining unknowns z_0, $z_{0,II}$ and $z_{\min}$ from equation (8.1) are defined by choosing a terrain category. There are five categories, presented in Table NA.4.1 in the standard, and shown graphically in Appendix A1. Lerkendal Hotel is significantly higher than any of the surrounding structures. As a result, the best suited terrain category would be category III.

The turbulence intensity is given by §4.4. It describes the turbulence component of the wind flow for a given height. It is given by

$$I_v(x) = \frac{0.19 \cdot \left(\frac{z_0}{z_{0,II}} \right)^{0.07} \cdot k_l \cdot v_b}{V_m(x)} \tag{8.2}$$

The factor k_l is a turbulence factor, which is set to 1.0. The numerator of equation (8.2) describes the standard deviation of the wind flow, like indicated in equation (6.40).

8.3 Peak Factor k_p

The peak factor k_p is a way of describing the influence of a standard deviation over a given time span. It depends on whether the response is narrow- or broad banded. For instance, a process described by a single harmonic would have a theoretical peak factor $k_p = \sqrt{2}$ [1]. Generally, the peak factor takes on values between 2 and 5. Details regarding k_p can be found for example in Dyrbye & Hansen [2]. For a Gaussian process, Dyrbye & Hansen gives the following expression for the peak factor:

$$k_p = \sqrt{2 \cdot \ln(\nu T)} + \frac{\gamma}{\sqrt{2 \cdot \ln(\nu T)}} \tag{8.3}$$

ν is the zero-upcrossing frequency while T is the relevant time span. γ is Euler's constant, equal to 0.557.

Although the relevant formulas for calculating ν is given by Dyrbye & Hansen, the approach given in NS-EN 1991-1-4 appendix B is adopted. The basis is quite similar to the one presented by Dyrbye & Hansen, but several of the design code calculations have already been done in Section 7.1.1. The formula for calculating k_p in §B.2(3) is similar to equation (8.3),

except for γ, which is set to 0.6. T is set to 600 seconds (10 minutes). The only parameter needed is the zero-upcrossing frequency, which is given as

$$\nu = n_{1,x}\sqrt{\frac{R^2}{R^2 + B^2}} \tag{8.4}$$

The resonance factor R^2 and the structural factor B^2 has been calculated in Section 7.1.1 for both directions. The first eigen frequency estimate $n_{1,x} = 0.613[Hz]$ is found from Appendix F in the standard. It could be argued that the natural frequencies found in SAP 2000 should be used to calculate the peak factor. However, since the peak factor is estimated from the standard, using the standard estimate for eigen frequency would be the most consistent option. The peak factors obtained for the assumptions above have already been calculated in Section 7.1.1, and they are given in Table 7.1.

8.4 Drag Coefficients

As can be seen in Section 6.2.2.2, three drag and lift coefficients are needed; $\bar{C}_D$, C'_D and $\bar{C}_L$. Estimating these quantities proved to be difficult. Usually, they are determined from the drag and lift forces on a model obtained by wind tunnel experiments. Wind tunnel testing was not possible to include in this thesis, and thus the coefficients had to be determined through literature or by estimates.

In literature, it is common to refer to the force coefficient C_f , which equals the drag coefficient C_D when the force acts parallel to wind, and the lift factor C_L when force acts perpendicular to wind. The coefficients will normally vary over the height of the structure, but this effect will be neglected here.

Calculations in this thesis are performed for wind acting perpendicular to the sides of the structure, e.g. only on one side at a time. With this in mind, there is no reason that wind forces should have a component perpendicular to the wind flow. As a result of this, the lift coefficient $\bar{C}_L$ is assumed equal to zero. After consulting Einar Strømmen [24], it has been decided that the drag slope coefficient C'_D could be assumed equal to zero. In other words, only the average drag coefficient $\bar{C}_D$ needs to be estimated.

8.4.1 Eurocode Estimate for C_f

NS-EN 1991-1-4 [11] provides an estimate for the force coefficient C_f . §7.6 states that

$$c_f = c_{f,0} \cdot \psi_r \cdot \psi_\lambda \tag{8.5}$$

The $c_{f,0}$ factor describes rectangular cross sections with sharp edges, while the ψ -factors account for round corners and slenderness of the structure. The structure at hand has sharp corners, thus only $c_{f,0}$ and ψ_λ needs to be taken into account. Table 8.1 shows all used factors

found from §7.6 and §7.13. The solidity ratio from §7.13(3) is assumed to be 1.0, because all surfaces are solid. Assuming a rectangular 45 times 15 meter cross section, the following is obtained:

Wind direction	**Depth/Width**	**Slenderness λ**	**Slenderness factor ψ_λ**	**Rect. factor $c_{f,0}$**	**Force coeff. C_f**
On Short Side (Mode 1)	$\frac{d}{b}=\frac{45}{15}=3.0$	$1.4\frac{h}{b}=7.0$	0.68	1.3	**0.88**
On Long Side (Mode 2)	$\frac{d}{b}=\frac{15}{45}=0.33$	$1.4\frac{h}{b}=2.33$	0.63	2.1	**1.32**

Table 8.1: Estimated drag coefficients from NS-EN 1991-1-4

The force coefficients calculated here represent forces parallel to wind, and thus they are equal to the average drag coefficient $\bar{C}_d$.

8.4.2 Other Estimates in Literature

As mentioned above, drag and lift coefficients are determined by wind tunnel experiments. Therefore, there are few general values provided in literature. Lin et.al [25] has studied several rectangular tower models to investigate the force coefficients. Considering height variation, it is found that for a width ($\perp$ to wind flow) to depth ratio d/b at about 0.33 (wind against the long side), the drag coefficient lies in the range 1.0 - 1.4. For d/b at about 3 (wind against the short side), the drag coefficient obtains values between 0.6 and 1.0. Looking at the values found in Table 8.1, it is clear that the Eurocode estimates for the drag coefficient corresponds well to the ones found by Lin.

8.5 Mass Estimate

Calculations demand for a normalized modal mass, $\tilde{m}$. The easiest way to obtain $\tilde{m}$ is to estimate the mass for each floor and create a mass matrix. Then the modal mass matrix could easily be calculated using the modal shapes, and finally $\frac{\tilde{M}}{\int_L \phi^2 dx}=\tilde{m}$. Since all floors (except the ground floor and the top floor) are equally built, it is assumed that all floors have the same mass. This mass will be estimated in the following.

The mass estimate is done by considering the blueprints of the 5th floor (see Appendix 8). The following is included:

- Walls included in the load carrying system
- Slabs
- Bathroom modules
- Live load for hotel

- Applied dead load on floors and facades

Area of walls and slabs are estimates from the blueprints. The weight of concrete is assumed to be 25 kN/m^3. Bathroom modules weigh about 1500 kg each [26]. On an average floor there are 21 rooms, containing one bathroom module each. NS-EN 1991-1-1 Tables NA.6.1 and NA.6.2 indicates a live load of 2 kN/m^2 for hotel rooms and 5 kN/m^2 for hallways [27]. Norconsult have provided applied dead loads for floors and facades of 1 kN/m^2 [28].

Another aspect of the calculations is load factors given by NS-EN 1990 [14]. In the forthcoming calculations, both cross sectional forces, accelerations and displacements are considered, i.e. both ultimate limit state (ULS) and service limit state (SLS). Load combinations are found using tables NA.A1.1 and NA.A1.2 together with §6.4.3.2 and §6.5.3. Looking at equations (6.52) and (6.83) describing the standard deviations of displacements and cross sectional forces, it is clear that an increased mass would decrease the response quantities. A high mass will therefore be favorable to the structural response. To be conservative, load coefficients from table NA.A1.2 have been chosen to obtain the lowest possible mass. This entails that variable loads are neglected for the ULS.

From the assumptions made above, the mass per floor has been estimated to 624.360 kg per floor for ULS, and 765.600 kg per floor for SLS. Calculations are shown in Appendix 5.

8.6 Estimation of EI and GA

To calculate both force and displacement quantities, the bending stiffness EI about both main axes of the structure is required, together with the shear stiffness GA. Since the structure is treated as a cantilevered beam, EI should be a scalar. The simplest way to estimate the stiffness when the structure at hand is treated as a beam, is simply to calculate the 2nd moment of inertia for the cross section, letting all vertical load carrying elements provide stiffness contributions. Young's Modulus could be found for instance from the concrete standard NS-EN 1992-1-1.

8.6.1 2nd Moment of Inertia

This is a basic quantity within mechanics, and could easily be calculated by hand. However, given the complexity of the cross section. hand calculations would be tedious. The computer program CrossX [29], developed at NTNU, provide the opportunity to model a cross section graphically. The program calculates all cross sectional properties.

The cross section was modeled as thin walled. CrossX demands that all parts of the cross section must be connected. This is not the case for the structure at hand. The solution chosen was to connect the load carrying elements by VOID elements, which does not provide any additional stiffness. VOID elements are meant to replace empty space in the program [29]. The basis used for the CrossX cross sectional model is shown in Figure 8.1, with color codes presented in Table 8.2.

Wall Thickness	Color used in Figure 8.1
200 mm	
250 mm	
300 mm	
VOID elements	

Table 8.2: Color codes used in cross sectional sketch

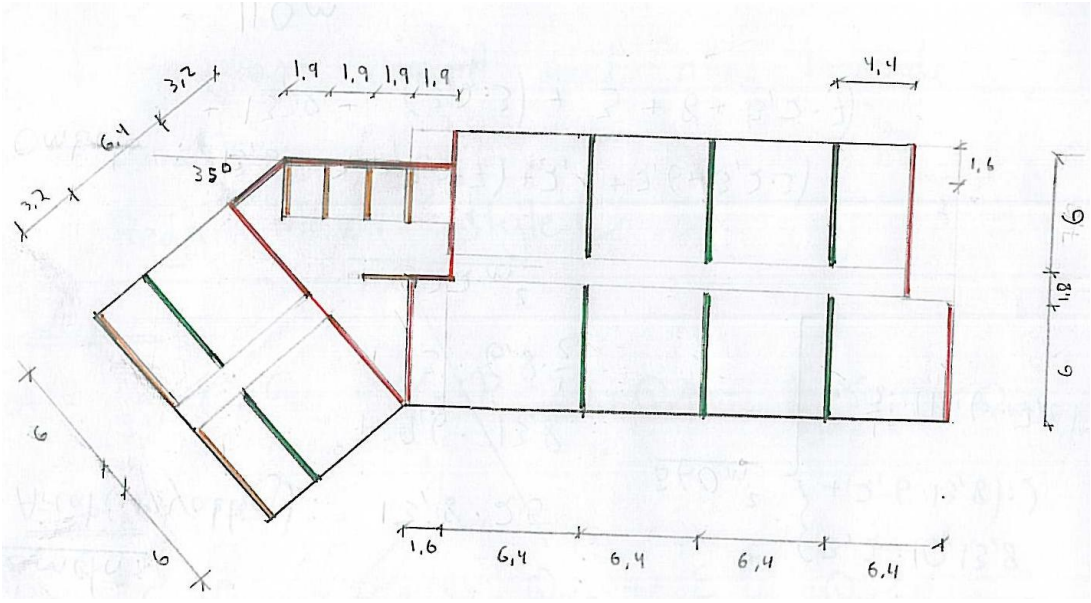

Figure 8.1: Basis for cross sectional estimation in CrossX

CrossX provides I both with respect to major axes and reference axes. Since the modal displacements for modes 1 and 2 consists of movement in the longitudinal and transversal directions respectively, I has been obtained with respect to the reference axes displayed in Figure 8.2, which shows a screenshot of the CrossX model.

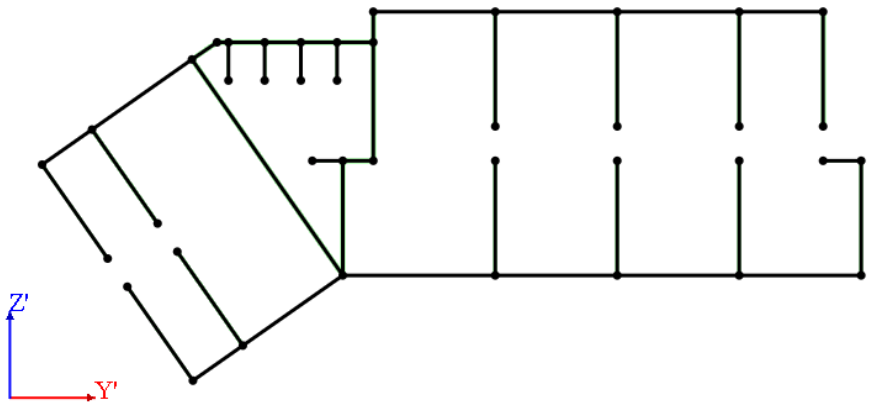

Figure 8.2: Cross sectional model from CrossX

2nd Moment of Inertia was found to be $I_{y'} = 6.99 \cdot 10^{14}\ mm^4$ for bending about the Y' axis in Figure 8.2, and $I_{z'} = 4.94 \cdot 10^{15}\ mm^4$ for bending about the Z' axis. The cross section has the highest bending stiffness about the Z' axis. Although there are few elements providing high bending stiffness about the Z' axis, the Huygens-Steiner Theorem adds significant amounts of stiffness because of the extent of the cross section.

8.6.2 Young's Modulus

One important aspect when deciding on a Young's modulus, is whether the concrete will crack or not. The study building will, as could be understood from Section 8.5, have a tremendous total mass. Therefore, the lower concrete elements will be exposed to vast pressure. In addition, wind loading by itself will not suffice to create cracks in the concrete. As a result of the above, the concrete is assumed uncracked.

In addition to cracking, the reinforcement will increase Young's modulus by some amount. Since there are given no indications regarding the reinforcement, an estimate has to be made. Rules for minimum reinforcement of concrete walls are found from §NA.9.6.2 and §NA.9.6.3 in the concrete standard NS-EN 1992-1-1 [30]. The paragraphs states that vertical and horizontal reinforcement in total should equal no less than $A_S = 0.0025 \cdot A_C$, where A_C is the concrete area. Since the walls carry significant load, it is assumed that $A_S = 0.01 \cdot A_C$. It is given in the blueprints that the concrete quality is B 30 for most of the structure, while the reinforcement is given as B500NC. The two have Young's modules of 33 000 MPa and 200 000 MPa respectively. It could then be approximated that

$$E_{tot} = 0.99 \cdot E_{cm} + 0.01 \cdot E_S \simeq 34700 MPa .$$

The total bending stiffness is given in Table 8.3, with respect to the axes given in Figure 8.2.

Axis	Bending Stiffness, [Nmm^2]
$EI_{Y'}$ (Stiffness for loading on long the side)	$2.425 \cdot 10^{19}$ $(= 2.425 \cdot 10^{13}\ Nm^2)$
$EI_{Z'}$ (Stiffness for loading on the short side)	$1.715 \cdot 10^{20}$ $(= 1.715 \cdot 10^{14}\ Nm^2)$

Table 8.3: Bending stiffness about principle axes

8.6.3 Shear Stiffness GA

When it comes to the shear stiffness, the calculations are easier. According to the concrete standard NS-EN 1992-1-1 §3.1.4(6), the Poisson ratio for concrete is approximately 0.2. Again assuming an uncracked cross section, the Shear Modulus G is found from basic theory of elasticity

$$G = \frac{E}{2(1+\nu)} = \frac{34700}{2 \cdot 1.2} \simeq 14500 \ [MPa] \tag{8.6}$$

According to CrossX, the total area of the cross section is $3.2 \cdot 10^7$ mm^2, which gives a total shear stiffness $GA = 14500 \cdot 3.2 \cdot 10^7 = 4.62 \cdot 10^{11}$ N.

8.7 The Shear Factor k

Section 6.2.1 shows how the static displacements are calculated using the unit load method. To calculate the shear-dependent part, the shear factor k is needed. This factor in particular carries a high amount of uncertainty. It describes the effect that the cross sectional shape has on the distribution of shear stresses. Evaluating it by hand for the given cross section is not a straightforward operation. The program CrossX calculates k, but the fact that all cross sectional parts are not really connected makes these results unreliable.

The solution finally chosen is based on estimation formulas given by Clausen [31]. He states that the shear factor k for hollow core sections and IPE profiles could be estimated by

$$k_i \approx \frac{A_{tot}}{A_{web}} \tag{8.7}$$

The area of the webs is the area where the majority of the shear stresses are located. Using the total area provided by CrossX, and making a quick estimate of the web area for both directions using blueprints (Appendix 8), the shear factors shown in Table 8.4 are obtained.

	Total area A_{tot} [mm^2]	Web area A_{web} [mm^2]	Shear factor k
Load on short side	$3.6 \cdot 10^7$	$5.8 \cdot 10^6$	**5.52**
Load on long side	$3.6 \cdot 10^7$	$2.62 \cdot 10^7$	**1.22**

Table 8.4: Shear factor for principle directions

These factors are rough estimates. Nonetheless, they give an indication of what kind of static displacement that is brought on by shear strain energy.

8.8 Derivatives of modal shapes

As shown in Section 6.3.3, the resonant part of the cross sectional forces contains the 2nd and 3rd derivatives of the considered mode shape, evaluated at the base $(x = 0)$. Finding these derivatives has proven to be problematic. Normally, these quantities should be obtained by derivation of the mode shapes that were found from SAP2000. However, these modal shapes contain a low number of points, which makes derivation inaccurate. Although extra points are added in MATLAB like described in Section 8.1, these points are distributed linearly, thus the 2nd and 3rd derivatives are equal to zero.

To overcome the problem above, the meshing in SAP2000 was refined to get a modal displacement output containing a higher amount of points. Refining of the mesh near $x = 0$ revealed that the curvature of the modal displacement curve increased when the spacing between points decreased. Obtaining converged values for ϕ'' and ϕ''' from the SAP2000 output was therefore impossible. The reason for this behavior is unknown. A likely explanation is that the fixed boundary condition at $x = 0$ in the SAP2000 model results in an infinite curvature in the FEM analysis.

After considering several other options for obtaining ϕ'' and ϕ''', theory for cantilevered beams was chosen. According to Strømmen [32], a general solution for the shape function of a cantilevered beam could be obtained from

$$\phi(\hat{x}) = a_1 \sin(\lambda\hat{x}) + a_2 \cos(\lambda\hat{x}) + a_3 \sinh(\lambda\hat{x}) + a_4 \cosh(\lambda\hat{x}) \tag{8.8}$$

where $\hat{x}$ is the normalized height coordinate (dimensionless) and λ is a normalized wave length obtained from cross sectional data of the given beam. For a cantilevered beam, both the displacement and angle at $x = 0$ are equal to zero. In addition, the moment and shear force at $x = L$ are equal to zero. Using these boundary conditions and equation (8.8), the displacement function for a cantilevered beam is obtained

$$\phi_n(\hat{x}) = \sin(\lambda_n\hat{x}) - \sinh(\lambda_n\hat{x}) + \frac{\sin(\lambda_n) + \sinh(\lambda_n)}{\cos(\lambda_n) + \cosh(\lambda_n)}\left[\cos(\lambda_n\hat{x}) - \cosh(\lambda_n\hat{x})\right] \tag{8.9}$$

From the differential equation of dynamic equilibrium, it is found that

$$\begin{aligned} \omega_{z,n} &= \lambda_n^2 \sqrt{\frac{EI_y}{m_z L^4}} \\ \rightarrow \lambda_n &= \sqrt{\omega_{z,n}} \cdot \sqrt[4]{\frac{m_z L^4}{EI_y}} \end{aligned} \tag{8.10}$$

It is seen from equation (8.10) that λ_n for mode n could be obtained from known mass and stiffness properties of the structure. Using Wolfram|Alpha [33], ϕ_n'' and ϕ_n''' are obtained as

$$\begin{aligned} \phi_n''(\hat{x}) &= \lambda_n^2(-\sin(\lambda_n\hat{x}) - \sinh(\lambda_n\hat{x})) + \frac{\sin(\lambda_n) + \sinh(\lambda_n)}{\cos(\lambda_n) + \cosh(\lambda_n)}\left[\lambda_n^2(-\cos(\lambda_n\hat{x}) - \cosh(\lambda_n\hat{x}))\right] \\ \phi_n'''(\hat{x}) &= \lambda_n^3(-\cos(\lambda_n\hat{x}) - \cosh(\lambda_n\hat{x})) + \frac{\sin(\lambda_n) + \sinh(\lambda_n)}{\cos(\lambda_n) + \cosh(\lambda_n)}\left[\lambda_n^3(\sin(\lambda_n\hat{x}) - \sinh(\lambda_n\hat{x}))\right] \end{aligned} \tag{8.11}$$

The formulas above are valid for a normalized $\hat{x}$, spanning from 0 to 1. In other words, the real x value is given by $x = \hat{x} \cdot L$. This influences the derivatives. Given that $dx = d\hat{x} \cdot L$, it is obtained that

$$\frac{d\phi}{dx}\cdot\frac{d\hat{x}}{d\hat{x}}=\frac{d\phi}{d\hat{x}}\cdot\frac{d\hat{x}}{dx}=\frac{d\phi}{d\hat{x}}\cdot\frac{1}{L} \tag{8.12}$$

And, correspondingly

$$\begin{aligned}\frac{d^2\phi}{dx^2}&=\frac{d^2\phi}{d\hat{x}^2}\cdot\frac{1}{L^2}\\ \frac{d^3\phi}{dx^3}&=\frac{d^3\phi}{d\hat{x}^3}\cdot\frac{1}{L^3}\end{aligned} \tag{8.13}$$

Using the above, and evaluating the two derivatives from equation (8.11) at $x=0$, it is obtained that

$$\begin{aligned}\phi_n''(x)&=\frac{1}{L^2}\cdot\frac{\sin(\lambda_n)+\sinh(\lambda_n)}{\cos(\lambda_n)+\cosh(\lambda_n)}\left[\lambda_n^2(-2)\right]\\ \phi_n'''(x)&=\frac{1}{L^3}\cdot\lambda_n^3(-2)\end{aligned} \tag{8.14}$$

Table 8.5 shows the mass and stiffness properties for modes 1 and 2 (gathered from sections 8.5 and 8.6.2), and the corresponding λ_n-values and derivatives ϕ_n'' and ϕ_n''' calculated from equations (8.10) and (8.14). The length L equals 75 meters. The application of the derivatives is calculation of cross sectional forces, and therefore the ULS mass is assumed.

Mode #	ω_n [rad/s]	EI_y [Nm^2]	m_z [kg/m]	λ_n	ϕ_n''	ϕ_n'''
1	3.75	$1.715\cdot10^{14}$	183 640	0.830	$\mathbf{9.77\cdot10^{-5}}$	$\mathbf{2.71\cdot10^{-6}}$
2	6.71	$2.425\cdot10^{13}$	183 640	1.812	$\mathbf{8.49\cdot10^{-4}}$	$\mathbf{2.82\cdot10^{-5}}$

Table 8.5: Modal shape derivatives and key parameters from the calculation

9 Results from MATLAB Calculations

MATLAB calculations have been performed using the theoretical basis presented in Section 6. Input values are presented in Sections 3.2, 5.5 and 8. All the used MATLAB scripts and functions are shown in Appendix 6, and additional MATLAB output is shown in Appendix 7.

The MATLAB program uses a main script TotalResponse.m. This script calls other scripts and functions which performs calculations. It then provides output that describes all relevant response parameters of the structure. Although an effort has been made to make the program as general as possible, several special considerations has been made to fit the given structure and the available input data. As mentioned earlier, single component response has been calculated for modes 1 and 2 separately. Response and forces referred to as Mode 1 values describes results for wind loading against the short side of the building, which excites the first structural mode. Similarly, response and forces referred to as Mode 2 values describes results for wind loading against the long side of the building, which excites the second mode.

9.1 Wind Field

The wind field specifics have been given in Section 8.2. The script Input.m calculates the mean wind velocity and the turbulence intensity as a function of height above ground, terrain category and return period. Both wind velocity and turbulence intensity are independent of structural properties. Figure 9.1 shows the wind field as a function of height.

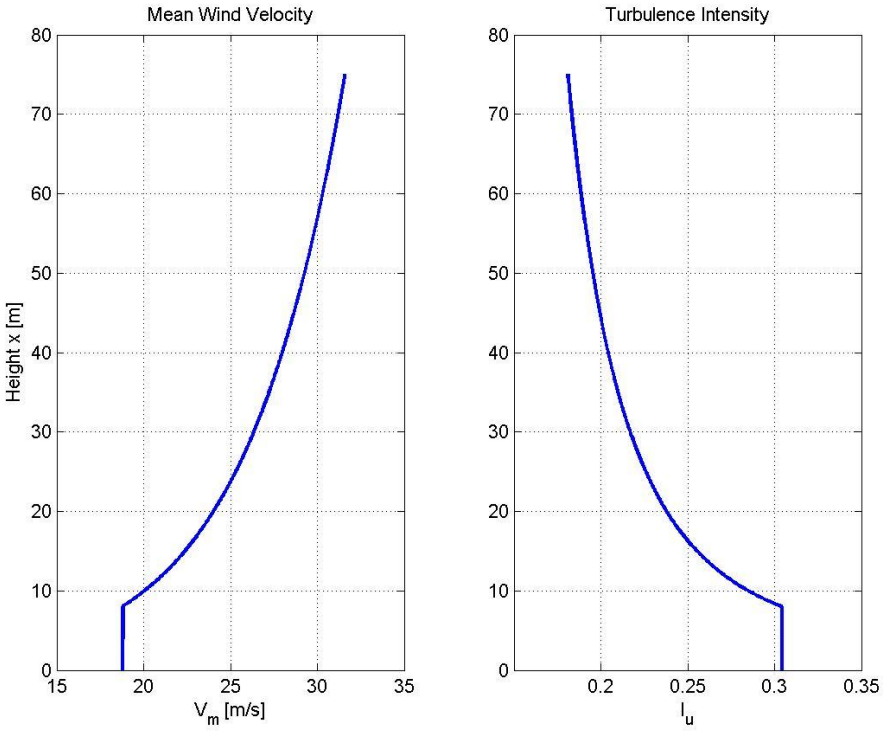

Figure 9.1: Wind field properties for Trondheim

As Figure 9.1 shows, the wind velocity increases from about 18 m/s at ground level to almost 32 m/s at the tower top. As mentioned earlier, the basic wind velocity corresponds to a 50 year return period wind. 32 m/s equals a violent storm on the Beaufort-scale [34].

The turbulence intensity decreases with height. The wind field will fluctuate near ground level, and be dominated by a steady flow further up.

9.2 Frequency Response Function

The next quantity to be obtained is the FRF, calculated by the function FrequencyResponse.m. The FRF includes imaginary terms, but only its absolute value is used within the calculations. FRF describes how the structure reacts to different excitation frequencies. When the excitation frequency matches a natural frequency of the structure, the FRF peaks. This effect is known as resonance. Figure 9.2 shows the FRF for modes 1 and 2.

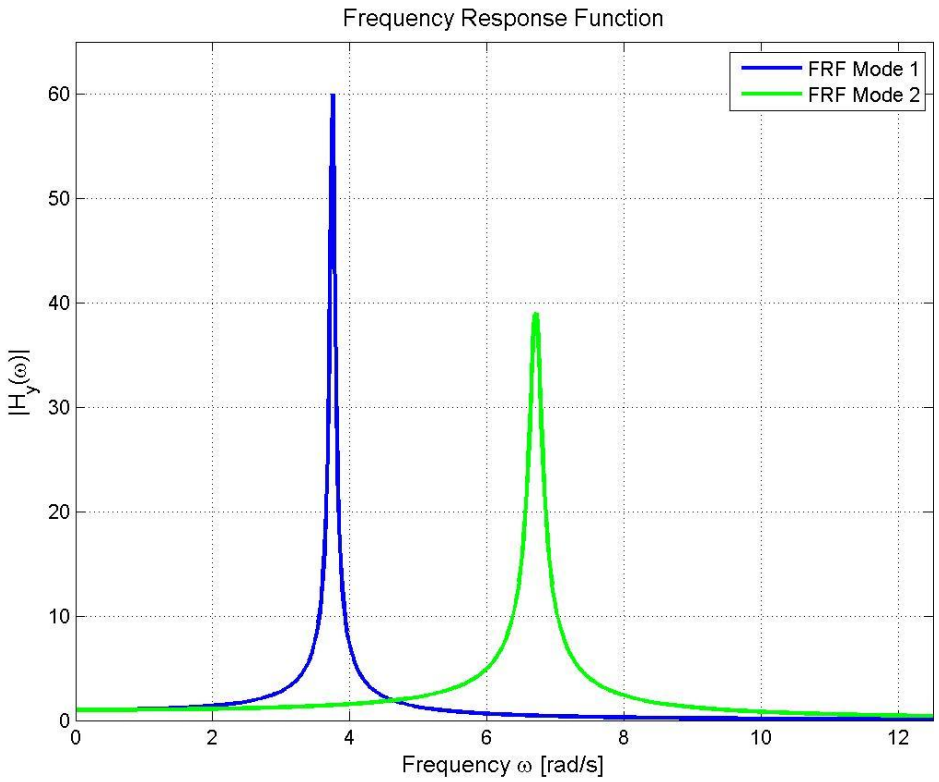

Figure 9.2: Frequency response function for modes 1 and 2

As the figure above clearly shows, the FRF peaks at the eigen frequencies (3.7 and 6.7 rad/s for modes 1 and 2 respectively). For both modes, the FRF approaches zero for high frequencies. It is noted that the maximal value of the FRF could be approximated as $\frac{1}{2\zeta}$ (see equation (6.49) with $\omega = \omega_i$). Using total damping values (given in Table 11.2), it is found

that $\left|\hat{H}_1\right|_{\max} = \frac{1}{2 \cdot 0.0083} = 60.2$ and $\left|\hat{H}_2\right|_{\max} = \frac{1}{2 \cdot 0.0127} = 39.4$, which confirms the results shown in Figure 9.2.

9.3 Joint Acceptance Function

The Joint Acceptance Function, calculated by Jointacceptance.m, is somewhat more complex than the FRF. Initially, the Kaimal spectral density (see Section 6.2.2.3) is obtained. This quantity is a function of frequency, and it is calculated for both *u* and *v* turbulence. Figure 9.3 shows the *u*-component Kaimal spectral density multiplied by the frequency of Mode 1.

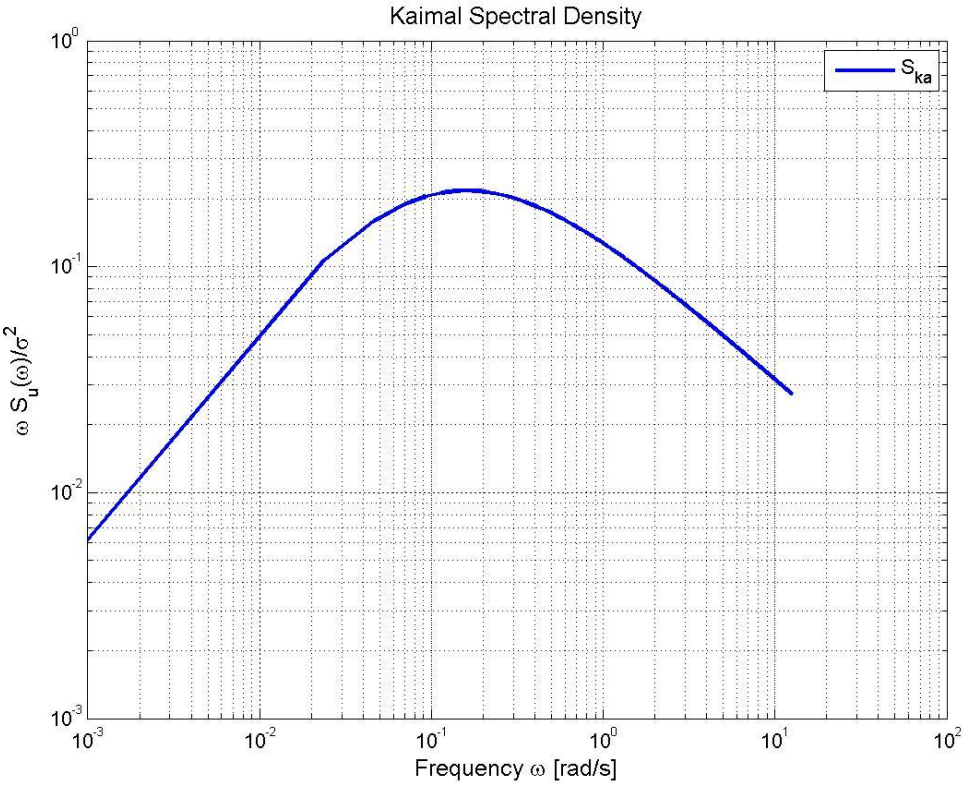

Figure 9.3: Normalized Kaimal spectral density, u-component

It should be mentioned that the resolution of the ω-vector combined with the logarithmic plotting makes the function look linear for low values of ω. However, this has little effect for the calculations. It is seen that S_{ka} decreases for high frequencies. Physically, the figure illustrates the density of fluctuations of a given frequency. It is seen that wind fluctuations with a frequency between 0.02 and 2 rad/s are most frequently experienced.

As mentioned in Section 6.2.2.3, the wind velocity is included when the JAF is calculated. This results in values that are way higher than what could normally be expected for the JAF. Figure 9.4 shows the JAF for modes 1 and 2.

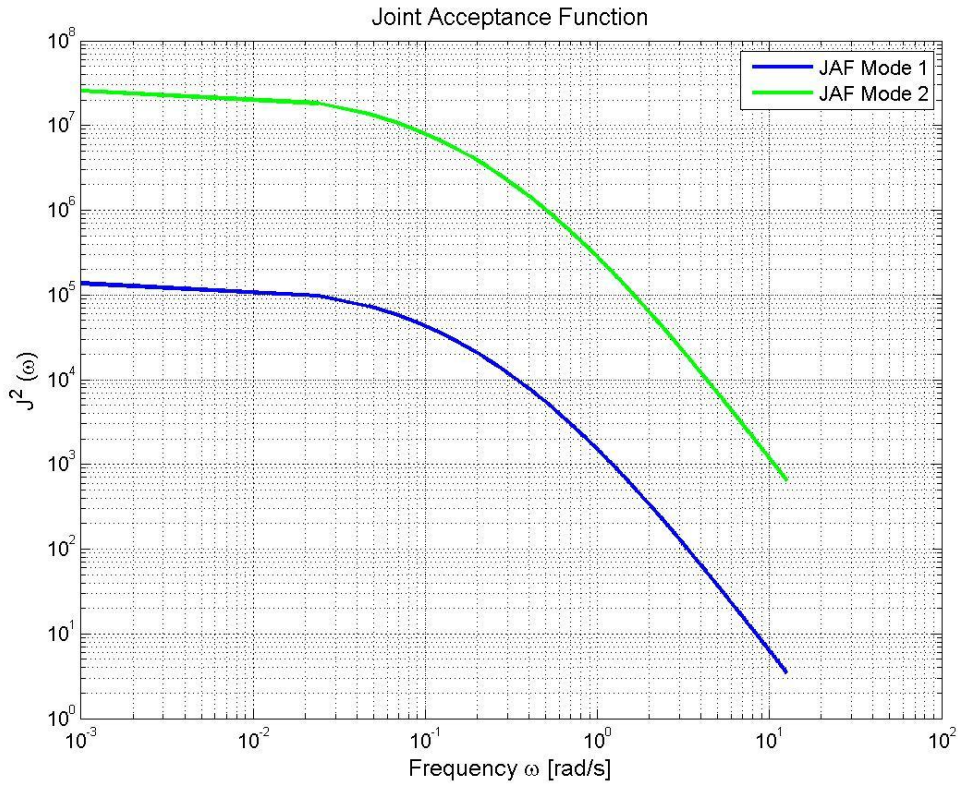

Figure 9.4: Joint acceptance function for modes 1 and 2

It is seen that the JAF has maximal values of about 10^5 for Mode 1, and 10^7 for Mode 2. The wind velocity is included in the JAF integral in the fourth power, and thus the contribution from V_m to the total JAF should approach 10^6. This argues that the value of the JAF is reasonable (between 0.1 and 10 for low frequencies). It is noted that the JAFs decrease for high frequency values.

In Strømmen's *Theory of Bridge Aerodynamics* [1], Appendix B, joint acceptance functions for several shape functions have been plotted. The JAFs in this thesis correspond well to the JAF obtained by Strømmen for the shape $\phi = x$, which has been shown in Section 3.2.1 to correspond fairly well to the actual modal shapes of the structure. In other words, the JAFs in Figure 9.4 resemble what could be expected for the given modal shapes.

9.4 Response Spectra

Response Spectrums for acceleration and displacement are crucial in the calculations. To illustrate these quantities, they are shown for Mode 1 in Figure 9.5. The following has been calculated by the script AccelSpectra.m.

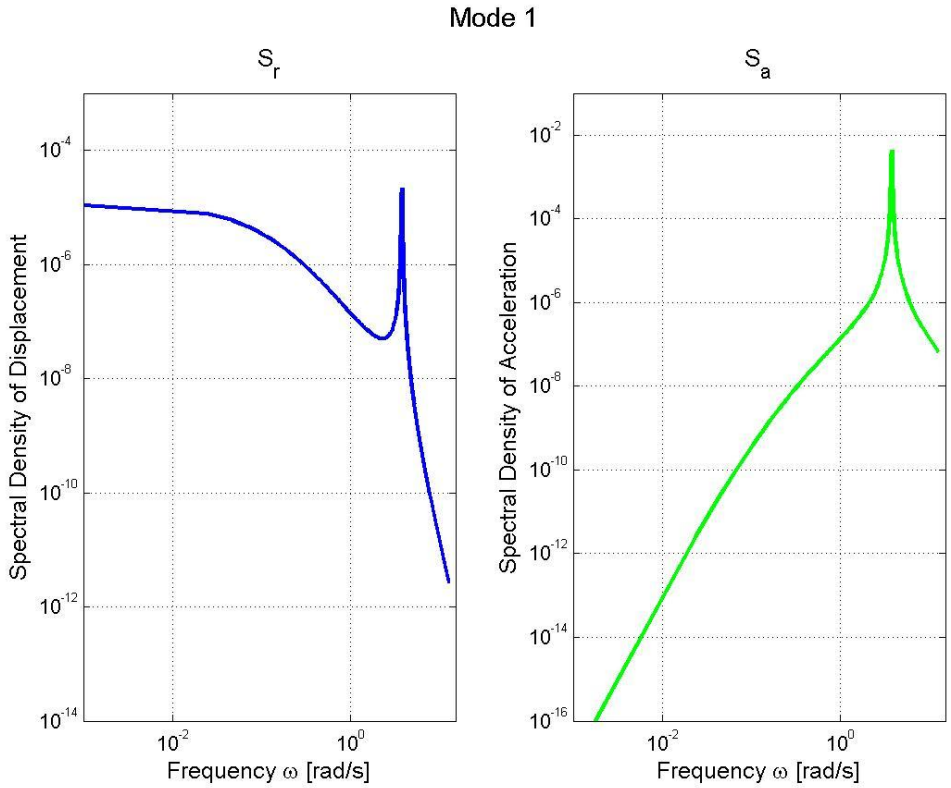

Figure 9.5: Spectral densities of displacement and acceleration

As expected, both response spectrums have clear peaks for the eigen frequency of Mode 1. It is seen that contributions to the acceleration from low frequencies are almost negligible, while low frequencies will contribute somewhat more to the displacement.

As mentioned in 6.2.2.1, time series simulations of spectral densities could be obtained. Such simulations illustrate the structural motion, and indicates which values could be expected for dynamic displacements and accelerations. Using the script TimeSim.m, simulations are performed for both modes for displacement and acceleration. It is noted that results vary with the used phase angle, and thus plots will be different for every calculation (see equation (6.19)). Time domain plots for Mode 1 are shown in Figure 9.6. The considered time span is 10 minutes, 600 s.

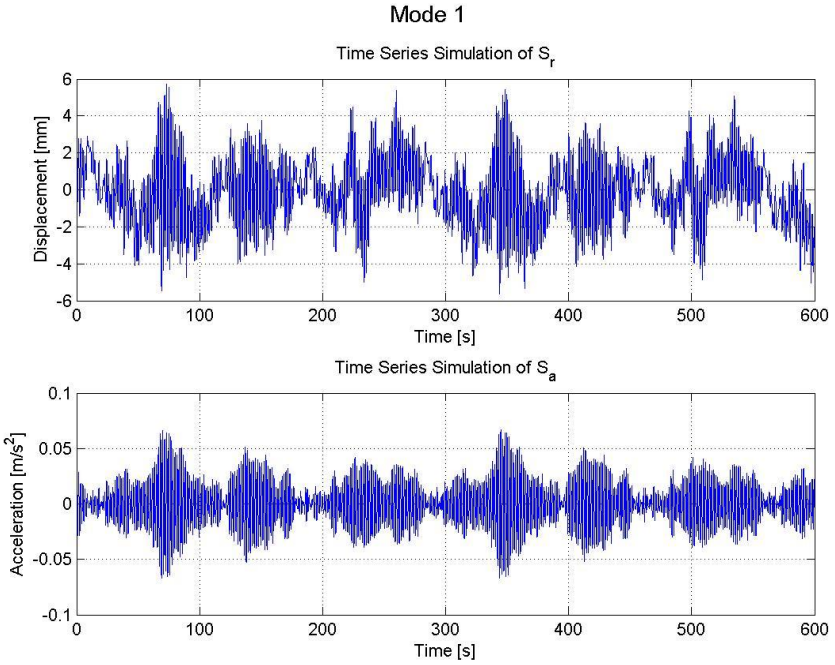

Figure 9.6: Time domain simulation of displacement and acceleration, Mode 1

It is seen that the dynamic displacements have maximal values close to 6 mm. The acceleration seems to have maximal values of about 0.06 m/s^2. It seems as the acceleration comes in pulses, with peaks every 1-2 minutes. The time domain simulations for Mode 2 are shown in Figure 9.7.

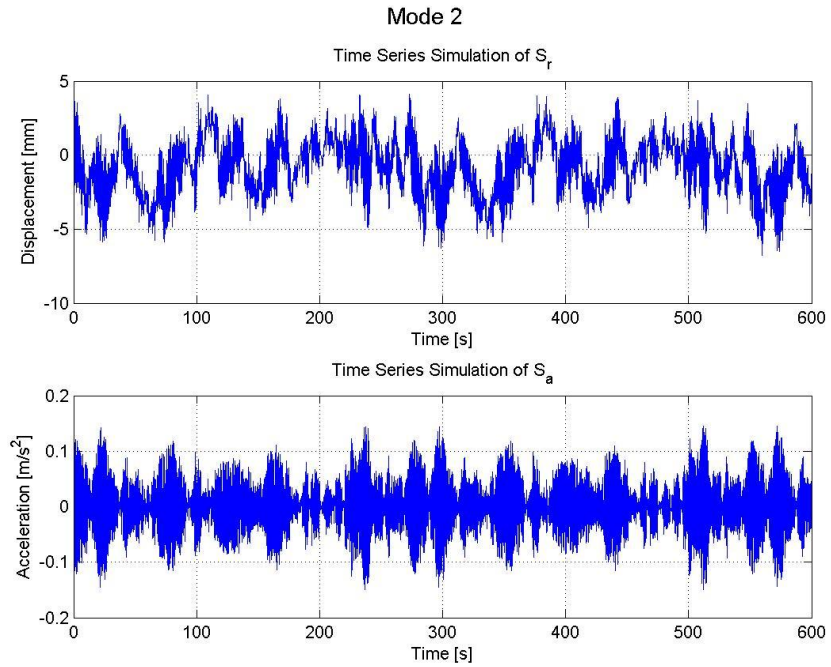

Figure 9.7: Time domain simulation of displacement and acceleration, Mode 2

Looking at Figure 9.7, it is seen that the dynamic displacements have maximal values of about 6 mm, the same as for Mode 1. The acceleration once again comes in pulses, but these are more closely spaced than what was observed for Mode 1. The maximal acceleration of Mode 2 seems to approach 1.5 m/s^2.

9.5 Force Calculations

The next step is calculation of the cross sectional forces. As shown in Section 6.3, the calculations are split into two main parts; static and dynamic.

The static forces are calculated straightforward by integrating the static wind loading over the height. This is done by the function StaticForce.m. The static wind loading on both sides of the structure is shown in Figure 9.8. Since the tower is considered as a line like cantilever, the unit is N/m.

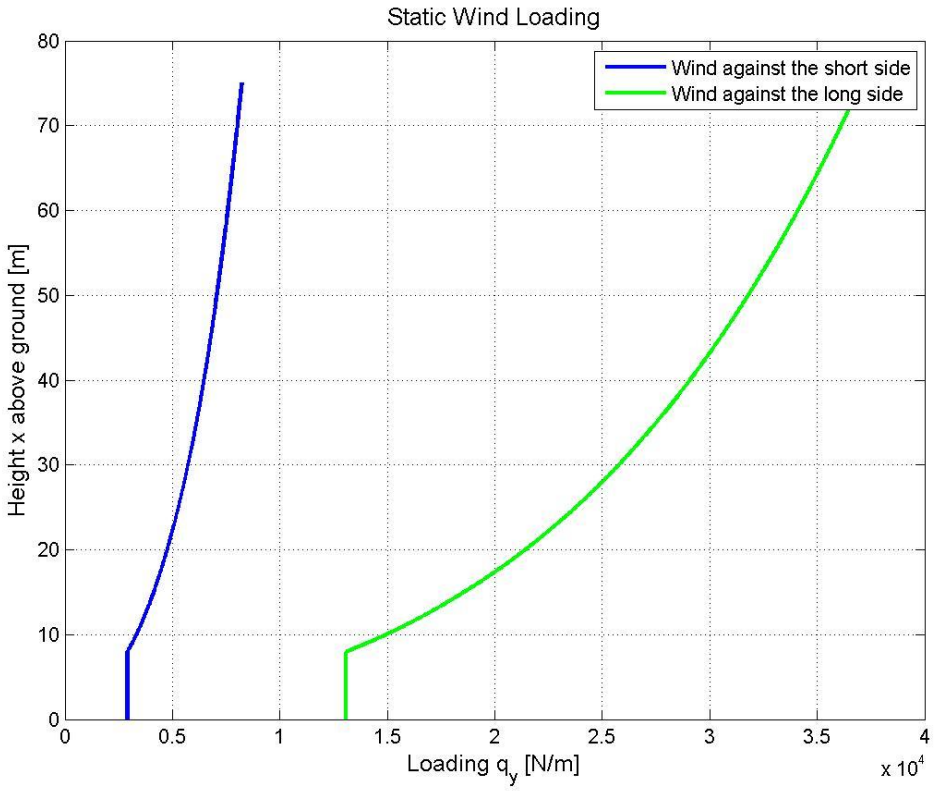

Figure 9.8: Static wind load on the structure

As expected, the static load has the same distribution over the height as the velocity field shown in Figure 9.1. The loading is defined in equation (6.6), and is dependent of the width of the cross section perpendicular to main flow. For wind against the short side, this width is 15 meters. The load at the tower top is approximately 8 kN/m, which corresponds to a pressure of about 550 Pa. For wind against the long side the width is three times higher, and the drag coefficient is larger. In total, this results in a load of about 37 kN/m at the tower top.

The objective of the force calculations is to obtain the base reactions. Therefore, the output from both static and dynamic calculations are scalars. Values of the static cross sectional forces will be shown later.

The dynamic forces are calculated as a background part and a resonant part, using the function SigmaForce.m. The variance for each part is calculated using the basis presented in Section 6.3, and then the two are combined using SRSS technique (Square Root Sum of Squares). The dynamic contribution is then weighted by the peak factor, and added to the static force.

Neglecting the SRSS combination and peak factor weighting, it is interesting to look at the size of the two standard deviations and the static contribution compared to each other. Figure 9.9 shows the size of the three contributions relative to each other for wind against the short side.

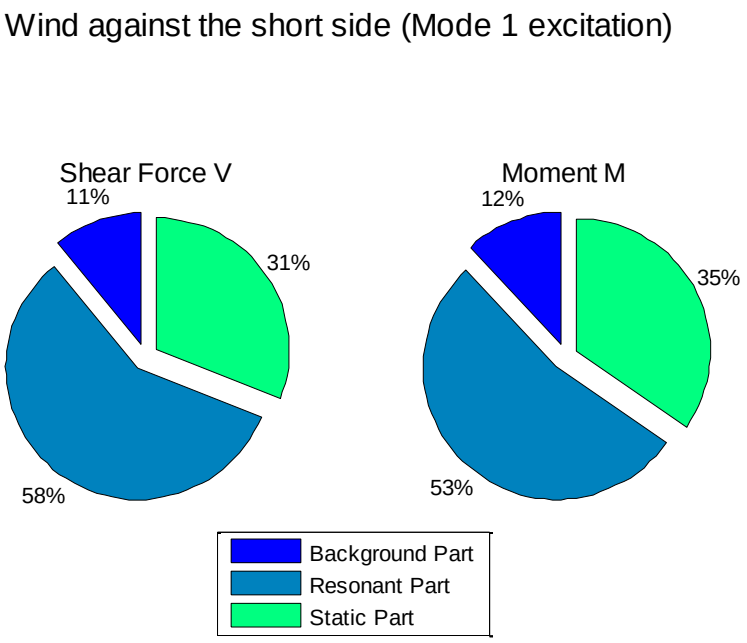

Figure 9.9: Cross sectional force contributions, Mode 1 excitation

As the figure shows, the resonant standard deviation, $\sigma_{Rs,1}$, dominates for both base shear and base moment. The same relation is shown for wind against the long side in Figure 9.10.

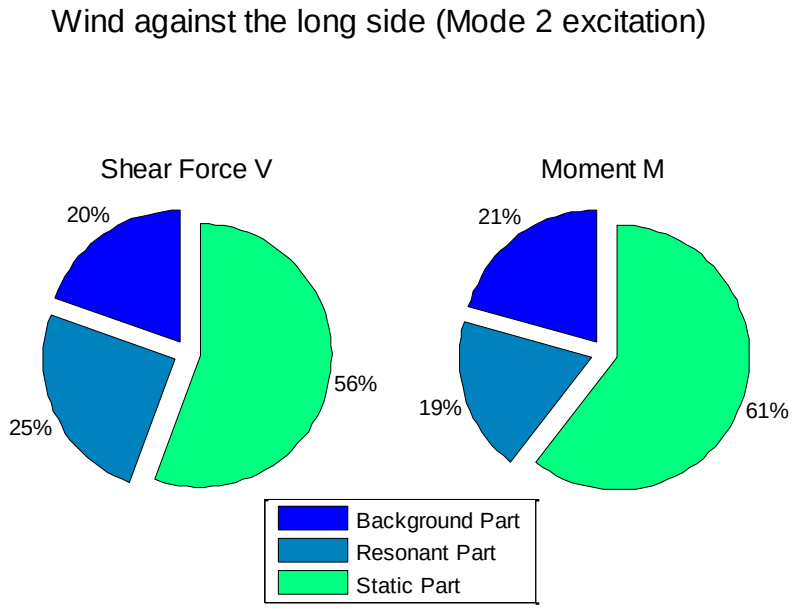

Figure 9.10: Cross sectional force contributions, Mode 2 excitation

For wind against the long side the relation is somewhat different than for wind against the short side. Static contributions dominate for both base shear and moment, while the resonant and background parts takes on relatively equal shares. The fact that the loaded area is different for the two cases makes the static contribution more dominant for wind against the long side. The resonant part, σ_{Rs}, is small because the eigen frequency of Mode 2 is relatively high. σ_{Rs} contains the JAF, which like mentioned earlier decreases for higher frequencies. In addition, the bending stiffness is lower about the axes that corresponds to Mode 2 oscillations.

Now to the actual size of the cross sectional forces. These quantities are scalars, and therefore best illustrated in a table. Table 9.1 shows the cross sectional forces for wind acting on the short side. Values are rounded to the nearest 5 kN or 10 kNm.

Wind against the short side - Mode 1 excitation		
Contribution	**Shear Force [kN]**	**Moment [kNm]**
Static contribution	445	19 400
Resonant Part σ_{Rs}	830	29 900
Background Part σ_B	155	6 620
Peak Factor k_p	3.42 [-]	3.42 [-]
Total Base Reaction	**3 330 [kN]**	**124 150 [kNm]**

Table 9.1: Cross sectional forces, wind on the short side

The total cross sectional forces from wind load on the short side of the structure are dominated by the dynamic contribution. As an example, the total base shear in Table 9.1 is more than 7 times higher than the static contribution. The resonant part of the forces was seen in Figure 9.9 to be higher than the static value, and when weighted by the peak factor the dynamic contributions dominate completely.

For wind acting on the long side, the total forces are expected higher since the loaded area is greater. Table 9.2 shows the cross sectional forces in the same manner as in Table 9.1.

Wind against the long side - Mode 2 excitation		
Contribution	**Shear Force [kN]**	**Moment [kNm]**
Static CS Forces in relevant direction	2 000	87 290
Resonant Part σ_{Rs}	898	27 030
Background Part σ_B	705	29 780
Peak Factor k_p	3.32 [-]	3.32 [-]
Total Base Reaction	**5 790 [kN]**	**220 800 [kNm]**

Table 9.2: Cross sectional forces, wind on the long side

The dynamic parts of the cross sectional forces are not as dominant for wind against the long side as for wind against the short side. The total base shear is about 2.9 times higher than the static contribution. Comparing results for the two directions, it is seen that the resonant parts the of cross sectional forces, σ_{Rs}, are fairly equal. The background part σ_B is more than four times higher for Mode 2 than it is for Mode 1. As mentioned under Figure 9.10, it could be expected that the resonant part takes on a lower value relative to the other contributions because of the higher eigen frequency of Mode 2 and the lower EI about the relevant axis. However, the fact that the loaded area and the drag coefficient has higher values makes σ_{Rs} obtain approximately the same value for both modes.

The background part, σ_B, is not affected by the eigen frequency or EI. The reason for the higher Mode 2 value is therefore almost entirely the increased width and drag coefficient. For the same reason, the static force for wind against the long side is higher than for wind against the short side.

Looking closer at the effect caused by cross sectional width and drag coefficient, it is seen that σ_B and the static forces for wind loading on the long side are about 4.5 times higher than for wind acting on the short side. Using the drag coefficients $\bar{C}_D$ found in Section 8.4 together

with the fact that the cross sectional width is three times higher for width against the long side, it is easily shown that $F_2 = \frac{1.32 \cdot 3}{0.88} \cdot F_1 = 4.5 \cdot F_1$, which confirms the obtained results.

9.6 Displacements and Accelerations

The next step of the response calculations is obtaining displacements and accelerations. Like for the cross sectional forces, displacements are calculated as a static and a dynamic part (see Section 6.2). The dynamic part is once again weighted by the peak factor. Acceleration is calculated as shown in Section 6.2.3.

The dynamic part of the displacement is calculated for buffeting response only, using the function SigmaR.m. Calculations include both the FRF and the JAF shown above, integrated over the entire frequency domain. Figure 9.11 shows the standard deviations $\sigma_{R,1}$ and $\sigma_{A,1}$ for Mode 1. σ_A has not been frequency weighted.

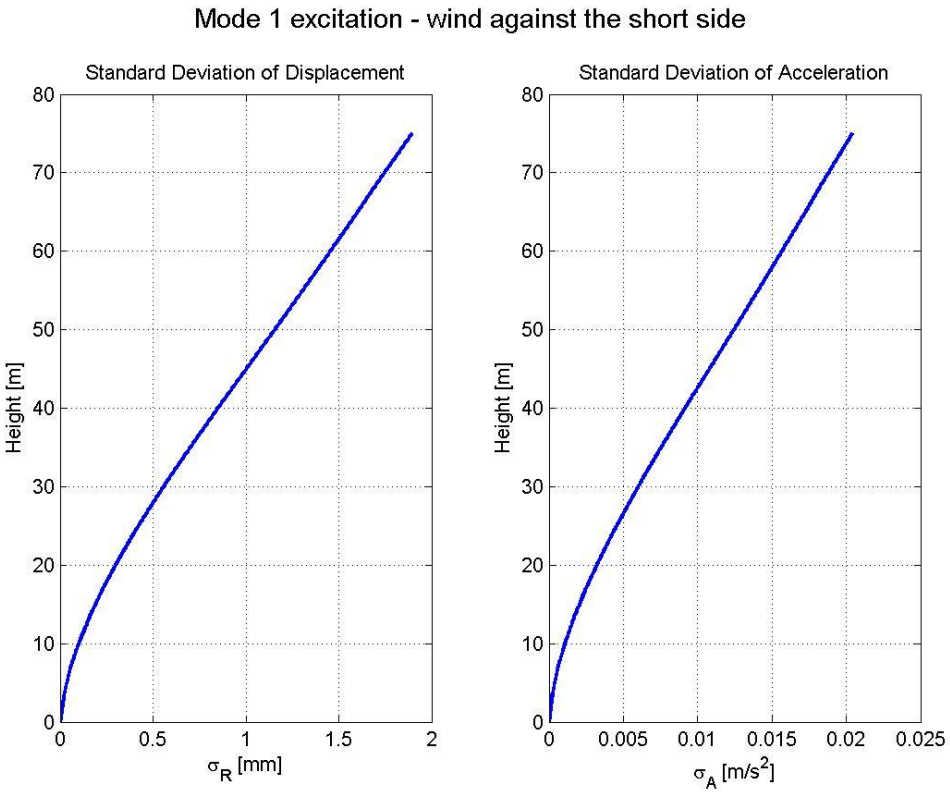

Figure 9.11: Standard deviations of displacement and acceleration, Mode 1

The two plots clearly have the same shape. $\sigma_{R,1}$ takes a value at the tower top of about 1.9 mm. $\sigma_{A,1}$ has a value of about 0.02 m/s^2 at the top of the building. The plots obtained for wind against the long side are shown in Figure 9.12.

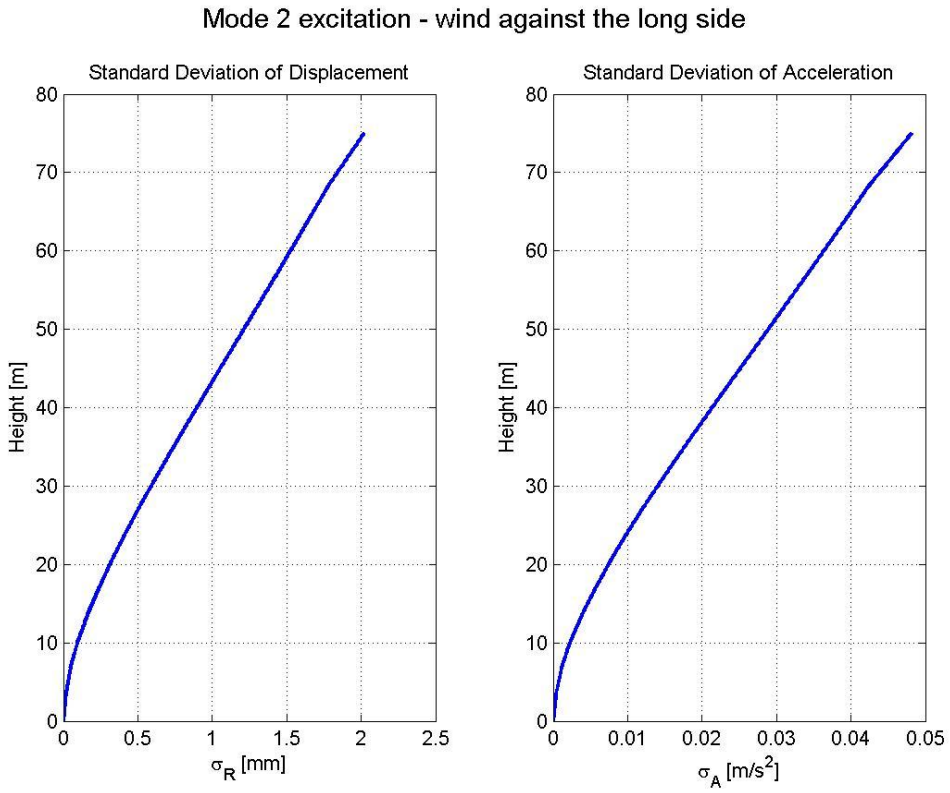

Figure 9.12: Standard deviations of displacement and acceleration, Mode 2

$\sigma_{R,2}$ takes a value of about 2.0 mm at the tower top, while $\sigma_{A,2}$ takes a value of 0.048 m/s^2. Comparing modes 1 and 2 it is seen that the standard deviations of displacement are fairly equal. When it comes to acceleration, $\sigma_{A,2}$ is more than two times higher than $\sigma_{A,1}$. The latter is easily explained by referring to the physical motion. The two mode shapes fluctuates with approximately the same amplitude, but Mode 2 has a frequency that is almost twice as high, and therefore it reaches the same displacement as Mode 1 at about half the time. Accordingly, the acceleration has to be considerably higher. Using the peak factors calculated in Section 7.1.1, the following maximal accelerations are obtained:

$$0.020 \cdot 3.42 = 0.069 \ [m/s^2]$$
$$0.048 \cdot 3.32 = 0.160 \ [m/s^2]$$

for modes 1 and 2 respectively. It is noted that the acceleration values resemble the ones seen from the time domain simulation performed in Section 9.4.

The static displacements are calculated by using the function UnitLoad.m, utilizing the theory shown in Section 6.2.1. Results are shown in Table 9.3.

Mode/Contribution	Shear Contribution [mm]	Moment Contribution [mm]	Total Static Disp.[mm]
Wind against short side	0.23	0.17	**0.40**
Wind against long side	0.23	5.34	**5.57**

Table 9.3: Static displacement of the structure

Looking at the values in Table 9.3, it is clear that the results are corrupted in some way. A static displacement of less than 6 mm for both directions is way too low.

As mentioned, the total displacement is obtained by multiplying the dynamic contribution by the peak factor, before adding the static contribution. The obtained values for both directions are shown in Table 9.4.

Contribution	**Wind against short side** (Excitation of Mode 1) Displacement [mm]	**Wind against long side** (Excitation of Mode 2) Displacement [mm]
Static contribution in relevant direction	0.40	5.57
Dynamic Contribution	1.90	2.02
Peak Factor	3.42	3.32
Total Displacement	**6.88**	**12.28**

Table 9.4: Total structural displacements

As the table above shows, the dynamic contributions make up the majority of the total displacement for both directions. Although the situation is somewhat more likely for wind against the long side than it is for wind against the short side, the total displacements are lower than what was expected in advance. The anticipated result was a total displacement of somewhere between 10 and 30 cm, where the static contribution dominated. It is noted that the dynamic contribution times the peak factor resembles the values seen from the time domain plots in Section 9.4.

This thesis aims to investigate the dynamic response of the structure, and therefore the dynamic parts of the displacement are of more interest than the static parts. With this in mind, the static displacement will not be pursued further. Factors affecting the dynamic displacements and accelerations will be further investigated in Sections 11 and 12.

10 Comparison to Eurocode Values

To determine whether the response parameters calculated using MATLAB are reasonable or not, values are compared to Eurocode estimates obtained in Sections 0 and 7. Standards are in general known to be conservative, and thus overestimate forces and accelerations. The same trend is expected here.

10.1 Cross Sectional Forces

Table 10.1 shows the cross sectional forces for wind against the short side calculated both from the Eurocode and by using MATLAB. All values are rounded to the nearest 10 kN or 10 kNm.

Wind against the short side - excitation of Mode 1		
Parameter	Base Shear [kN]	Base Moment [kNm]
Eurocode, Force Coefficient	1 510	61 580
Theoretical, MATLAB	3 330	124 150
Deviation from closest value	**120 %**	**102 %**

Table 10.1: Eurocode vs. theoretical forces, wind against the short side

The theoretical values are considerably higher than the values obtained by codes for both base shear and base moment. Corresponding values for wind against the long side are shown in Table 10.2.

Wind against the long side - excitation of Mode 2		
Parameter	Base Shear [kN]	Base Moment [kNm]
Eurocode, Force Coefficient	7 250	279 790
Theoretical, MATLAB	5 790	220 800
Deviation from closest value	**-20 %**	**-21 %**

Table 10.2: Eurocode vs. theoretical forces, wind against the long side

Comparing the results from the two tables above, it is seen that the trend for the two directions are different. For wind against the long side, results are as expected. The results obtained from aerodynamic theory are about 20 % lower than the Eurocode estimates.

The results for wind against the short side deserves some extra attention. The theoretical results are 120 % and 102 % higher than Eurocode values for base shear and base moment respectively. As shown in Figure 9.9 and Table 9.1 in Section 9.5, the resonant part of the dynamic forces dominated the totals for Mode 1. In advance it was expected that the two

dynamic parts would contribute more evenly. The peak factor weighted dynamic contribution was expected to be close to the static part, but in reality it is more than 6 times higher. It is therefore reasonable to assume that the reason for the high cross sectional forces for wind against the short side lays somewhere within the resonant part. σ_{Rs} depends on modal derivatives and bending stiffness, both of which are calculated from rough estimates. As will be discussed in Section 12.1.2, the bending stiffness should probably be lower, which would lead to better correspondence between design code forces and forces calculated from theory. Other parameters that influences the dynamic forces are discussed in Section 11.

It should be mentioned that the concept of cross-sectional forces has been used in its simplest way in this thesis. The structure has been assumed as a solid beam, where the given wind load induces a total shear force and a total moment in the structural base. In reality, the force distribution is way more complex. The point of the simplified approach is to compare theory and design procedures without detailed calculations that involves single structural components. Although Eurocode estimates could be expected to be conservative compared to theoretical calculations, the nature of the performed calculations could eliminate the expected differences between the two methods. For wind against the long side, the results are as good as one could expect, with deviations between aerodynamic theory and building codes of about $1/5$. For wind against the short side, theoretical and design code estimates deviate by more than 100 %, which could not be interpreted as a good match.

10.2 Accelerations

Acceleration estimates have already been calculated using Eurocode methods (see Section 0). In addition, design limits for accelerations have been obtained from different design codes. Table 10.3 shows the accelerations obtained both by theoretical calculations and by Eurocode estimates.

Calculation Procedure	**Mode 1 - wind against short side** Acceleration [m/s^2]	**Mode 2 - wind against long side** Acceleration [m/s^2]
Method B (EC)	0.029	0.084
Method C (EC)	0.037	0.104
Theoretical Value	0.069	0.160

Table 10.3: Eurocode vs. theoretical accelerations

As the table clearly shows, the theoretical calculations provides accelerations considerably higher than design codes.

The next step is comparing the frequency weighted accelerations to the perception demand, like described in Sections 4.3 and 6.2.3. Calculations are performed using the function AccelSpectra.m. To demonstrate the calculation process, some key quantities are presented here. The frequency weighting function is shown in Figure 10.1.

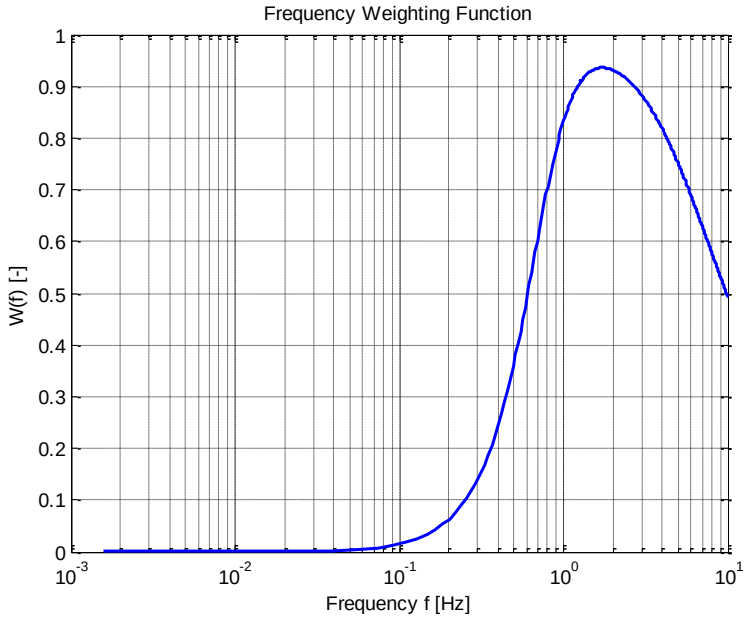

Figure 10.1: Frequency weighting function from ISO 2631

It is clear that frequencies between 0.1 and 10 Hz are most crucial for human comfort. The weighting function is defined for frequencies up to 80 Hz, but given the nature of wind and the structural behavior, the previously defined frequency spectrum (see Section 8.1) has been used. Figure 10.2 shows the spectral density of acceleration and the frequency weighted spectral density of acceleration for Mode 1, calculated as shown in Section 6.2.3. Corresponding plots for Mode 2 are given in Appendix 7.

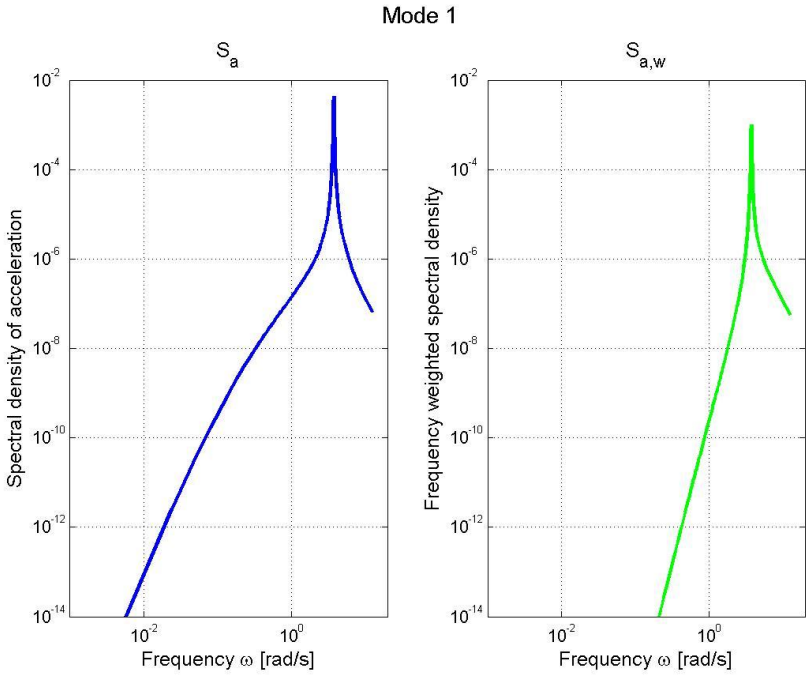

Figure 10.2: Spectral density of acceleration, Mode 1

Like one would expect, the frequency weighted acceleration spectrum has lower values than the original acceleration spectrum. Low frequencies are almost removed from the chart. After integrating over the entire frequency domain and multiplying by the peak factor, the following frequency weighted acceleration values are obtained (Table 10.4).

Mode #	Frequency weighted acceleration a_w
Mode 1 (wind against the short side)	0.034 [m/s^2]
Mode 2 (wind against the long side)	0.137 [m/s^2]

Table 10.4: Frequency weighted acceleration, modes 1 and 2

It is clear that the frequency weighted accelerations for both modes 1 and 2 are significantly higher than the perception limit given in Section 4.3, which had an upper value of 0.02 [m/s^2]. a_w for Mode 1 is about 70 % higher than the upper perception limit. For Mode 2, a_w is almost 7 times higher than the upper perception limit.

Comparing the values to the ones estimated from NS-EN 1991-1-4 (see Table 10.3), it is seen that the frequency weighted accelerations correspond much better than the actual maximal accelerations given in Table 10.3. a_w for Mode 1 is located between the estimates given by Eurocode methods B and C. For Mode 2, a_w is found to be 32 % higher than the estimate obtained from Method C. Although this does not provide any improvement regarding the perception limit, the similarity confirms that high design accelerations could be expected for the structure, and thus the obtained results for a_w are strengthened.

11 Parameter Studies

To explore the effect of crucial parameters on the obtained response, a selection of parameter studies have been performed. These studies aim both to verify the obtained results, and to investigate the uncertainty that is introduced through input parameters. In addition, the studies tests the impact caused by assumptions made in the calculation process. Two of the response parameters have been selected to illustrate the parameter studies, namely the frequency weighted acceleration at the tower top, and the base moment. These two quantities include all relevant calculations, and will therefore be representative for the theoretical basis. It is noted that the static contribution of the base moment is included, and thus referring to modal shapes describes the relevant loading direction.

11.1 Velocity Assumptions in S_{ka} and Co

As mentioned in Section 6.2.2.3, the velocity term within the Kaimal spectral density S_{ka} and the Davenport Co-spectrum $\hat{C}o$ was assumed constant. The original assumption was the maximal possible velocity over the height, about 31.5 m/s. However, this approach will render conservative results. To investigate the effect of a reduced velocity, response calculations has been performed for velocities between 31.5 m/s and 17.5 m/s, which is equal to the upper and lower velocities experienced over the tower height. The effect of this variation for wind against the short side (excitation of Mode 1) is shown in Figure 11.1.

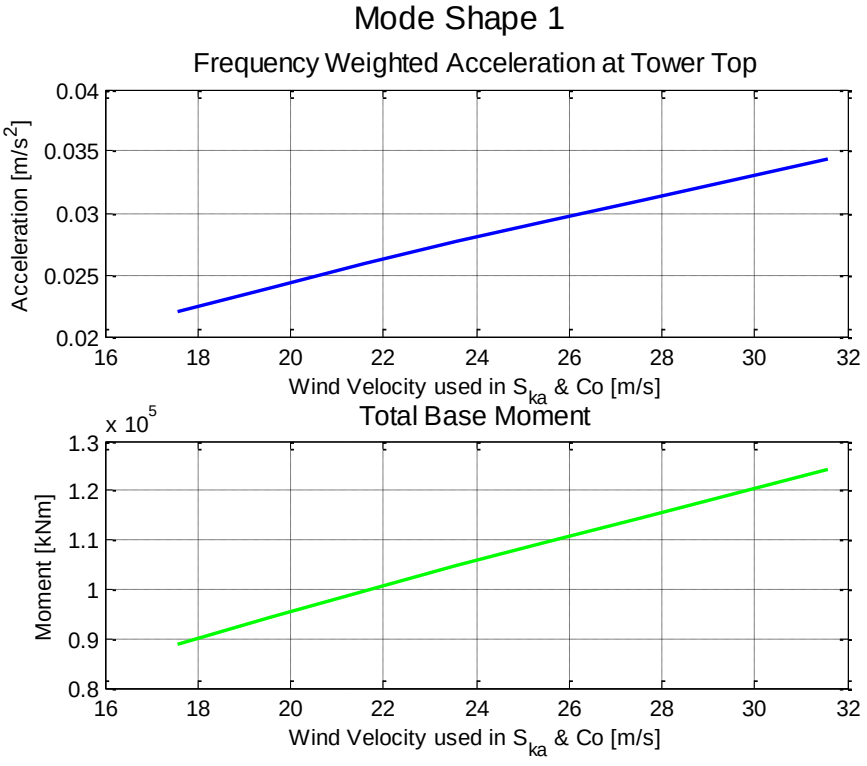

Figure 11.1: Variation induced by velocity assumption, wind against the short side

As the figure shows, both the base moment and the top acceleration decrease when the assumed velocity decreases. It is seen that the variation is almost linear. The difference between using the lowest and highest possible velocity is a change in acceleration of about 34 %. Also for the base moment, it seems that the variation caused by the velocity assumption is nearly linear. The velocity assumption only effects the resonant part of the moment, where it is included in the JAF evaluated at the eigen frequency (see Section 6.3.3). Using the lowest possible velocity instead of the highest one results in a reduction of base moment by about 28 %, which is less than what was seen for the acceleration.

For wind against the long side (excitation of Mode 2), the situation is the same. The variation of acceleration and base moment is shown in Figure 11.2.

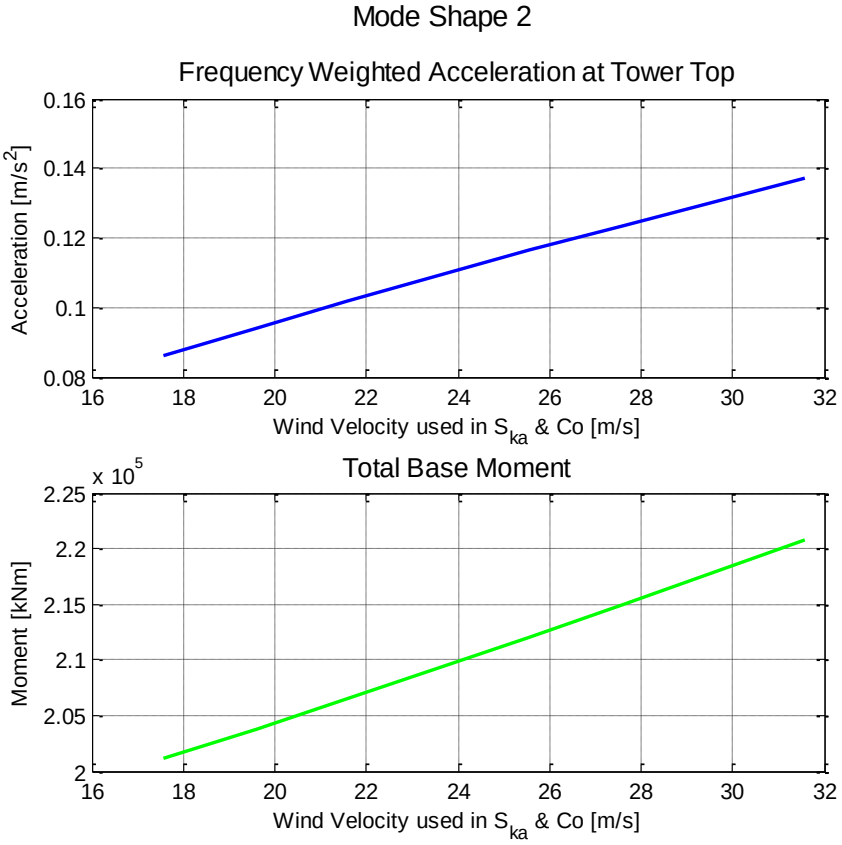

Figure 11.2: Variation induced by velocity assumption, wind against the long side

To start with the base moment, the velocity assumption results in the same trend as for wind against the short side: the base moment decreases in a linear manner when the velocity is reduced. However, the effect is less apparent for wind against the long side than it was for wind against the short side. The reduction obtained for the latter by using the lowest possible velocity is only about 9 %. In Section 9.5, it was shown that the resonant part of the base moment accounted for a smaller part of the total for Mode 2 than for Mode 1. It is therefore

logical that the effect of the velocity assumption is less significant for wind against the long side than for wind against the short side when it comes to base moment.

For the acceleration of Mode 2, the effect is again linear. Checking the values, it is seen that the difference between using maximal and minimal velocity assumption is a 37 % reduction in acceleration, which is somewhat more than what was seen for Mode 1.

Looking to the theory section, the effect of the velocity assumption could be explained. For the frequency weighted acceleration, the velocity assumption affects the JAF through the term shown in equation (6.48), which is the product between the Davenport Co-spectrum and the Kaimal spectral density. It is seen directly from equation (6.48) that a reduced velocity would reduce both the mentioned quantities, and thus the observed behavior is expected. The same explanation is valid for the base moment.

To conclude on what effect the velocity assumption has on the calculated response, an assessment of a realistic velocity value needs to be done. As mentioned earlier, the maximal possible velocity was chosen to obtain the highest possible response values. However, the average velocity over the height is about 26.5 m/s. Looking at Figure 11.1 and Figure 11.2 it is seen that lower response values are obtained if a velocity of 26.5 m/s is used. It is therefore reasonable to assume that the actual response of the structure should be somewhat lower. How much lower differs for each response parameter and direction.

11.2 Height Used in the Integral Length Scales

As mentioned in Section 6.2.2.3, the integral length scale, ${}^{s}L_n$, represents the eddy size in a given direction. The length scales are included in the Kaimal spectral density, and the covariance coefficient used when calculating the background part of cross sectional forces. According to equation (6.46), length scales are dependent on the height x_f above ground, and will increase with increasing height. The original assumption was that the length scales could be evaluated for the maximal height, H = 75 m. In the following, heights between 10 m and 80 m have been tested. Figure 11.3 shows the frequency weighted acceleration at the top and the base moment as functions of the height used in ${}^{s}L_n$ for wind loading against the short side of the structure.

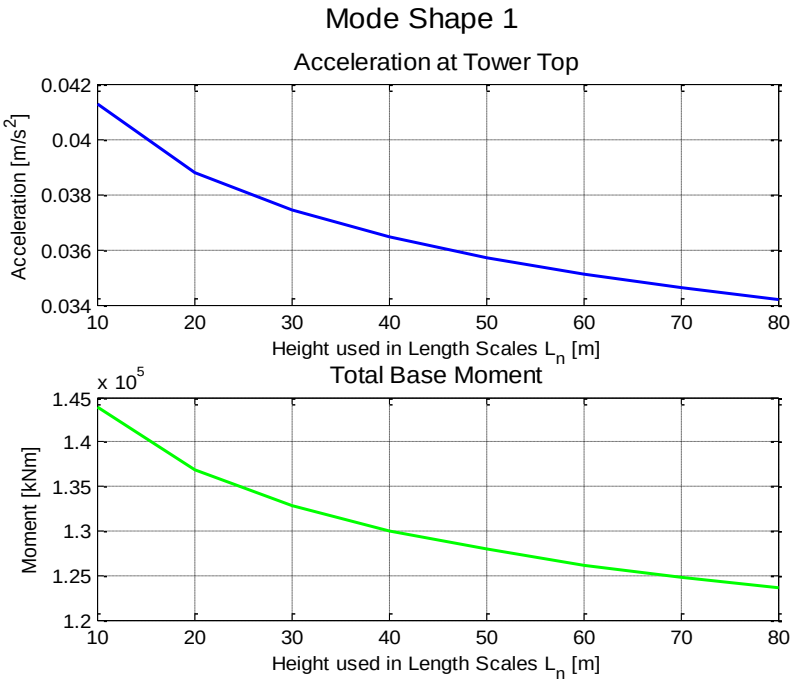

Figure 11.3: Variation induced by height assumption in integral length scales, excitation of Mode 1

As the figure shows, both the acceleration and the base moment increases when the height used in the length scales is decreased. The acceleration value is approximately 20 % higher when a height of 10 m is used. For the base moment, the increase is about 16 %. The corresponding quantities for wind against the long side are shown in Figure 11.4.

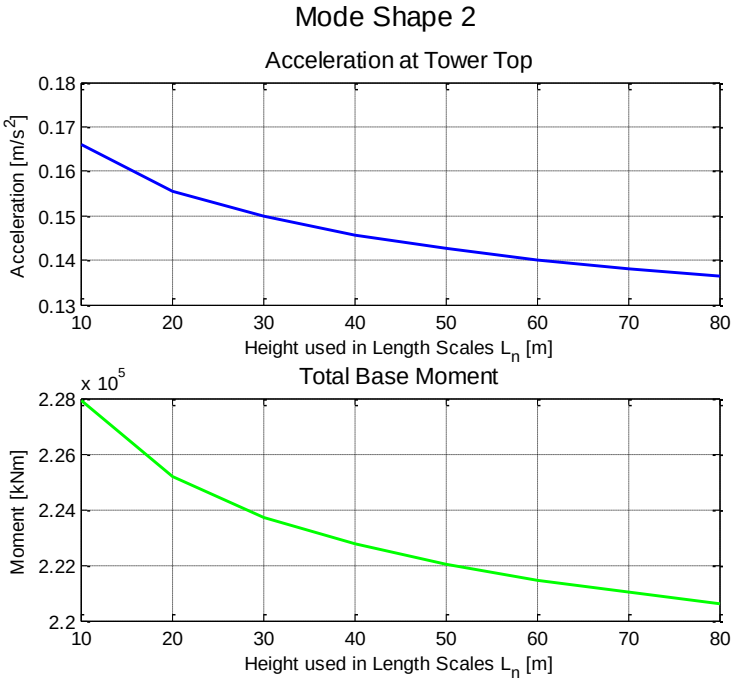

Figure 11.4: Variation induced by height assumption in integral length scales, excitation of Mode 2

Starting with the base moment, Mode 2 follows the same pattern as Mode 1. The base moment is estimated about 3 % higher when the height is set to 10 m. For the frequency weighted acceleration, the trend is the same. a_w increases by about 21 % when the height is reduced from 75 to 10 meters.

To explain the effect of ${}^{s}L_n$, it is easiest to start with the base moment. As mentioned, ${}^{s}L_n$ is included in the background part of the base moment through a covariance coefficient, given in equation (6.69) as $\rho_{nn}(\Delta x) \approx e^{\frac{-\Delta x}{{}^{x}L_n}}$. If the height in the length scale is reduced, the length scale is reduced as well. This will result in a higher covariance coefficient, which again provides a higher base moment.

When it comes to the acceleration, the length scale is included in the Kaimal spectral density S_{ka}. According to Section 6.2.2.3, an increase in S_{ka} would lead to an increase in response. It is seen from equations (6.45) and (6.46) that reducing the height x_f will reduce the normalized frequency f_L. When f_L is reduced , the Kaimal Spectral Density will increase, which again makes the frequency weighted acceleration increase.

Looking at the results obtained above, it is clear that the cross sectional forces (represented by the base moment) would be higher if the height dependence of ${}^{s}L_n$ was included in the calculations. By what amount differs between the two modes. The same conclusion is valid for the frequency weighted acceleration, but the effect is more apparent. It is noted that the effect is smaller than what was demonstrated for the velocity assumption above. In addition, the behavior caused by the height dependence is not linear. Changing x_f from 40 to 10 meters gives twice the impact that is obtained by changing x_f from 75 to 40 meters.

11.3 Mass Estimate

The mass was estimated based on the assumptions given in Section 8.5. Estimates were made for SLS and ULS separately, to be used when calculating displacements and forces respectively. To check the effect of the mass used in calculations, the following scenarios have been tested (Table 11.1):

Scenario	ULS mass [kg/floor]	SLS mass [kg/floor]
Original Mass	624 360	765 600
10 % increase	686 800	842 160
10 % reduction	561 920	689 040
No variable loads for SLS	-	693 730
Maximal load coeff. for ULS	1 256 200	-

Table 11.1: Mass scenarios used in parameter studies

Figure 11.5 shows the frequency weighted acceleration and the base moment for wind against the short side, calculated with all the mass scenarios.

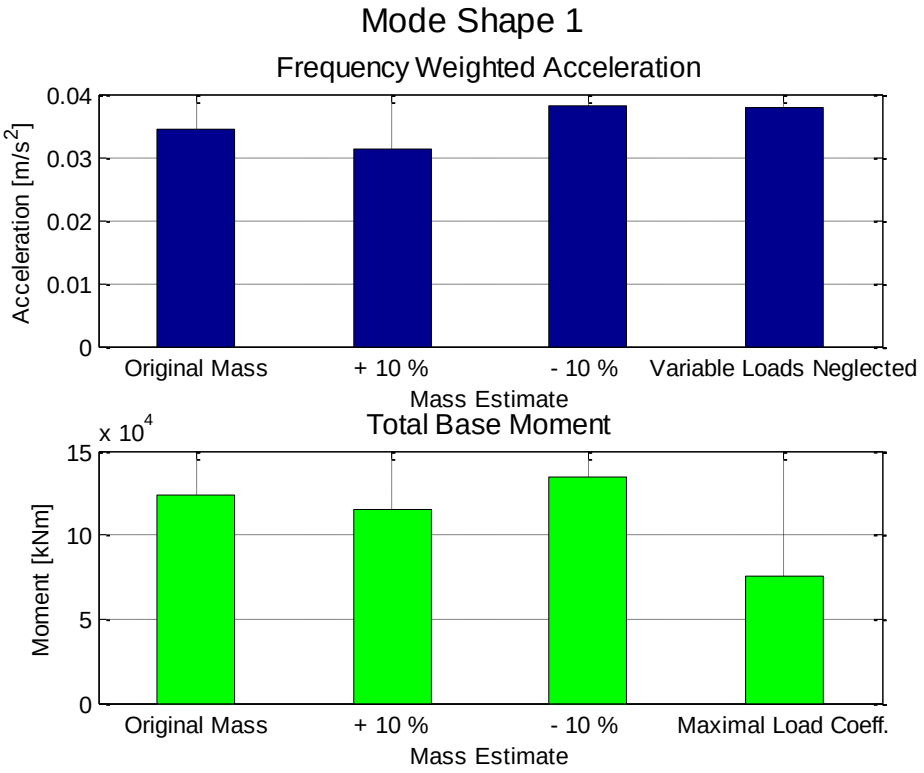

Figure 11.5: Effect of mass scenarios, wind against the short side

Figure 11.5 illustrates the assumption that was made when the original mass was estimated. If the mass is reduced, the resulting response will be higher than the original value, and vice versa.

A closer look at the base moment is required. By reducing the mass 10 %, the total base moment increases 8.5 %. A mass increase of 10 % will result in a base moment reduction of 7.3 %. The mass is included in the resonant part of the cross sectional forces, both directly and through the aerodynamic damping. In other words, a linear relation between mass and base moment could not be expected. Referring to equation (6.50), a smaller mass will provide a higher aerodynamic damping, and therefore a higher total damping. From equation (6.83) it is seen that an increase in damping will lead to a reduction in the base moment. The mass is also included directly in equation (6.83), and looking at the results obtained above it is clear that the latter contribution dominates.

For the frequency weighted acceleration, the same effect is observed. A mass reduction of 10 % results in an acceleration that is about 10.5 % higher than the original value. Increasing the mass by 10 % will reduce the acceleration by about 9 %. Similar to the base moment, the mass is included in the acceleration both directly, and through the aerodynamic damping

which is a part of the frequency response function. The reasons for the observed effects are similar to the ones explained above.

The two last scenarios investigate the effect of load factors. When variable loads are neglected for SLS, the acceleration increases approximately 10 %. In Section 2.2 it was mentioned that the hotel will be booked from the bottom floors and up, thus the scenario of reduced variable load is relatively likely. However, with no occupancy on the upper floors, there will be no complaints on structural motion.

The scenario where maximal load coefficients are used is meant to illustrate the effect of load factors being favorable. If the maximal load factors are introduced, the mass is increased by more than 100 % for the ULS (see Table 11.1). The resulting base moment is reduced by 40 % compared to the original value.

Assessing the data found above and the considerations made when estimating the mass (Section 8.5), it is clear that the original ULS mass estimate is conservative for cross sectional force calculations. For the displacement and acceleration calculations, even more conservative results could be obtained by neglecting the variable load. However, according to NS-EN 1990 (see mass estimate in Section 8.5 and Appendix 5) the lowest load factor possible for the variable load in SLS calculations is 0.3. Applying this factor would reduce the mass by less than 4 %, and looking at the trends seen in Figure 11.5, this would result in an increase of acceleration by less than 5 %.

For wind against the long side, which excites Mode 2, the situation is similar to the one shown for wind against the short side. The effects of a +/- 10 % mass change on the acceleration are the same as for wind against the short side. This is much expected since the main mass effect is independent on modal data. The effects on the base moment are smaller than for Mode 1, less than 3 % for both cases. The reason for the latter is that the static part of the cross sectional forces is more dominant compared to the resonant part (where the mass is included) for wind against the long side (see Figure 9.10). The mass changes will therefore have a lower impact on the total value. A graphical representation is shown in Figure 11.6

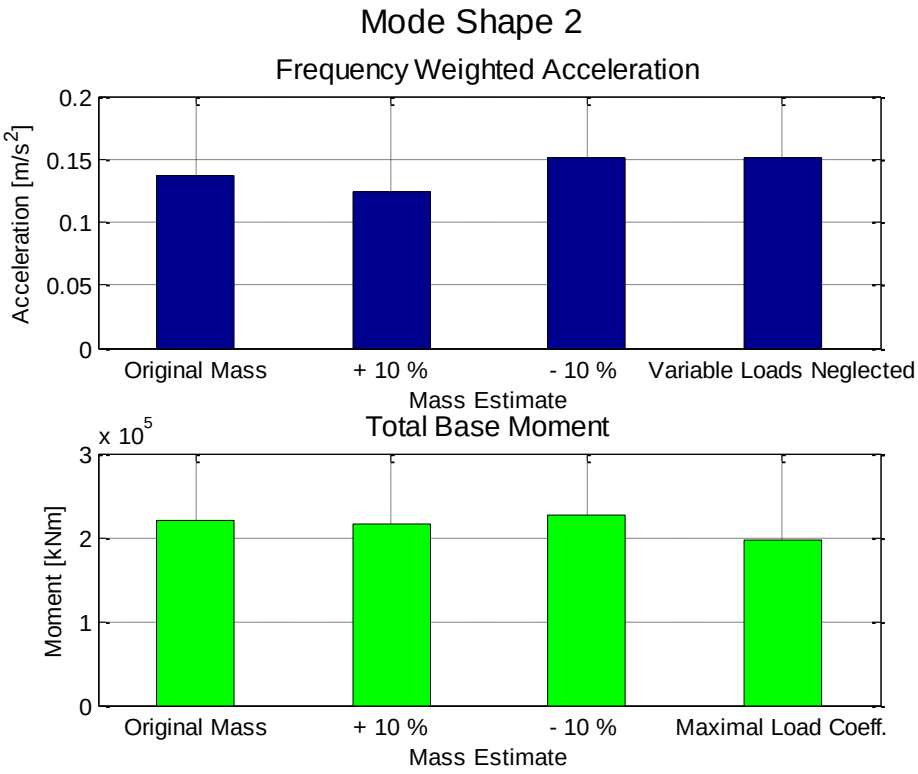

Figure 11.6: Effect of mass scenarios, wind against the long side

In total, the original mass estimates seem to be reasonable. If the actual mass is lower than the estimate, the cross sectional forces, accelerations and displacements will increase correspondingly. However, since the original mass estimates are conservative, it is unlikely that the actual structural mass is even lower.

11.4 The Effect of Damping

Damping of the structure was determined Section 5, using different estimates found in literature. The chosen damping was higher for Mode 2 than for Mode 1, and was based on the frequency estimates obtained from SAP2000. It goes without saying that an increase in damping will result in lower response, while lower damping will increase response parameters. The objective of this parameter study is therefore to map the magnitude of response changes caused by damping deviations. In addition, the contribution from aerodynamic damping will be investigated.

11.4.1 Structural Damping

The original damping estimates were based on Satake (see Section 5.5), and resulted in damping ratios of 0.008 (0.8 %) for Mode 1 and 0.012 (1.2 %) for Mode 2. However, other estimates gave somewhat different values. This was especially the case for Mode 1, where other estimates indicated higher damping ratios. To check the effect of damping, the top acceleration and base moment has been calculated for damping ratios deviating +/- 0.003 and + 0.007 from the original values for both modes. Figure 11.7 shows the results for Mode 1.

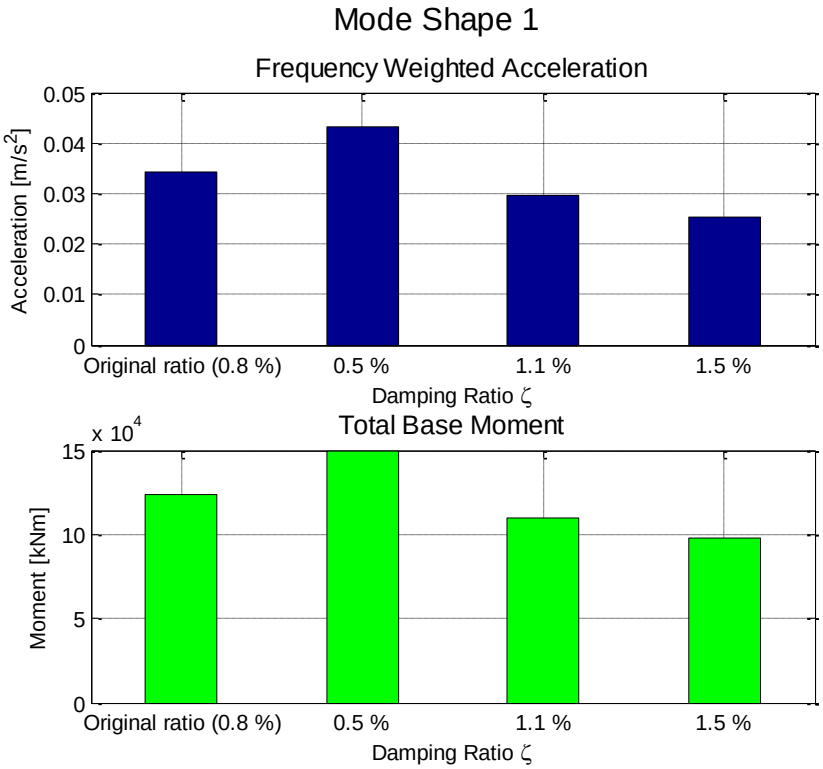

Figure 11.7: Effect of damping ratio changes, Mode 1

The figure confirms the expected trend. A damping ratio of 0.005, corresponding to a reduction of 0.003, increases the acceleration by about 25 %. The base moment increases by 20 % compared to the original value. Increasing the damping ratio by 0.003 will result in a 14 % reduction of top acceleration compared to the original value. The base moment is reduced by about 11 %.

To explain why the change in ζ has a larger impact on the frequency weighted acceleration than on the base moment, it is once again referred to Section 9.5. The damping ratio only affects the resonant part of the dynamic cross sectional forces, while σ_B and the static base moment are independent of ζ .

For Mode 2, the top acceleration and base moment are shown in Figure 11.8.

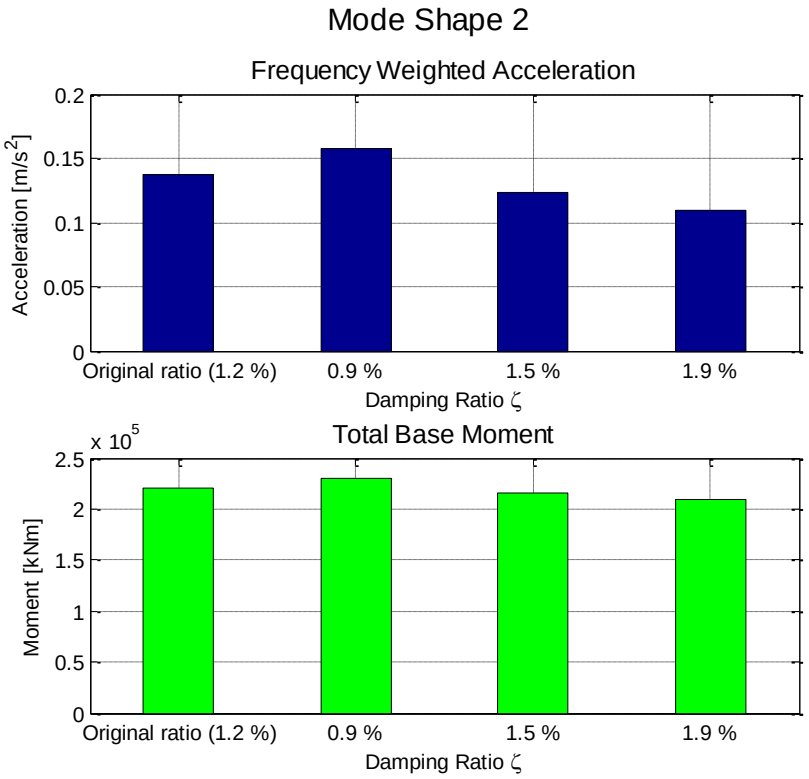

Figure 11.8: Effect of damping ratio changes, Mode 2

To start with the base moment, one would expect that the difference induced by a 0.003 reduction in damping ratio would be smaller than for Mode 1. The reason for this is that the damping ratio is included in the resonant part of the base moment, which is less dominant for Mode 2 than for Mode 1. Checking the values, it is found that reducing ζ by 0.003 increases the base moment by about 4 % compared to the original value. This is less than for Mode 1, like expected.

Checking the acceleration values, it is seen that a decrease in damping ratio of 0.003 increases the top acceleration by about 15 %. This is less than for Mode 1. However, changes in damping ratio has a more significant effect for low damping ratios than for high ones. The reason for this could be seen from $\hat{H}(\omega)$, given in equation (6.49). As a function of damping ration, the FRF will obtain high values for small ζ, and small values for high ζ. The original damping ratio of Mode 2 is higher than for Mode 1, which explains why a similar change in damping ratio has less effect for Mode 2. The effect is illustrated by the low changes induced by a damping ratio of 1.9 % in Figure 11.8.

Increasing the damping ratio for Mode 2 by 0.003 will result in a base moment that is 2.6 % lower than the original value. Similarly, the frequency weighted acceleration is reduced by about 10 %.

11.4.1 Aerodynamic Damping

The aerodynamic damping ζ_{ae} also deserves some attention. Relative to the structural damping, the aerodynamic damping of Mode 2 could be expected higher than for Mode 1. The reason for this is that the motion of Mode 2 is perpendicular to the longest side of the structure, and thus the area that interacts with the air flow is larger. The aerodynamic damping is a function of mass. Since two different mass estimates has been used for the ULS and SLS, there will be two different aerodynamic damping ratios for each mode. Table 11.2 shows the aerodynamic damping ratios, and compares them to the structural damping.

	Mode 1		**Mode 2**	
Damping contribution	ULS	SLS	ULS	SLS
Structural, ζ	0.8 %	0.8 %	1.2 %	1.2 %
Aerodynamic, ζ_{ae}	0.036 %	0.030 %	0.091 %	0.074 %
Total, ζ_{tot}	0.836 %	0.830 %	1.291 %	1.274 %
ζ_{ae} share of ζ_{tot}	**4.3 %**	**3.6 %**	**7.0 %**	**5.8 %**

Table 11.2: Effect of aerodynamic damping

Table 11.2 confirms the expectation of higher aerodynamic damping ratios for Mode 2 than Mode 1. ζ_{ae} values for Mode 2 are about 2.5 times higher than the ones obtained for Mode 1. Furthermore, it is seen that the SLS mass gives lower aerodynamic damping ratios. As discussed in Section 11.3, a higher mass provides smaller response, and it is therefore logical that the aerodynamic damping is smaller.

Looking at the aerodynamic damping compared to the total damping, it is seen that the contribution from ζ_{ae} is small. The highest contribution is found for ULS calculations concerning Mode 2, where the aerodynamic damping only accounts for 7 % of $\zeta_{tot,ULS}$. The parameter tests in Section 11.4.1 changed the damping ratio by +/- 0.003, which corresponds to almost 40 % of the original damping ratio of Mode 1, and 25 % of the original damping ratio of Mode 2. In other words, the effects of the aerodynamic damping on acceleration and base moment is at the most less than a third of the effects displayed in Figure 11.7 and Figure 11.8.

To conclude upon the effect of structural and aerodynamic damping, it is seen that deviations in damping give relatively large changes in frequency weighted acceleration. For the base moment, the effect is somewhat lower, especially for Mode 2. For Mode 1, the most conservative damping estimate was used in the original calculations (see Section 5.5). The damping ratio of Mode 1 could probably have been higher. This makes the 20 % increase in base moment and the 25 % increase of acceleration unlikely to occur. Despite of this, it must

be kept in mind that changes in the structural damping could be significant for the total response. The effect of aerodynamic damping is almost negligible compared to the structural contribution.

11.5 The Peak Factor

As mentioned in Section 8.3, the peak factors k_p were calculated using an eigen frequency estimate obtained from NS-EN 1991-1-4, Appendix F. This frequency estimate (0.613 Hz) is a relatively good match for Mode 1, but a poor match for Mode 2. To check the effect of the frequency assumption in the calculations, peak factors have been re-calculated using the Eurocode method with the actual eigen frequencies estimated by SAP2000 (0.596 Hz for Mode 1, 1.067 Hz for Mode 2). Calculations will not be shown, but the used formulas and parameters are given in Section 8.3 and demonstrated in Appendix 2.

Performing the calculations, it is seen that the changes in k_p are minimal. For Mode 1, the peak factor changes from 3.42 to 3.41. Mode 2 has a peak factor change from 3.32 to 3.30. It is seen that both peak factors decrease compared to the original value. Since one frequency is decreased while the other one is increased in the calculations, it was expected that the two peak factors would change in different directions. However, given the complexity of the calculations, this effect will not be investigated.

Values for top acceleration and base moment for the different peak factors are given in Table 11.3.

Parameters	**Mode 1**		**Mode 2**	
	Frequency weighted acceleration	Base Moment	Frequency weighted acceleration	Base Moment
Old k_p	0.0344 m/s^2	124 150 kNm	0.137 m/s^2	220 800 kNm
New k_p	0.0343 m/s^2	123 840 kNm	0.136 m/s^2	220 000 kNm
Difference	-0.3 %	-0.25 %	-0.7 %	-0.4 %

Table 11.3: Effect of frequency change in peak factor calculations

As the table clearly illustrates, recalculating k_p for the right eigen frequencies provides negligible changes to response parameters. Since the peak factor directly scales the top acceleration, it is clear that major changes in k_p are crucial to peak values. For cross sectional forces and displacements, the total values includes static parts, which reduces the effect of the peak factor. However, the effect of the peak factor is easily tracked and understood, and thus no further parameter tests will be performed for k_p.

It is worth to notice that the peak factor also is included in the structural factor $c_s c_d$, which is a part of the NS-EN 1991-1-4 cross sectional force estimation in Section 7. In those calculations, the frequency estimate from appendix F was used for oscillations in both directions. The fact that the peak factor barely changed when the used frequency was altered, suggests that the peak factor assumption has limited effect on the Eurocode cross sectional force estimates as well.

11.6 Return Period in Acceleration Design

As seen in Section 10.2, the frequency weighted acceleration a_w exceeded the found perception limit for both modes. The perception limit from ISO 2631 does not come with any return period. As mentioned in Section 0, NS-EN 1991-1-4 provides a method for reducing the base wind velocity for a given return period. Using this method, the frequency weighted top acceleration has been calculated for return periods from 50 down to 1.5 years. Results are shown in Figure 11.9.

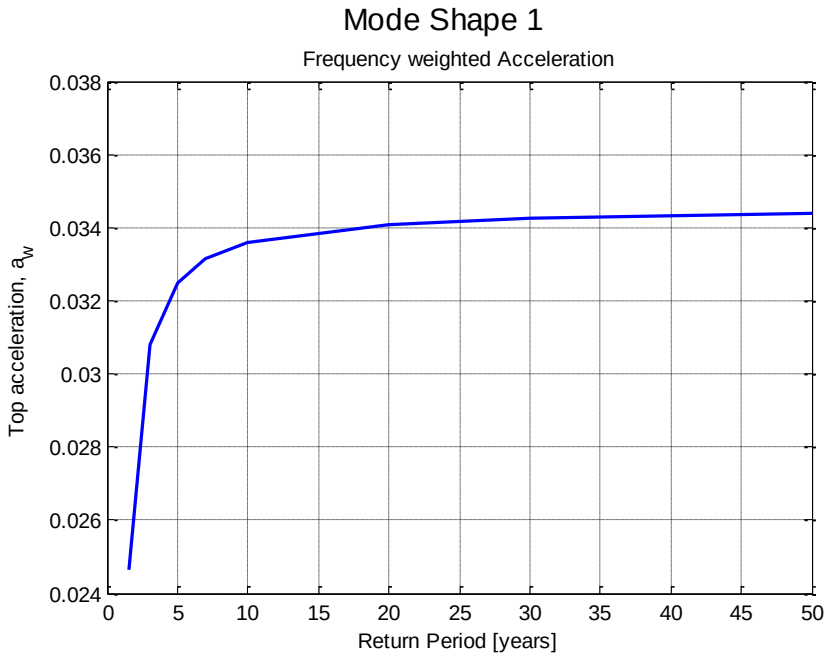

Figure 11.9: Change in frequency weighted acceleration caused by return period

As the figure clearly illustrates, the formula for base wind velocity reduction is extremely sensitive for low return periods. a_w is reduced by almost 30 % when the return period is decreased from 50 years to 1.5 years. The resulting a_w is only 24 % higher than the upper perception limit of 0.02 m/s^2.

It goes without saying that similar calculations for Mode 2 results in an equal plot, and thus there is no use in displaying the graph. The frequency weighted acceleration is again reduced by about 30 % when the return period is set to 1.5 years. However, since the initial value of

a_w is much higher for Mode 2, the acceleration value for a 1.5 years return period will still be almost 5 times higher than the perception limit.

In total, it is seen that reduction of return periods for wind will result in major changes of the frequency weighted acceleration. However, there is no return period given with the perception limit from ISO 2631, and thus a return period has to be determined for the given project. Regardless of this, it is seen that a_w will be higher than the perception limit even for low return periods.

11.7 Bending Stiffness EI

It was observed in Sections 9.6 and 10.1 that the static displacements and the resonant part of the cross sectional forces obtained values different from what was expected in advance. The reason proposed was that the estimated bending stiffness was too high. Although the influence of EI is relatively straightforward to trace both for displacements and forces (see equations (6.7) and (6.83)), the effect is shown graphically to see how much EI must change before results approach values that was expected in advance. The procedure chosen is to reduce the bending stiffness by 25 % 15 times. The lowest EI considered will then be about 1.3 % of the original value.

Since this study aims to illustrate the effect of EI, calculations have only been performed for wind loading on the short side of the building, corresponding to excitation of Mode 1. Figure 11.10 shows the variation of base moment and static displacement when the bending stiffness is reduced.

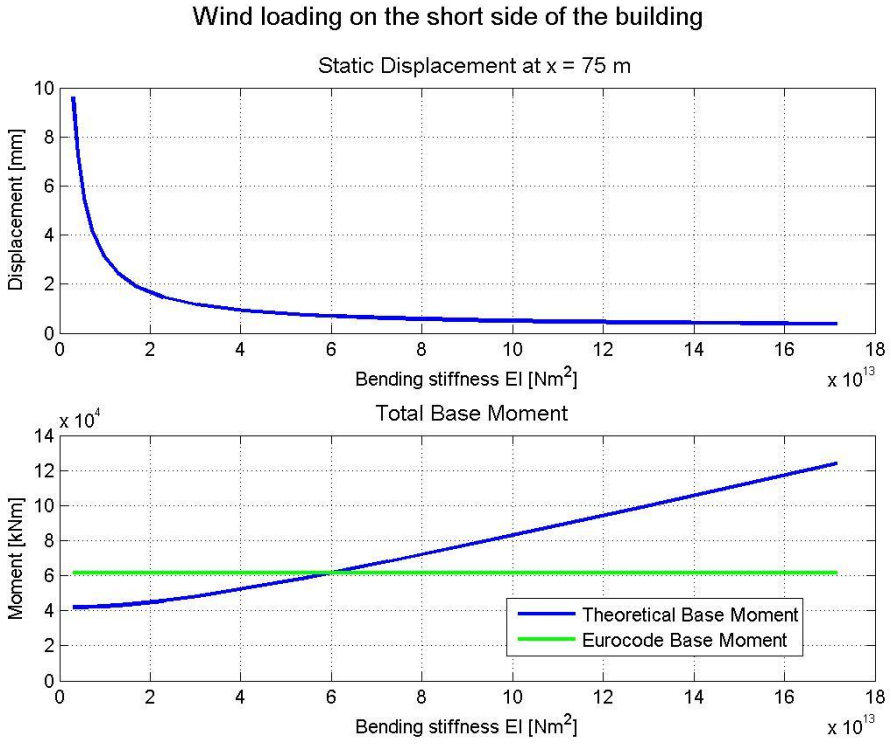

Figure 11.10: Effect of bending stiffness reduction

As the figure clearly illustrates, both static displacement and base moment approaches more realistic values when the bending stiffness is reduced. The static displacement is inversely proportional to EI. When the bending stiffness is reduced to less than 10 % of the original value, the static displacement starts to approach realistic values.

The base moment is plotted together with the moment obtained by using building design codes. The two moments are equal for a bending stiffness of about 35 % of the original value.

To sum up the above, it is seen that a substantial change in bending stiffness is needed to obtain trends that was expected in advance. Further discussion of the bending stiffness is done in Section 12.1.2.

11.8 Effect of the Parameter Studies

In this section, the effect of several parameters on the structural response has been demonstrated. To summarize the impact from different parameters, all studies are listed in Table 11.4 together with their effect on response. Percentages and trends given in the table are based on the probable values of the parameters given above. Green background indicate a reduction in response or cross sectional forces. Further explanation follows below.

	Acceleration		**Base Moment**	
	Wind against the short side (Mode 1)	**Wind against the long side** (Mode 2)	**Wind against the short side** (Mode 1)	**Wind against the long side** (Mode 2)
V in S_{ka} and $\hat{Co}$	-12 %	-13 %	-10 %	-3 %
z in ${}^{s}L_{n}$	+ 6 %	+6 %	+5 %	+1 %
Mass estimate	-	-	-	-
Damping estimate	-		-	
Peak factor k_p				
Return Period	(-)	(-)		
Bending Stiffness EI			(-)	(-)

Table 11.4: Summarized effects of parameter studies

To start from the top, the velocity used in S_{ka} and $\hat{Co}$ was seen to reduce both displacement response and cross sectional forces. The percentage given in Table 11.4 is based on an average velocity of 26.5 m/s. The height used in the integral length scales ${}^{s}L_{n}$ was seen to increase the response and cross sectional forces in three of four cases. The percentages in Table 11.4 are found for a height x_f of 40 meters, which is approximately the middle of the

possible range. Although this increases the output, the increase is less than the reduction caused by the velocity assumption above.

For the last five parameter tests, no clear percentage change is stated. The reason for this is that there is no way of saying whether the parameters really are higher or lower than the original estimates. In spite of this, assumptions that led to the original values could indicate what effect the parameters could have on the total response. For the original mass estimate an effort was made to keep the mass as low as possible, which again increased displacement, acceleration and cross sectional forces. Although the SLS mass could have been estimated even lower, the general effects of the mass estimates are probably conservative.

For damping, original estimates were made using literature. For Mode 1, the estimate chosen was the lowest of all estimates obtained. In other words, it is more likely that the damping of Mode 1 is assumed too low than too high. The result of this is that response and cross sectional forces for Mode 1 probably are conservative. For Mode 2, all damping estimates were relatively equal, and therefore there is no reason to expect any changes.

When recalculating peak factors for the real eigen frequencies, it was found that response and cross sectional forces decreased by a negligible percentage. In general, the peak factor has great effect on both dynamic displacement, acceleration and cross sectional forces. However, there are no other clear indications suggesting that the peak factor should be increased or reduced compared to the original value. The return period proved to reduce the frequency weighted acceleration by some amount. However, no conclusions could be made with respect to design acceleration without defining a return period acceptable for the project.

Finally, the cross sectional forces was seen to depend linearly on the bending stiffness EI. It is reasonable to assume that the bending stiffness is estimated too high, and thus the cross sectional forces would be correspondingly lower. Further discussions are done in Section 12.1.2.

In total, the effects described above are likely to reduce both response and cross sectional forces. While the influence of the different parameters vary, the total trend is that most of the parameters tested could give lower values for all response quantities. Although no changes will be made to the original calculated values, it must be kept in mind that the obtained results probably are conservative.

12 Considerations and Conclusion

In this master thesis, aerodynamic theory has been used to predict the response of a high rise concrete structure. Obtained results have been compared to values estimated by design codes, both to check validity of the results, and whether design limits are complied. In the following, possible error sources in the calculations are described and discussed. Then, the obtained results and findings are concluded upon. A short summary of additional work that could be performed is included at the end.

12.1 Error Sources

Before concluding on the obtained results, some important error sources should be mentioned. The calculations performed in this thesis include several parameters, which has been estimated to fit the given structure and the given conditions. It is clear that every estimation entails uncertainty and error potential. The effect of uncertainty from a given parameter could cause negligible response changes, or it could change conclusions completely. Small errors in each parameter could eliminate each other, or they could accumulate a significant error in the total result. To list every possible error source in this thesis would be impractical. The effect of changes in several parameters has already been investigated in Section 11. Below, some of the assumptions that could lead to errors in the calculations, or could have large impact on the results, have been accounted for.

12.1.1 Single Mode Single Component Assumption

The results obtained in this thesis demands that the modes of the system at hand are uncoupled. This implies that the eigen frequencies of each mode are sufficiently separated to avoid modal interaction. Although this assumption is used quite often in literature, there are few clear definitions of "well separated". To get an indication of whether the assumption is fulfilled, the bridge-part of the seismic standard NS-EN 1998-1-1 [35] is considered. §4.2.1.3 provides an expression for checking if two modes could be considered as closely spaced or not. The two periods T_i and T_j are closely spaced if

$$\frac{0.1}{0.1+\sqrt{\zeta_i\zeta_j}} \leq \frac{T_i}{T_j} \leq 1+10\sqrt{\zeta_i\zeta_j} \tag{12.1}$$

ζ represents the damping ratios for each mode. Looking at the periods obtained in Section 3.2, Table 3.2, it is easily seen that modes 1 and 2 are not closely spaced. Modes 2 and 3 on the other hand has frequencies that are relatively closely spaced. To ensure that Mode 2 could be calculated by a single mode single component approach, the test from equation (12.1) is applied to modes 2 and 3.

The natural periods are 0.936 and 0.819 seconds for modes 2 and 3 respectively. Using the values estimated from Section 5.5, the two relevant damping ratios are 0.012 and 0.017 for modes 1 and 2 respectively. Equation (12.1) gives

$$\frac{0.1}{0.1+\sqrt{0.012\cdot 0.017}} \le \frac{0.819}{0.937} \le 1+10\cdot\sqrt{0.012\cdot 0.017}$$

$$0.875 \le 0.874 \le 1.143 \tag{12.2}$$

It is seen from equation (12.2) that the condition is not satisfied, i.e. the two modes are not closely spaced. If modes 2 and 3 had been closely spaced, the combination of transversal and rotational motion should have been checked. This effect is called flutter, and is characterized as an instability problem.

12.1.2 Bending Stiffness EI

The bending stiffness was estimated in Section 8.6 by using CrossX and the concrete standard. Looking at the obtained static displacement and the resonant part of cross sectional forces obtained in Sections 9.6 and 10.1, there is reason to believe that the used bending stiffness is too high.

For the cross sectional forces, one could expect that fluctuations in the wind field would induce less forces than the static part. This is not the case for either modes, especially when the peak factor is included. When it comes to the static displacements, it is clear that less than a centimeter displacement for both directions is not correct for the structure when wind velocities approach hurricane strength. It is clear that a lower bending stiffness would both increase the static displacement and reduce the resonant part of cross sectional forces. It was shown in Section 11.7 that reduction of the bending stiffness (for loading on the short side) by 65 % or more would result in a base moment lower than what was obtained from design codes. Realistic values of the static displacement would demand a reduction of EI by more than 90 %.

The estimate of 2nd moment of inertia made in Section 8.6.1 rests on the assumption that every element of the cross section stretches over the entire height, which in reality would imply that the entire structure is casted at the construction site. However, the structure is built using precast elements. Adjacent elements are connected by reinforcement, and the pressure from the structural weight will stiffen each joint. Despite this, connections will not be as stiff as the elements themselves.

As a result of the above, it seems that the actual stiffness of the building is probably lower than the estimate. How much lower is impossible to say. Estimating the stiffness as a constant EI for the entire building could be characterized as a rough approximate at best. For accurate design procedures, a FEM model with distributed stiffness would be considerably more precise.

12.1.3 Derivation of Modal Shapes

When derivatives of modal shapes were estimated, it was assumed that the modal shapes resembled the theoretical shape function of a cantilevered beam. This approximation deserves some extra attention. Figure 12.1 shows mode shapes 1 and 2 plotted over the tower height. The two normalized shapes are almost identical. It is seen that the curvatures of the two

shapes are quite high for the first 20 meters, and thereafter the displacement increases linearly.

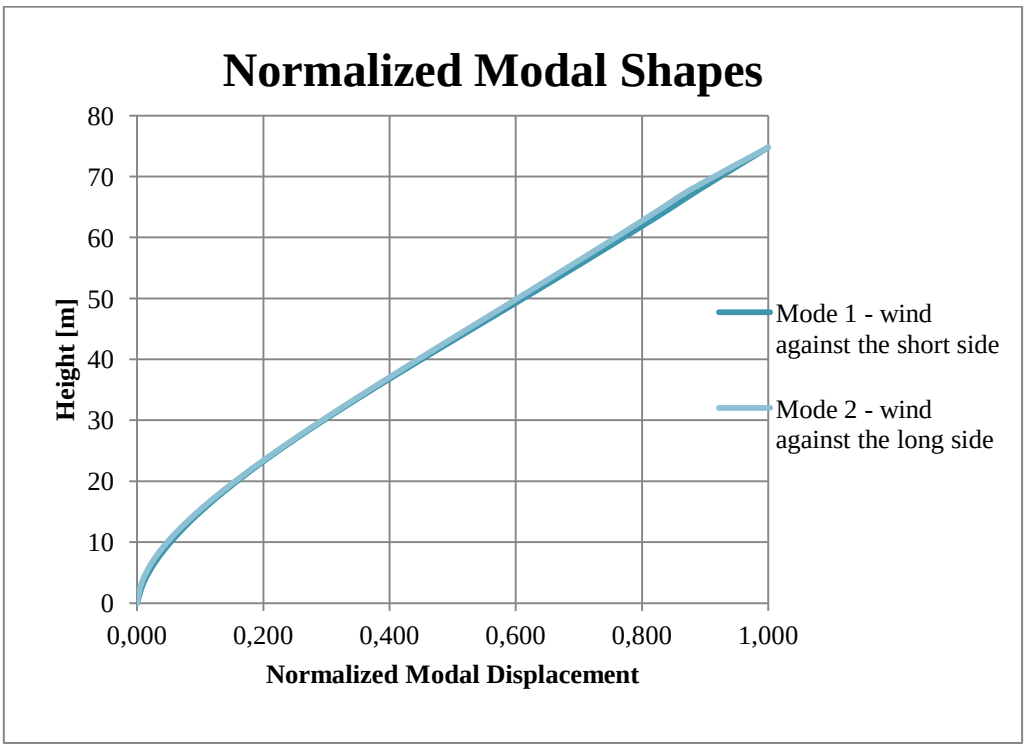

Figure 12.1: Normalized modal shapes, modes 1 and 2

As shown in equation (6.83), the resonant part of response depends on the 2nd and 3rd derivatives of the modal shapes. For the shapes shown in Figure 12.1, the linear displacement variation in the interval $x = [20m \rightarrow 75m]$ will have 2nd and 3rd derivatives approximately equal to zero. In other words, only the lower 20 meters of the structure contributes to the resonant cross sectional forces. Figure 12.2 shows mode shapes 1 and 2 alongside the theoretical cantilever estimates from Section 8.8 for the lower 15 meters of the structure.

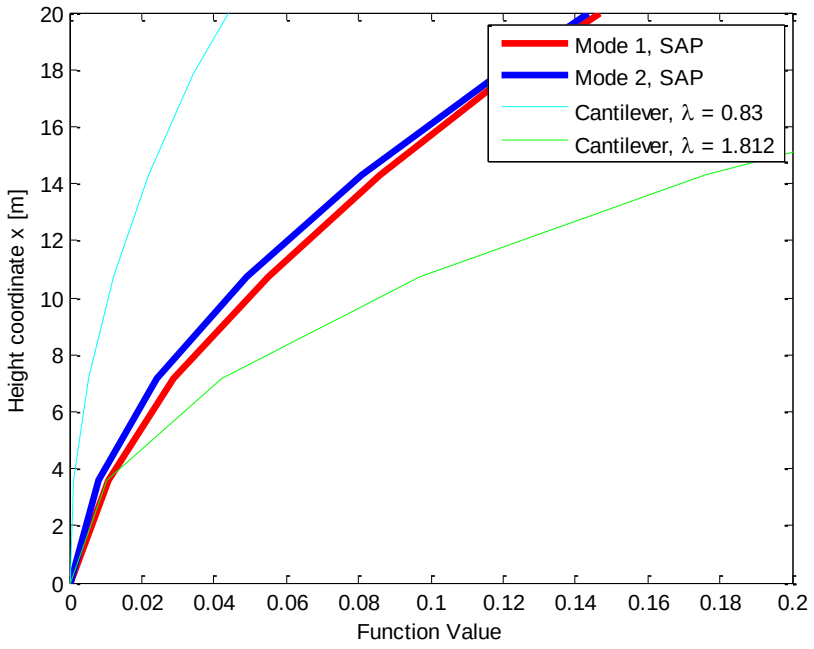

Figure 12.2: Theoretical cantilever vs. actual mode shapes, 0 - 15 meters

As the figure shows, the theoretical cantilever with calculated λ_n-values fails to predict the actual modal shapes. Modal shapes obtained from SAP2000 behave like cantilevers only for the lower 20 meters. The bending stiffness used to calculate the λ_n-values does not necessarily reflect the stiffness of the 3D FEM model from SAP2000. The mass is also somewhat different. If the SAP2000 modal shapes and cantilever estimates coincided, it would be a coincidence rather than an expected result.

It should be mentioned that curve fitting of the modal shapes from SAP2000 was attempted. This was abandoned as the SAP2000 modal shapes had curvatures that approached infinity when x approached 0.

The effect of the modal derivatives is restricted to the resonant part of cross sectional forces. This contribution was shown in Section 9.5 to dominate cross sectional forces for wind against the short side. For wind against the long side, the contribution was smaller, but still significant. Like mentioned above when discussing the bending stiffness, the resonant part was expected to be less significant for the total cross sectional forces. Such a result would be obtained if the mode shape derivatives were smaller.

12.1.4 Shape of the Building and Wind Direction

Although the building was modeled in SAP2000 with approximately the exact cross sectional shape (see Section 3.1.2), all response calculations have been performed for a simplified rectangular cross section. In the forthcoming, some possible effects of this simplification are

accounted for. Figure 12.3 shows the actual cross sectional shape, and the different principal wind directions.

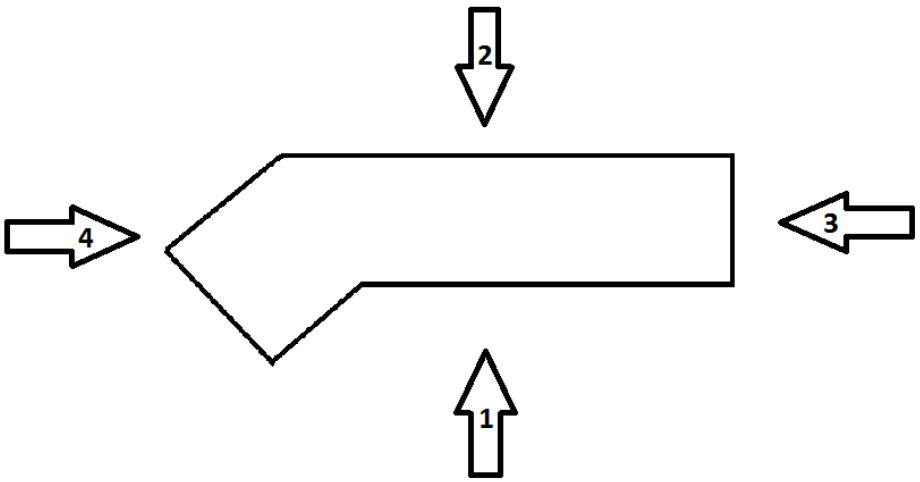

Figure 12.3: Cross sectional shape and wind directions

Wind acting on the long side, which excites Mode 2, could have increased or decreased effect depending on the wind direction. If the main flow is directed like flow 1 in Figure 12.3, the middle bend would increase the wind pressure, resulting in increased displacements and cross-sectional forces. Similarly, if the main flow is directed like flow 2 in Figure 12.3, the wind could flow easier past the left side of the building sketch, decreasing the wind pressure on the structure.

The actual cross sectional shape could affect results for main wind flow in directions 3 and 4 as well. Although it was shown in Section 6.1.3 that Vortex Shedding was not a problem for the rectangular estimate, the same conclusion is not as easily made for the actual cross sectional shape.

A rectangular cross section would induce little or no response perpendicular to the main flow directions from Figure 12.3. For the actual cross section, wind flow in the directions indicated in Figure 12.3 would result in force components perpendicular to flow, which would give response in more than one direction. This effect disappears when the cross section is assumed rectangular.

Another aspect of the calculations that has been neglected is wind at an angle, i.e. main flow in a direction different from the ones indicated in Figure 12.3. The original assumption of wind flow parallel to the main directions of the structure creates maximal response for each of the considered modes. Wind at an angle would change the response pattern. Several modes would be excited at the same time. In addition, "lift" forces perpendicular to the main flow direction would be induced. The total response situation would be much more complicated than the one assumed in this thesis, and a multi mode response calculation would be required to evaluate the system.

12.1.5 Including a Rotational Mode

As stated in Section 6, only the two first translational modes have been considered in the response calculations. The theoretical basis needed to calculate the response of the rotational Mode 3 is quite similar to what has been used for the two translational modes. Thus, including the rotational mode would not increase the learning outcome. However, the rotational Mode 3 is included as an error source because it could provide response that is relevant for the total results. Considering cross sectional forces, a rotational mode would induce a torsional base moment, which is not of much interest. When it comes to displacements and accelerations, a rotational motion could induce considerable accelerations at the upper corners of the structure. Referring to Table 3.2 in Section 3.2, it is seen that Mode 3 has an eigen frequency within the least favorable area when it comes to human comfort (see Figure 4.1). Accelerations given by Mode 3 oscillations could therefore be crucial for design.

12.1.6 FEM-Model in SAP2000

Like mentioned on several occasions, the FEM-modeling in SAP2000 was done to resemble the structure as much as possible. The output gathered from SAP2000 was modal shapes and eigen frequencies. To start with the modal shapes, displacement values was gathered from each floor, providing 22 output points. This meshing of the modal shapes removed the displacement pattern between floors. Like mentioned in Section 8.1, the displacement between floors was approximated by a linearization. However, the study building resembles a shear frame, which does not deform linearly between floors. A comparison between a general shear frame displacement and the obtained modal shapes is shown in Figure 12.4.

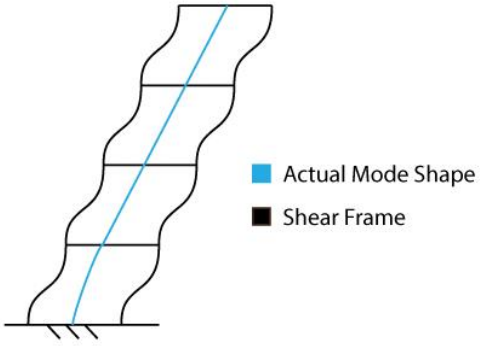

Figure 12.4: Shear frame vs. SAP2000 modal shapes

It is seen that the displacement pattern between floors for a shear frame does not resemble the linear behavior demonstrated by the actual modal shapes. Modal shape vectors are included in all calculations. Thus, the effect of a change in the ϕ-vectors would affect all response parameters obtained in this thesis.

The eigen frequencies found in SAP2000 have been used for most calculations that does not involve building design code estimation. Like mentioned in Section 3.1.2, the FEM model

included no live loads. The applied dead loads used in the mass estimate from Section 8.5 were not included either. This results in a lower mass for the model than what could be expected for the real structure. The result of a lower mass would be higher eigen frequencies, which again would affect response calculations.

12.2 Considerations Regarding Acceleration

The most important response parameter calculated in this thesis is acceleration at the tower top. This value could be decisive for building design, because high accelerations on the upper floors leads to discomfort for occupants. In Section 4, an upper perception limit of 0.02 m/s^2 given by ISO 2631-1 was established. It was stated that inhabitants of buildings tend to complain if the frequency weighted acceleration exceed the perception limit.

To check whether accelerations at the top of Lerkendal Hotel are acceptable, the peak acceleration was calculated both by using building codes and aerodynamic theory with frequency weighting. Both methods gave accelerations that were considerably higher than the perception limit. The fact that accelerations estimated from building codes and frequency weighted accelerations calculated from theory was relatively similar indicates that the calculated accelerations are correct, and thus that perception demands for the top of Lerkendal Hotel are not fulfilled.

Some additional comments should be made about the acceleration considerations. The first one concerns the concept of perception. Although oscillations in a structure are perceptible, they do not necessarily cause discomfort for inhabitants. The next comment regards the building use. As mentioned in Section 2.2, the lower floors of the hotel will be booked first to reduce energy consumption. On lower floors, the displacement amplitude and therefore the acceleration will be significantly lower than at the top where design values are calculated. In light of the two comments made above, it could be argued that the perception limit is too strict for design of the given structure.

There are several measures that could be implemented to reduce the acceleration in a structure. One of the most basic measures is to change the mass- or stiffness properties. A higher mass would result in both lower eigen frequencies and lower displacement amplitudes, which would reduce the acceleration. Another alternative is tuned mass dampers. These consists of masses that are tuned to move opposite of the structures eigen frequency oscillations. This motion will reduce the response amplitudes of the structure, and therefore also the accelerations.

12.3 Considerations Regarding Cross Sectional Forces

Wind-induced cross sectional forces at the base of the structure have been calculated both by building design codes and by aerodynamic theory. The calculated cross sectional forces are not calculated for design purposes, but rather to compare aerodynamic theory to building design codes. Forces were calculated for oscillations in two directions. For the direction corresponding to Mode 1, aerodynamic theory provided larger forces than building design codes. For the direction corresponding to Mode 2, the forces estimated by building design codes were larger than the ones calculated by aerodynamic theory.

Building design codes are generally conservative, which would imply that forces calculated by the building design codes could be expected higher than the ones calculated from aerodynamic theory. This was the case only for one of the two calculated directions. A possible explanation for the unexpected results for wind against the short side is given Section

12.1.2. For wind against the long side, the deviation between cross sectional forces obtained by design codes and aerodynamic theory was about $1/5$, which is acceptable given all the uncertainty included in both calculation methods.

12.4 Conclusion

Summing up the considerations made above, it is found that the cross sectional forces calculated for the structure deviate by some amount from Eurocode estimates. The high values obtained for wind against the short side are probably caused by the high bending stiffness used in the resonant cross sectional forces. The results for wind against the long side are fairly reasonable.

Acceleration at the top of the structure is found to be high. To compare the acceleration to perception limits found in building codes, it has been weighted by a frequency filter. The frequency weighted acceleration corresponds well to acceleration estimated by the wind standard NS-EN 1991-1-4. This supports the considerable size of the accelerations calculated by aerodynamic theory.

The frequency weighted acceleration is found to be 70 % higher than the upper perception limit for Mode 1 (wind against the short side), and almost 7 times higher than the upper perception limit for Mode 2 (wind against the long side). The calculated values raises a demand for special measures to reduce the displacement and acceleration in the building. However, given the pattern of use for the hotel, the 50 year return period of wind velocity and the difference between perception and comfort, the perception limit used may be too strict.

Throughout the calculations, key quantities have been tracked to ensure that they obtain reasonable values. Parameter studies have been performed to investigate the effect of assumptions made in the calculations. The parameter studies indicate that calculated values could have been somewhat lower. However, the possible changes would not have major effect on the considerations and conclusions made in this thesis.

12.5 Further Work

Although a substantial effort has been put into the theoretical research, calculations and considerations of this thesis, there is potential for additional exploration of the subject. The following describes shortly some of the aspects that could be investigated, and what effect they could have.

- Wind tunnel testing could be used to establish exact values for drag and lift coefficients. This would lead to higher accuracy in all calculations, and enable calculation of wind at an angle with the correct coefficients.
- Although the effects of Flutter and Vortex Shedding are shown to be irrelevant, calculating the response caused by the two phenomena would illuminate the impact they have on the total response. It would also provide a great learning outcome.
- As mentioned, the rotational Mode 3 has not been included in the calculations. It would be interesting to check the response of this mode, especially considering acceleration.
- If three or more modes were included in the calculations, a multi mode calculation process would be the most convenient calculation procedure. The three first modes would be calculated together, resulting in response in both transversal directions and rotation. Such an approach would also allow calculating wind at an angle. The response from such calculations could differ from what is obtained in this thesis.
- FEM analysis could be conducted using response spectrums or time series to simulate the wind field. This would enable calculation of forces in individual structural components, which is required for design.

13 References

1. Strømmen, E.N., *Theory of Bridge Aerodynamics*. 2010, Berlin: Springer.

2. Dyrbye&Hansen, *Wind Loads on Structures*. 1999, Chichester: Wiley.

3. Wikipedia. *Liste over høye bygninger i Norge*. http://no.wikipedia.org/wiki/Liste_over_h%C3%B8ye_bygninger_i_Norge 2012 [cited 2013 23.04].

4. Anleggsmaskinen, *Bygger Trondheims nye landemerke*, in *Anleggsmaskinen 10-2012*, Maskinentreprenørenes Forbund MEF: http://www.mef.no/ikbViewer/page/mef/fakta-om-bransjen/anleggsmaskinen.

5. ScandicHotels.no. *Scandic Lerkendal*. http://www.scandichotels.no/Hotels/Countries/Norge/Trondheim/Hotels/Lerkendal/#.UXZ15rV7Kp0 2012 [cited 2013 23.04].

6. Rambøll. *Utvikler Løsninger til "Verdens mest energivennlige hotell"*. http://www.ramboll.no/news/viewnews?newsid=A18AFABB-F69E-4B67-90C8-316CDEE016BE 2012 [cited 2013 23.04].

7. NVE. *Energimerking.no - Energimerking for bygninger*. http://www.energimerking.no/no/Energimerking-Bygg/Om-energimerkesystemet-og-regelverket/Energimerkeskalaen/ 2011 [cited 2013 23.04].

8. TEK10, *TEK 10: Forskrift om tekniske krav til byggverk (byggteknisk forskrift): 26. mars 2010 nr. 489. Updated, 28. mach 2012 og 15. june 2012* ed. N.K.-o. regionaldepartementet. 2012, Oslo: Norsk byggtjenestes forlag.

9. Sweco. *Miljø-og energieffektivitet ved Lerkendal hotell*. http://www.sweco.no/no/norway/Markedsomraader/Bygninger/Kontorer/Verdens-mest-energieffektive-hotell/ 2012 [cited 2013 23.04].

10. Chopra, A.K., *Dynamics of structures : theory and applications to earthquake engineering*. 2007, Upper Saddle River, N.J.: Pearson Prentice Hall.

11. StandardNorge, *Eurokode 1: Laster på konstruksjoner, Del 1-4, Allmenne laster. Vindlaster*. 2009, Lysaker: Standard Norge.

12. Ellis, B.R., *An assessment of the accuracy of predicting the fundamental natural frequencies of buildings and implications concerning the dynamic analysis of structures.* Proceedings of the Institution of Civil Engineers, Part 2, 1980. **69**: p. 763-776.

13. Lagomarsino, S., *Forecast models for damping and vibration periods of buildings.* Journal of Wind Engineering and Industrial Aerodynamics, 1993. **48**(2–3): p. 221-239.

14. StandardNorge, *Eurokode 0: grunnlag for prosjektering av konstruksjoner*. 2008, Lysaker: Standard Norge.

15. ISO, *ISO 10137:2007; Bases for Design of Structures - Serviceability of Buildings and Walkways Against Vibrations*, 2007: StandardNorge.

16. ISO, *NS-ISO 2631-1 and 2:1997: Mechanical Vibrations and Shock - Evaluation of Human Exposure to Whole-Body Vibration*, 1997: StandardNorge.

17. Satake, N., et al., *Damping Evaluation Using Full-Scale Data of Buildings in Japan.* Journal of Structural Engineering, 2003. **129**(4): p. 470-477.

18. Kareem, A. and K. Gurley, *Damping in structures: its evaluation and treatment of uncertainty.* Journal of Wind Engineering and Industrial Aerodynamics, 1996. **59**(2–3): p. 131-157.

19. Strømmen, E.N., *Guidance meeting, conversation regarding structural damping Aprl 21.*, K.H. Bjørnland, Editor 2013.

20. WMO. *Info Note 58: World Record Wind Gust*. http://www.wmo.int/pages/mediacentre/infonotes/info_58_en.html 2010 [cited 2013 19.05].

21. Irgens, F., *Fasthetslære*. 1999, Trondheim: Tapir.

22. Kaimal, J.C., et al., *Spectral characteristics of surface-layer turbulence.* Quarterly Journal of the Royal Meteorological Society, 1972. **98**(417): p. 563-589.

23. Davenport, A.G., *The Response of Slender, Line-Like Structures to a Gusty Wind.* Ice Proceedings, 1962. **23**: p. 389-408.

24. Strømmen, E.N., *Guidance meeting, conversation regarding aerodynamic coefficients, March 21.*, K.H. Bjørnland, Editor 2013.

25. Lin, N., et al., *Characteristics of wind forces acting on tall buildings.* Journal of Wind Engineering and Industrial Aerodynamics, 2005. **93**(3): p. 217-242.

26. SINTEF. *Teknisk Godkjenning: Contech Prefabrikkerte Baderomsmoduler*. 2012.

27. StandardNorge, *Eurokode 1: Laster på konstruksjoner, Del 1-1, Allmenne laster : Tetthet, egenvekt og nyttelaster i bygninger*. 2008, Oslo: Standard Norge.

28. Vagnildhaug, Ø., *E-mail correspondance regarding cross sectional data, April 8.*, K.H. Bjørnland, Editor 2013.

29. Kolbein Bell, O.B., Lars Wollebæk, *CrossX*, 2000: NTNU Trondheim. p. A Windows-based program for computation of parameters for and stress distribution on arbitary beam cross sections.

30. StandardNorge, *Eurokode 2: Prosjektering av betongkonstruksjoner, Del 1-1, Allmenne regler og regler for bygninger*. 2008, Lysaker: Standard Norge.

31. Clausen, A.H., *Lecture Note 3: Tøyningsenergi, Mechanics 3*, in *TKT4124, NTNU*2010.

32. Strømmen, E., *Continous Systems, Eigen value calculations for simple beams*. 2013, Springer: Berlin.

33. WolframResearchCompany. *Wolfram|Alpha: http://www.wolframalpha.com/*. web calculator [cited 2013 18.04].

34. Harstvedt, S.N.L.P.D.K.E. *Wind http://snl.no/vind*. 2012 [cited 2013 26.04].

35. StandardNorge, *Eurokode 8: Prosjektering av konstruksjoner for seismisk påvirkning, Del 2, Bruer*. 2005, Lysaker: Standard Norge.

36. Kreyszig, E., H. Kreyszig, and E.J. Norminton, *Advanced engineering mathematics*. 2011, Hoboken, N.J.: Wiley.

APPENDIX 1:
Modal Displacements from SAP2000

Height	**SAP2000**	**Mode 1**	**SAP2000**	**Mode 2**	**Appendix F.3**	**Appendix F.3**
z [m]	Mode 1	Normalized	Mode 2	Normalized	ξ = 1	ξ = 1.5
0	0.000	0.000	0.000	0.000	0.000	0.000
3.4	0.188	0.011	0.077	0.008	0.045	0.010
6.8	0.516	0.029	0.246	0.024	0.091	0.027
10.2	0.967	0.055	0.502	0.049	0.136	0.050
13.6	1.523	0.086	0.827	0.081	0.182	0.078
17	2.167	0.122	1.206	0.119	0.227	0.108
20.4	2.886	0.163	1.628	0.160	0.273	0.142
23.8	3.670	0.207	2.083	0.205	0.318	0.179
27.2	4.507	0.255	2.565	0.252	0.364	0.219
30.6	5.388	0.304	3.066	0.302	0.409	0.262
34	6.303	0.356	3.584	0.353	0.455	0.306
37.4	7.244	0.409	4.113	0.405	0.500	0.354
40.8	8.202	0.463	4.650	0.458	0.545	0.403
44.2	9.171	0.518	5.193	0.511	0.591	0.454
47.6	10.144	0.573	5.737	0.565	0.636	0.508
51	11.115	0.628	6.280	0.618	0.682	0.563
54.4	12.079	0.682	6.821	0.671	0.727	0.620
57.8	13.033	0.736	7.357	0.724	0.773	0.679
61.2	13.974	0.789	7.888	0.776	0.818	0.740
64.6	14.906	0.842	8.412	0.828	0.864	0.803
68	15.803	0.893	8.932	0.879	0.909	0.867
74.8	17.702	1.000	10.160	1.000	1.000	1.000

APPENDIX 2:
NS-EN 1991-1-4 Acceleration Estimate

Calculations performed in this appendix are based on NS-EN 1991-1-4 [11]. Two methods are used to calculate the peak acceleration at the top of the study building as a result of wind loading. The two methods used are given in Appendix B and C in the standard. According to the Norwegian Annex § NA.6.3.2, none of the two methods are preferable to the other.

Generally About the Methods

Both calculation methods provides a peak acceleration value by multiplying the standard deviation of acceleration by a factor k_p. The resulting product gives the characteristic top value of acceleration. Calculations are performed for wind acting on both sides of the building.

Since this is a simplified approximation, the building is assumed to have rectangular cross section of 45 times 15 meters. The height is set to 75 meters. Terrain category is assumed to be category III (Appendix A in the standard). Furthermore, §6.3.1(2) gives $z_s = 45m$, while Table 4.1 gives $z_0 = 0.3m$. For Trondheim, Table NA.4(901.1) gives $v_b = 26$ m/s. Also the first natural frequency of the building needs to be determined. Appendix F §F.2(2) suggests for buildings higher than 50 m that $n_{1,x} = \frac{46}{h} = 0.613\text{Hz}$. NA.4.5 gives the density of air as $\rho_{air} = 1.25\left[kg/m^3\right]$

The factor k_p is given by §B.2. The zero upcrossing frequency ν should according to §B.4(4) and §C.4(3) be set equal to the estimated eigen frequency $n_{1,x} = 0.613\text{Hz}$. Using Figure B.2, it is obtained that $k_p = 3.6$.

Because two modes are calculated, there will be two sets of values for each method. The upper value in all equations equals wind loading on the long side (Mode 2), while the bottom value equals wind loading on the short side (Mode 1).

Appendix B - Method B

Method B states the following expression for standard deviation of the acceleration in the wind direction (B.10):

$$\sigma_{a,x} = \frac{c_f \cdot \rho \cdot b \cdot I_v(z_s) \cdot v_m^2(z_s)}{m_{1,x}} \cdot R \cdot K_x \cdot \Phi_{1,x}(z)$$

The force factor c_f is given by §7.6(1) as $c_f = \psi_r \cdot \psi_\lambda \cdot c_{f,0}$

It is assumed that $\psi_r = 1$. Using §7.13, it is found that

$$\lambda = 1.4 * \mathrm{h}/\mathrm{b} = \begin{cases} 2.33 \text{ for b} = 45 \text{ m} \\ 7 \text{ for b} = 15 \text{ m} \end{cases}$$

For the found λ values, figure 7.36 with $\varphi = 1$ provides that $\psi_\lambda = \begin{cases} 0.63 \\ 0.68 \end{cases}$

From figure 7.23, with $b/d = \begin{cases} 3.0 \\ 0.33 \end{cases}$, it is obtained that $c_{f,0} = \begin{cases} 2.1 \\ 1.3 \end{cases}$

The resulting force factors are given by

$$c_f = \begin{cases} 1 \cdot 0.64 \cdot 2.2 = 1.323 \\ 1 \cdot 0.68 \cdot 1.3 = 0.884 \end{cases}$$

$I_v(z_s)$ is turbulence intensity at height $z_s = 45m$, given by

$$I_v(z_s) = \frac{k_r v_b k_l}{v_m(z_s)}.$$

The mean wind velocity is given by

$$v_m(z_s) = c_r(z_s) \cdot v_b \cdot c_0(z_s).$$

By using § 4.4, 4.3.1, table NA.4.3.2 and 4.3.2, it is obtained that

$$k_r = 0.22,\ c_r = k_r \cdot \ln(\frac{z}{z_0}) = 1.102,\ c_0 = 1,\ k_l = 1$$

$$v_m(z_s) = 1 \cdot 26 \cdot 1.102 = 28.7\left[m/s\right]$$

$$I_v(z_s) = \frac{1.102 \cdot 26 \cdot 1}{28.7} = 0.199.$$

$m_{1,x}$ is the equivalent mass in the wind direction. It can be approximated using §F.4(2), which states that m_e could be set as the average mass over the top third of the structure. This mass has been estimated for SLS in Appendix 5 to be approximately 225 200 kg/m.

R represents the resonant part of response, and is given by § B.2(5) as

$$R = \sqrt{\frac{\pi^2 \cdot S_L \cdot R_h \cdot R_b}{2 \cdot \delta}}$$

§ B.1 gives

$$S_L = \frac{6.8 \cdot f_L}{(1 + 10.2 \cdot f_L)^{5/3}}$$

$$f_L(z_s, n_{1,x}) = \frac{n_{1,x} \cdot L(z_s)}{v_m(z_s)}.$$

$$L(z_s) = L_t \cdot \left(\frac{z_s}{z_t}\right)^{0.67+0.05\ln(z_0)} = 300 \cdot \left(\frac{45}{200}\right)^{0.67+0.05\cdot\ln(0.3)} = 120.8, \text{ and thus}$$

$$f_L(z_s, n_{1,x}) = \frac{0.613 \cdot 120.8}{28.7} = 2.58, \text{ which gives}$$

$$S_L = \frac{6.8 \cdot 2.58}{(1+10.2 \cdot 2.58)^{5/3}} = 0.071$$

§ B.2(6) states that

$$R_{h,b} = \frac{1}{\eta_{h,b}} - \frac{\left(1-e^{-2\cdot\eta_{h,b}}\right)}{2\cdot{\eta_{h,b}}^2}$$

Values found above gives that $\eta_h = 7.37,\ \eta_{b,45} = 4.42$ and $\eta_{b,15} = 1.47$.
Inserting the η-values, it is obtained that $R_h = 0.126,\ R_{b,45} = 0.201$ and $R_{b,15} = 0.461$.

The total logarithmic decrement of damping, δ, is given by appendix F.5 as

$$\delta = \delta_s + \delta_a = (\text{Table F.2}) + \frac{c_{f,i} \cdot \rho \cdot b \cdot v_m(z_s)}{2 \cdot n_{1,x} \cdot m_e} = \begin{cases} 0.1 + \dfrac{1.323 \cdot 1.25 \cdot 45 \cdot 28.7}{2 \cdot 0.613 \cdot 225200} = 0.108 \\ 0.1 + \dfrac{0.884 \cdot 1.25 \cdot 15 \cdot 28.7}{2 \cdot 0.613 \cdot 225200} = 0.102 \end{cases}$$

In total, R is found as

$$R = \begin{cases} \sqrt{\dfrac{\pi^2 \cdot 0.071 \cdot 0.126 \cdot 0.201}{2 \cdot 0.108}} = 0.287 \\ \sqrt{\dfrac{\pi^2 \cdot 0.071 \cdot 0.126 \cdot 0.461}{2 \cdot 0.102}} = 0.447 \end{cases}$$

K_x is a dimensionless factor. It can be approximated by utilizing the mode shape suggested in § F.3, which says that $\Phi_1(z) = \left(\frac{z}{h}\right)^{\zeta}$, where it is assumed that $\zeta = 1$. This gives the following expression:

$$K_x = \frac{(2\cdot\zeta+1)\cdot\left\{(1+\zeta)\cdot\left[\ln\left(\frac{z_s}{z_0}\right)+0.5\right]-1\right\}}{(\zeta+1)^2\cdot\ln\left(\frac{z_s}{z_0}\right)} = \frac{3\cdot\left\{2\cdot\left[\ln\left(\frac{45}{0.3}\right)+0.5\right]-1\right\}}{4\cdot\ln\left(\frac{45}{0.3}\right)} = 1.5$$

It is noted that the mode shape function has value 1 at the top, where the acceleration is calculated. Now, all the different terms of the $\sigma_{a,x}$ - expression have been obtained, and thus

$$\sigma_{a,x,B} = \frac{c_f \cdot \rho \cdot b \cdot I_v(z_s) \cdot v_m^2(z_s)}{m_{1,x}} \cdot R \cdot K_x \cdot \Phi_{1,x}(z)$$

$$= \begin{cases} \dfrac{1.323 \cdot 1.25 \cdot 45 \cdot 0.199 \cdot 28.7^2}{225200} \cdot 0.287 \cdot 1.5 \cdot 1 = 0.0233 \\ \dfrac{0.884 \cdot 1.25 \cdot 15 \cdot 0.199 \cdot 28.7^2}{225200} \cdot 0.447 \cdot 1.5 \cdot 1 = 0.0081 \end{cases}$$

The peak acceleration at the top of the building is then

$$a_{peak,B} = \sigma_{a,x,B}(z) \cdot k_p = \begin{cases} 0.0233 \cdot 3.6 \simeq \mathbf{0.084\,m/s^2}, & \text{Wind on long side} \\ 0.0081 \cdot 3.6 \simeq \mathbf{0.029\,m/s^2}, & \text{Wind on short side} \end{cases}$$

Appendix C - Method C

Appendix C provides the following expression for the standard deviation of acceleration:

$$\sigma_{a,x} = \frac{c_f \cdot \rho \cdot I_v(z_s) \cdot v_m^2(z_s)}{\mu_{ref} \cdot \Phi_{\max}} \cdot R \cdot K_z \cdot K_y \cdot \Phi(y,z)$$

Most of the parameters above have already calculated. Since the acceleration is calculated at the top of the building, it is noted that $\dfrac{\Phi(y,z)}{\Phi_{\max}} = 1$.

The Resonant-factor is calculated differently in appendix C, namely

$R = \sqrt{\dfrac{\pi^2 \cdot S_L \cdot K_s}{2 \cdot \delta}}$, where K_s is a new factor given by

$$K_s(n) = \frac{1}{\sqrt{(G_y \cdot \phi_y)^2 + (G_z \cdot \phi_z)^2 + \left(\dfrac{2}{\pi} \cdot G_z \cdot \phi_z \cdot G_y \cdot \phi_y\right)^2}}$$

Using Table C.1 note 1, it is found that $G_y = 1/2,\ G_z = 3/8,\ \mathrm{K}_y = 1$ and $\mathrm{K}_z = 3/2$.

C.2(5) gives

$$\phi_{y,45} = \frac{c_y \cdot b_{45} \cdot n_{1,x}}{v_m(z_s)} = \frac{11.5 \cdot 45 \cdot 0.613}{28.7} = 11.05,$$

$$\phi_{y,15} = \frac{c_y \cdot b_{15} \cdot n_{1,x}}{v_m(z_s)} = \frac{11.5 \cdot 15 \cdot 0.613}{28.7} = 3.68,$$

$$\phi_z = \frac{c_z \cdot h \cdot n_{1,x}}{v_m(z_s)} = \frac{11.5 \cdot 75 \cdot 0.613}{28.7} = 18.42$$

In total,

$$K_s(n) = \begin{cases} \dfrac{1}{\sqrt{(0.5\cdot 11.05)^2 + ((3/8)\cdot 18.42)^2 + \left(\dfrac{2}{\pi}\cdot 0.5\cdot 11.05\cdot (3/8)\cdot 18.42\right)^2}} = 0.0387 \\ \dfrac{1}{\sqrt{(0.5\cdot 3.68)^2 + ((3/8)\cdot 18.42)^2 + \left(\dfrac{2}{\pi}\cdot 0.5\cdot 3.68\cdot (3/8)\cdot 18.42\right)^2}} = 0.0926 \end{cases}$$

R for Method C is then found as

$$R = \begin{cases} \sqrt{\dfrac{\pi^2\cdot 0.071\cdot 0.0387}{2\cdot 0.108}} = 0.354 \\ \sqrt{\dfrac{\pi^2\cdot 0.071\cdot 0.0926}{2\cdot 0.102}} = 0.564 \end{cases}$$

μ_{ref} represents the reference mass per unit area normal to wind direction. This corresponds to dividing m_e by the width b.

$$\mu_{ref} = \begin{cases} \mathrm{m}_e / b_{45} = 225200/45 = 5004\ \mathrm{kg/m^2} \\ \mathrm{m}_e / b_{15} = 225200/15 = 15013\ \mathrm{kg/m^2} \end{cases}$$

Now all the expressions are known, and thus;

$$\sigma_{a,x,C} = \frac{c_f\cdot\rho\cdot I_v(z_s)\cdot v_m^2(z_s)}{\mu_{ref}\cdot\Phi_{\max}}\cdot R\cdot K_z\cdot K_y\cdot\Phi(y,z)$$

$$= \begin{cases} \dfrac{1.323\cdot 1.25\cdot 0.199\cdot 28.7^2}{5004}\cdot 0.354\cdot 1\cdot 1.5 = 0.0288 \\ \dfrac{0.884\cdot 1.25\cdot 0.199\cdot 28.7^2}{15013}\cdot 0.564\cdot 1\cdot 1.5 = 0.0102 \end{cases}$$

The peak acceleration at the top of the building is then

$$a_{peak,C} = \sigma_{a,x,C}(z)\cdot k_p = \begin{cases} 0.0306\cdot 3.6 \simeq \mathbf{0.104\,m/s^2}, & \text{Wind on long side} \\ 0.0102\cdot 3.6 \simeq \mathbf{0.037\,m/s^2}, & \text{Wind on short side} \end{cases}$$

APPENDIX 3:
Damping Estimates, Excel

Period and Frequency Estimates

Frequencies and Periods	Mode 1		Mode 2		Mode 3	
	f [Hz]	T [s]	f [Hz]	T [s]	f [Hz]	T [s]
Ellis (NS-EN 1991-1-4)	0.6133	1.6305	0.7733	1.2932	0.96	1.0417
Lagomarsino	0.7333	1.3637	-	-	1.04	0.9615
SAP2000	0.596	1.6779	1.0677	0.9366	1.2214	0.8187

Damping Estimates

Damping Estimate	Frequency/Period Estimate	Mode 1		Mode 2	Mode 3
		Decrement	**Ratio ζ**	**Ratio ζ**	**Ratio ζ**
Lagomarsino	Ellis (NS-EN)	-	0.016	0.015	0.014
	Lagomarsino	-	0.015	-	0.014
	SAP2000	-	0.016	0.014	0.015
Satake	Ellis	-	0.009	0.012	0.017
	Lagomarsino	-	0.010	0.014	0.020
	SAP2000	-	**0.008**	**0.012**	**0.017**
NS-EN 1991-1-4	Ellis	0.110	0.018	-	-
	Lagomarsino	0.109	0.017	-	-
	SAP2000	0.111	0.018	-	-

* The green fields indicate damping ratios used in calculations.

Average Damping Ratios

	Mode 1	Mode 2	Mode 3
Lagomarsino	0.016	0.015	0.014
Satake	0.009	0.013	0.018
NS-EN 1991-1-4	0.017	-	-

APPENDIX 4:
NS-EN 1991-1-4 Force Calculations

Input Parameters Used in Force Calculations

Parameter	Value	Parameter	Value
k_p	0.22	$c_s c_d$ (b = 45 m)	0.894
k_l	1.00	$c_s c_d$ (b = 15 m)	0.918
z_o	0.30	Load coefficient γ	1.50
v_b	26.00	$c_{f,0}$ (b = 15 m)	1.30
ρ	1.25	$c_{f,0}$ (b = 45 m)	2.10

Force Factor Calculations: Wind on Long Side (b = 45 m)

z [m]	V_m [m/s]	I_v	q_p [N/m^2]	H_{zone} [m]	λ	ψ_λ	$c_{f,i}$	A_{eff} [m^2]	F_w [kN]	Arm [m]	Moment [kNm]
45	28.66	0.200	1 230.6	45	1.49	0.62	1.302	2 025	4 132	22.5	92 971
75	31.58	0.181	1 413.8	30	1.16	0.61	1.281	1 350	3 114	60	186 816
							Totals		**7 246**		**279 787**

Force Factor Calculations: Wind on Short Side (b = 15 m)

z [m]	V_m [m/s]	I_v	q_p [N/m^2]	H_{zone} [m]	λ	ψ_λ	$c_{f,i}$	A_{eff} [m^2]	F_w [kN]	Arm [m]	Moment [kNm]
15	22.38	0.256	872.9	15	2	0.63	0.819	225	221.5	7.5	1 661
30	26.34	0.217	1 092.9	15	2	0.63	0.819	225	277.4	22.5	6 239
45	28.66	0.200	1 230.6	15	2	0.63	0.819	225	312.3	37.5	11 710
60	30.31	0.189	1 332.5	15	2	0.63	0.819	225	338.1	52.5	17 750
75	31.58	0.181	1 413.8	15	2	0.63	0.819	225	358.7	67.5	24 215
							Totals		**1 508**		**61 577**

APPENDIX 5:
Mass Estimate

Geometrical and Structural Data			
# rooms / floor	21	**Circumference [m]**	110
Gravity Constant [m/s^2]	9.81	**Floor Height [m]**	3.4
	Length [m]	**Area [m^2]**	**Thickness [m]**
Total floor area		560	0.25
Total Hotel room area		405	
Total Hallway area		120	
200 mm Wall	25	85	0.2
250 mm Wall	50	170	0.25
300 mm Wall	50	170	0.3
Load Data			
	Mass [kg]	**Weight**	
Weight of Concrete		25.0	[kN/m^3]
Bathroom Module	1 500	309.0	[kN/floor]
Applied Dead Load Facade		1.0	[kN/m^2]
Applied Dead Load Floor		1.0	[kN/m^2]
Live Load Hotel Rooms		2.0	[kN/m^2]
Live load Hallways		5.0	[kN/m^2]
Load Coefficients			
	Permanent	**Variable**	
ULS	0.9	0	
SLS	1	0.5	
Load Contributions and Total Mass			
		Load [kN]	
Weight of slabs		2 800	
Weight of 200mm walls		425	
Weight of 250mm walls		1 063	
Weight of 300mm walls		1 275	
Facade Applied Dead Load		374	
Floor Applied Dead Load		560	
Live Load Rooms		810	
Live Load Hallways		600	
Bathroom Modules		309	
	Total Load [kN]	**Floor Mass [kg/floor]**	**Distributed Mass [kg/m]**
ULS	6 125	**624 359**	**183 635**
SLS	7 511	**765 598**	**225 176**

APPENDIX 6: MATLAB Code

Integration Method

During the calculation procedure, there are several integrations performed, both with respect to frequency and to height-variable x. Schemes for numerical integration are given by several sources, i.e. by Kreyszig [36]. The most basic method of performing numerical integration is the Rectangular rule, and is given by Kreyszig as

$$J = \int_a^b f(x) \approx h\left[f(x_1^*) + f(x_2^*) + \cdots + f(x_n^*) \right]$$

h is equal to the step size, given as $h = \left(\frac{a-b}{n} \right)$. The Rectangular rule is reckoned to be less accurate than for example the Trapezoidal rule. However, if the number of points n is sufficiently high, there is not much difference between the Rectangular rule and the Trapezoidal rule. Therefore, the Rectangular rule has been used for all integrations.

It should be mentioned that MATLAB has a built-in function for trapezoidal integration. This function has been tested together with the rectangular method for most integrals performed, and the results deviate by magnitudes of 0.1-0.4 %, which is seen as irrelevant compared to the uncertainty in the input parameters. The built in function has not been used simply because of the complexity of the functions that are integrated. Defining them as function handles in MATLAB would not simplify the scripts.

TotalResponse.m - Main Script for Response Calculations

```
%% RESPONSE CALCULATIONS FOR LINE-LIKE STRUCTURE %%
clear all, close all, clc, tic;

%% DEFINING RELEVANT INPUT VALUES %%

Input;

%% CALCULATING FREQUENCY RESPONSE FUNCTION AND JOINT ACCEPTANCE FUNCTION %%

[Hhat,HhatN] =
FrequencyResponse(zeta,m_sls,C_d,L1,w_i,w,Vm,H,finy,x,rho,Plott,MShape,FRFE);
[Su_ka,J2norm,Jw_i] =
Jointacceptance(x,Vtop,Cuu,w,H,Vm,finy,Iu,Iv,C_d,Cddot,C_L,L1,L2,Plott,w_i,JAFU);

%% CALCULATING STATIC DISPLACEMENT BY UNIT LOAD METHOD %%

[R_M,R_V] = UnitLoad(rho,C_d,L1,x,Vm,EI,Plott,MShape,kshear,GA,Qstat,Mdiag,Vdiag);

%% CALCULATING STANDARD DEVIATION OF DISPLACEMENT AND ACCELERATION %%

[Sigma_R,Sigma_A] =
SigmaR(rho,L2,finy,m_sls,w_i,HhatN,J2norm,w,x,Plott,MShape,Sigdisp);

%Frequency weighted acceleration
[SigmaA_w,Sr,Sa] =
AccelSpectra(HhatN,J2norm,w,rho,L2,m_sls,w_i,MShape,Plott,Weight,SrSa,SaSaw);
[TimeHA,ti] = TimeSim(Sr,Sa,w,MShape,Plott,TimeSi);

%% CALCULATION OF STATIC CROSS SECTIONAL FORCES %%

[M,V] = StaticForce(rho,C_d,L1,x,Vm);

%% CALCULATING STANDARD DEVIATION OF M AND V %%

[SigmaM,SigmaV] =
SigmaForce(x,Vm,H,C_d,C_L,Cddot,Iv,Iu,L2,L1,rho,m_uls,w_i,zeta,Jw_i,EI,F2,F3,finy,P
lott,M,V,MShape,Fshears);

%% CALCULATING REACTION FORCES, DISPLACEMENTs AND ACCELERATIONs %%

%Cross Sectional Forces:
disp('Static reaction forces at base (M [kNm],V [kN]):');
Static = [M V];
disp(Static);
disp('Standard deviations of base reactions (M [kNm],V [kN])');
StandardDevi = [SigmaM SigmaV];
disp(StandardDevi);
Mbase = M + kp*SigmaM;
Vbase = V + kp*SigmaV;
disp('Total base moment [kNm]');
disp(Mbase);
disp('Total base shear [kN]');
disp(Vbase);

%Displacement and Acceleration
Atop = kp*max(Sigma_A);
Atop_w = kp*SigmaA_w;
disp('Acceleration at tower top [m/s^2]');
disp(Atop)
disp('Frequency Weighted Design Acceleration at tower top [m/s^2]');
disp(Atop_w)
Rstat = R_M + R_V;
Rtop = Rstat + kp*max(Sigma_R);
```

```
disp('Static displacement at tower top [mm]');
disp(Rstat);
disp('Standard deviation of displacement [mm]');
disp(max(Sigma_R));
disp('Displacement at tower top [mm]');
disp(Rtop)

toc
```

Input.m - Defining Input Parameters

```
%% INPUT FILE%%

%Determines all input values needed for response calculations

%% PLOTTING %%

Plott = input('Do you want plotting of parameters? 1 = Yes, 0 = No: ');

%% DEFINGING FREQUENCY SPECTRUM, HEIGHT DATA AND BASIC CONSTANTS %%

H = 75;                                 %Building height [m]
x = linspace(0,H,551);                  %Height coordinate of the structure [m]
w = linspace(0.01,4*pi,551);           %Frequency spectrum 0-20pi [rad/sec]
rho = 1.25;                             %Air Density [kg/m3]
Cuu = 9;                                %Decay Constant (Davenport)

%% DEFINGING WIND FIELD %%

%Defining base wind velocity
Vr = input('Enter refrence wind velocity [m/s] (Trondheim = 26): ');

%Determining return period of wind from NS-EN 1991-1-4, NA.4.2(2)
Retur = input('Enter return period [years] (default = 50): ');
prob = 1/(Retur);                       %Probability of given return period
Cprob = sqrt((1-(0.2*(-log(1-prob))))/(1-(0.2*(-log(0.98)))));
Vr = V*Cprob;

%Defining terrain category
CAT = input('Enter terrain category: 0, 1, 2, 3 or  4 (3 for Lerkendal Hotel): ');
%The terrain description vectors give the following:
%[Roughness length z0, Terrain Roughness Factor kr, Minimum height zmin]

if CAT == 0
    Ter = [0.003,0.16,2];
elseif CAT == 1
    Ter = [0.01,0.17,2];
elseif CAT == 2
    Ter = [0.05,0.19,4];
elseif CAT == 3
    Ter = [0.3,0.22,8];
else
    Ter = [1.0,0.24,16];
end

%Calculating the Mean Wind Velocity
for i = 1:length(x)
    if  x(i) <= Ter(3)
        Vm(i) = Ter(2)*Vr*log(Ter(3)/Ter(1));
    else
        Vm(i) = Ter(2)*Vr*log(x(i)/Ter(1));
    end
end
Vtop = max(Vm);

% CALCULATING Standard deviation of turbulence and turbulence intensity
kr = Ter(2);
kl = 1.0;
Sig_V = kr*kl*Vr;
for i = 1:length(x)
    Iu(i)= Sig_V/Vm(i);
    Iv(i) = Iu(i)*(3/4);
end
```

```
%% DEFINING MODE SHAPES, FREQUENCIES AND CROSS-SECTIONAL PROPERTIES%%

%Choosing Modal Shape
Mode = input('Choose mode shape 1 or 2: ');

%Loading data for respective mode from .txt files
if Mode == 1
    Dat = importdata('Mode1.txt');
    MShape = 'Mode Shape 1';
elseif Mode == 2
    Dat = importdata('Mode2.txt');
    MShape = 'Mode Shape 2';
else
    Dat = importdata('Mode3.txt');
end

%Extracting parameters from the chose .txt file
fi = Dat.data(:,1);          %Modal shape vector
w_i = Dat.data(1,2);         %Natural frequency
EI = Dat.data(1,3);          %Bending stiffness [Nm^2]
C_d = Dat.data(1,4);         %Drag coefficient
zeta = Dat.data(1,5);        %Damping Ratio
L1 = Dat.data(1,6);          %With perpendicular to wind
L2 = Dat.data(1,7);          %Depth parallel to wind
F2 = Dat.data(1,8);          %2nd derivative of mode shape
F3 = Dat.data(1,9);          %3rd derivative of mode shape
kp = Dat.data(1,10);         %Peak factor based on Eurocode
kshear = Dat.data(1,11);     %Shear factor k
GA = Dat.data(1,12);         %Shear Stiffness [N]
C_L = 0;                     %Lift coefficient
Cddot = 0;                   %Drag coefficient slope

%Increasing number of points in modal shape vector using linearization
k = 0;
finy = zeros(1,length(x));
N = length(fi);
for i = 1:(N-1)
    delfi = fi(i+1)-fi(i);
    if i <= (N-2)
        dfi = delfi/25;          %Dividing each interval into 25
        for m = 1:25
            finy(m+k+1) = fi(i)+(m*dfi);
        end
    elseif i == (N-1)            %The last two points have double spacing
        dfi = delfi/50;
        for m = 1:50
            finy(m+k+1) = fi(i)+(m*dfi);
        end
    end
    k = k+25;
end
%Modal vector finy now contains (m*(i+2))+1 = 551 points instead of 21

%% CALCULATION OF MODAL MASS %%

%Performed for ULS (force calc.) and SLS (displacement calc.)
for pp = 1:2
    if pp == 1
        Mf = 765600;                    %Mass per floor in SLS [kg]
    elseif pp == 2
        Mf = 624360;                    %Mass per floor in ULS [kg]
    end
    M0 = diag(Mf*ones(1,22));           %Mass matrix
    Mmodal = fi'*M0*fi;                 %Modal mass matrix

    %Normalization by dividing by the integral of fi^2 over height x
    Istep = 0;
    N = length(fi);
```

```
    for p = 1:N
        Istep = Istep + (fi(p)).^2;
    end
    stepd = Istep*(H/N);
    Mass(pp) = (Mmodal)/stepd;          %Normalized Modal Mass
end
m_sls = Mass(1);
m_uls = Mass(2);

%% PLOTTING OF PARAMETERS%%

if Plott == 1
    figure,
    subplot(1,2,1),plot(Vm,x,'linewidth',2),title('Mean Wind Velocity')
    xlabel('V_m [m/s]'),ylabel('Height x [m]'),grid
    subplot(1,2,2),plot(Iv,x,'linewidth',2),title('Turbulence Intensity'),
    xlabel('I_v'),grid
    figure,
    plot(finy,x,'linewidth',3), title(MShape), xlabel('Modal Displacement')
    ylabel('Height (x) [m]'),grid
end
```

FrequencyResponse.m - Calculating the Frequency Response Function

```
function[Hhat,HhatN] =
FrequencyResponse(zeta,my,C_d,L1,w_i,w,Vm,H,fi,x,rho,Plott,MShape)

%% FREQUENCY RESPONSE FUNCTION %%

%Defining the aerodynamic and total damping for the system
zeta_ae = AeroDamp(H,fi,x,Vm,rho,C_d,L1,w_i,my);
zeta_tot = zeta - zeta_ae;

%Calculating the Frequency Response Function for the entire frequ. domain
for j = 1:length(w)
    Hhat(j) = 1/((1-(w(j)/w_i)^2)+(2*1i*zeta_tot*(w(j)/w_i)));
end

%Obtaining the absolute value used in calculations
HhatN = abs(Hhat);

%% PLOTTING OF PARAMETERS %%

if Plott == 1
    figure
    plot(w,HhatN), title('Frequency Response function vs. \omega'),grid,
    xlabel('\omega [rad/s]'), ylabel('|H_{y} hat|'), axis([0 (2*w_i) 0 45])
    legend(MShape)
end
```

Jointacceptance.m - Calculating the Joint Acceptance Function

```
function[Su_ka,J2norm,Jw_i] =
Jointacceptance(x,Vtop,Cuu,w,H,Vm,fi,Iu,Iv,C_d,Cddot,C_L,L1,L2,Plott,w_i)

%% JOINT ACCEPTANCE FUNCTION %%

%% DEFINING THE KAIMAL SPECTRAL DENSITY %%

N = length(x);
w(N+1) = w_i;           %Adding the eigen frequency to w, J(w_i) is needed

%Integral y Length Scale for u- and v turbulence
yfLu = 100*(H/10)^0.3;
yfLv = yfLu/4;

%Normalized Frequencies, V assumed constant
fl_u = (w*yfLu)/(2*pi*Vtop);
fl_v = (w*yfLv)/(2*pi*Vtop);

%Kaimal Spectral Density for u and v directions
Su_ka = (6.8*fl_u./w)./((1+(10.2*fl_u)).^(5/3));
Sv_ka = (6.8*fl_v./w)./((1+(10.2*fl_v)).^(5/3));

%% CALCULATING JOINT ACCEPTANCE FUNCTION %%

%Numerical integration over two variables using the Rectangular Rule
for k = 1:length(w)
    Jstep = 0;
    for i = 1:length(x)
        A1 = (2*C_d*L1*Iu(i)/L2);
        B1 = (((Cddot*L1/L2)-C_L)*Iv(i));
        for j = 1:length(x)
            A2 = (2*C_d*L1*Iu(j)/L2);
            B2 = (((Cddot*L1/L2)-C_L)*Iv(j));
            dx = abs(x(i)-x(j));
            Co_hat = exp((-Cuu*dx*w(k))/(2*pi*Vtop));
            Jstep = Jstep +
(fi(i)*fi(j)*(Vm(i)^2)*(Vm(j)^2)*((A1*A2*Su_ka(k)*Co_hat)+(B1*B2*Sv_ka(k)*Co_hat)))
;
        end
    end
    Jd(k) = Jstep;
end
J2 = Jd*((H/N)^2);              %Multiplying by step size

%Normalization: dividing by the integral of fi^2 over x.
fistep = 0;
for p = 1:N
    fistep = fistep + (fi(p)).^2;
end
fistepd = fistep*(H/N);
J2norm = (J2)/(fistepd^2);       %Normalized J^2

Jw_i = sqrt(J2norm(N+1));        %JAF evaluated at the eigen frequency
J2norm(N+1) = [];                %Removing the added terms
Su_ka(N+1) = [];
fl_u(N+1) = [];
w(N+1) = [];

%% PLOTTING OF PARAMETERS %%

if Plott == 1
    figure
```

```
    subplot(1,3,1),loglog(w,Su_ka), title('Kaimal Spectral Density for u component
turbulence vs. \omega'),
    xlabel('\omega [rad/s]'), ylabel('S_{u} Kaimal'),grid
    subplot(1,3,2),plot(w,fl_u), title('Normalized frequency for u component vs.
\omega'),
    xlabel('\omega [rad/s]'), ylabel('f_{l}'),grid
    subplot(1,3,3),loglog(w,J2norm), title('J^2 Normalized'),
    xlabel('\omega [rad/s]'), ylabel('J^2'),grid
end
```

UnitLoad.m - Calculation of the Static Displacement

```
function[R_M,R_V] = UnitLoad(rho,C_d,L1,x,Vm,EI,Plott,MShape,kshear,GA)

%% STATIC DISPLACEMENT %%

%% DEFINING TRANSVERSAL WIND LOAD, SHEAR AND MOMENT DIAGRAMS%%

qv = (rho*C_d*L1/2).*(Vm.^2);            %[N/m] transversal load
dx = x(2)-x(1);

%Defining Moment Diagrams
N = length(qv);
for i = 1:length(qv)
    k = length(qv)+1-i;
    M_(i)= 1*(x(k));
    if i == 1
        Mq(k) = qv(k)*dx.*(x(i));
    else
        MQ = 0;
        ii = 1;
        for pp = k:N
            MQ = MQ + qv(pp)*x(ii)*dx;
            ii = ii + 1;
        end
        Mq(k) = MQ;
    end
end

%Defining Shear Diagrams
for i = 1:length(x)
    k = (length(x)+1)-i;
    V_(i) = 1;
    if i == 1
        V(k) = qv(k)*dx;
    else
        V(k) = V(k+1)+ (qv(k)*dx);
    end
end

%% INTEGRATION OVER THE HEIGHT BY THE RECTANGULAR RULE %%

%Moment Part
Dstep = 0;
for j = 1:length(x);
    Dstep = Dstep + (Mq(j)*M_(j));
end

R_M = (Dstep*dx/EI)*1000;           %Bending part of displacement [mm]

%Shear Part
Dd = 0;
for j = 1:length(x)
    Dd = Dd + (V_(j)*V(j));
end

R_V = (Dd*dx*kshear/GA)*1000;       %Bending part of displacement [mm]

%% PLOTTING  OF PARAMETERS%%

if Plott == 1
    figure,
    plot(qv,x,'linewidth',2),grid, title('Static Wind Load'),legend(MShape)
    xlabel('Loading q_y [N/m]'),ylabel('Height x above ground [m]')
    saveas(gcf,Qstat,'jpeg')
```

```
    figure,
    subplot(1,2,1), plot(Mq,x,'linewidth',2),title('Wind induced moment diagram')
    xlabel('Moment M_q_y [Nm]'), ylabel('Height z above ground [m]')
    subplot(1,2,2), plot(M_,x,'linewidth',2),title('Unit load moment diagram'),
    xlabel('Unit load moment [Nm]'),suptitle(MShape)
    saveas(gcf,Mdiag,'jpeg')
    figure,
    subplot(1,2,1), plot(V,x,'linewidth',2),title('Wind induced shear diagram')
    xlabel('Shear Force V_q_y [N]'), ylabel('Height z above ground [m]')
    subplot(1,2,2), plot(V_,x,'linewidth',2), hold on
    plot(CC,DD,'linewidth',2), axis([0 1.5 0 80]), title('Unit load shear
diagram'),
    xlabel('V_ [N]'),suptitle(MShape)
    saveas(gcf,Vdiag,'jpeg')
end
```

SigmaR.m - Calculating Standard Deviation of Acceleration and Displacement

```
function[SigmaR,SigmaA] =
SigmaR(rho,L2,fi,my,w_i,HhatN,J2norm,w,x,Plott,MShape,Sigdisp)

%% STANDARD DEVIATIONS OF DISPLACEMENT AND ACCELERATION %%

%Using Rectangle method numerical integration
Sigstep = 0;
SigstepA = 0;
N = length(w);
for t = 1:length(w)
    Const(t) = fi(t)*(L2*rho/(2*my*(w_i^2)));
    Sigstep = Sigstep + ((HhatN(t)^2)*J2norm(t));
    SigstepA = SigstepA + ((w(t)^4)*(HhatN(t)^2)*J2norm(t));
end

%Standard deviation of displacement [mm]
SigmaR = 1000*Const.*sqrt(Sigstep*(max(w)/N));

%Standard deviation of acceleration [m/s^2]
SigmaA = Const.*sqrt(SigstepA*(max(w)/N));

%% PLOTTING OF PARAMETERS %%

if Plott == 1
    figure,
    subplot(1,2,1),
    plot(SigmaR,x,'linewidth',2), grid,
    title('Standard Deviation of Displacement','fontsize',11)
    xlabel('\sigma_{R} [mm]','fontsize',11),
    ylabel('Height [m]','fontsize',11)
    subplot(1,2,2),
    plot(SigmaA,x,'linewidth',2), grid,
    title('Standard Deviation of Acceleration','fontsize',11)
    xlabel('\sigma_{A} [m/s^2]','fontsize',11), ylabel('Height [m]','fontsize',11)
    suptitle('Mode 1 excitation - wind against the short side')
    saveas(gcf,Sigdisp,'jpeg')
end
```

AccelSpectra.m - Calculating the Frequency Weighted Acceleration

```
function[SigmaA_w,Sr,Sa] =
AccelSpectra(HhatN,J2norm,w,rho,L2,m_sls,w_i,MShape,Plott,Weight,SrSa,SaSaw)

%% FREQUENCY WEIGHTED PEAK ACCELERATION %%

N = length(w);
wmax = max(w);

%Defining frequenct weighting function parameters from ISO 2631-2

f1 = 0.794328;
f2 = 100;               %Constants
f3 = 5.684105;
fr = w./(2*pi);         %Frequency in [Hz]

%Calculating spectral density of displacement and weighting function
for i = 1:length(fr)
    Sr(i) = ((rho*L2/(2*m_sls*(w_i^2)))^2)*(HhatN(i)^2)*J2norm(i);
    Hh = sqrt((fr(i)^4)/((fr(i)^4)+(f1^4)));
    Hl = sqrt((f2^4)/((fr(i)^4)+(f2^4)));
    Ht = sqrt((f3^2)/((fr(i)^2)+(f3^2)));
    W(i) = Hh*Hl*Ht;
end

%Defining spectral density of acceleration (at tower top only)
%and performing frequency weighting.
for j = 1:length(w)
    Sa(j) = Sr(j)*(w(j)^4);
    Seff(j) = Sa(j)*(W(j)^2);
end

%Obtaining acceleration by integrating over the frequency domain
Int = 0;
for k = 1:length(w)
    Int = Int + Seff(k);
end

%Calculating standard deviation of frequency weighted acceleration
SigmaA_w = sqrt(Int*(wmax/N));

%% PLOTTING OF PARAMETERS %%

if Plott == 1
    figure
    semilogx(fr,W,'linewidth',2),grid, title('Frequency Weighting
Function','fontsize',13),
    ylabel('W(f) [-]','fontsize',12), xlabel('Frequency f [Hz]','fontsize',12)
    saveas(gcf,Weight,'jpeg')
    figure
    subplot(1,2,1),loglog(w,Sr,'linewidth',2), grid,
    title('S_{r}','fontsize',13), axis([0.001 15 10e-15 10e-4])
    xlabel('Frequency \omega [rad/s]','fontsize',12),
    ylabel('Spectral Density of Displacement','fontsize',12)
    subplot(1,2,2),loglog(w,Sa,'g','linewidth',2), grid,
    title('S_{a}','fontsize',13), xlabel('Frequency \omega [rad/s]','fontsize',12)
    ylabel('Spectral Density of Acceleration','fontsize',12)
    axis([0.001 15 10e-17 10e-2]),suptitle(MShape)
    saveas(gcf,SrSa,'jpeg')
    figure
    subplot(1,2,1),loglog(w,Sa,'linewidth',2)
    axis([0.001 20 10e-15 0.01]), grid
    title('S_{a}','fontsize',13), xlabel('Frequency \omega [rad/s]','fontsize',12)
    ylabel('Spectral density of acceleration','fontsize',12)
```

```
    subplot(1,2,2),loglog(w,Seff,'g','linewidth',2), axis([0.001 20 10e-15 0.01])
    grid, title('S_{a,w}','fontsize',13),
    xlabel('Frequency \omega [rad/s]','fontsize',12)
    ylabel('Frequency weighted spectral density','fontsize',12)
    suptitle(MShape)
    saveas(gcf,SaSaw,'jpeg')
end
```

TimeSim.m - Time Domain Simulations of Displacement and Acceleration

```
function[TimeHA,ti] = TimeSim(Sr,Sa,w,MShape,Plott,TimeSi)

%% TIME SERIES SIMULATION OF ACCELERATION AND DISPLACEMENT %%

dw = w(2)-w(1);
ti = linspace(0,600,10001);     %Time domain 10 minutes = 600 s

%Defining amplitude constants and phase angle
for l = 1:length(Sa)
    ckR(l) = sqrt(2*Sr(l)*dw);
    ckA(l) =  sqrt(2*Sa(l)*dw);
    Phase(l) = (2*pi*rand);
end

%Summation over the frequency domain for each time step
for mm = 1:length(ti)
    TistepR = 0;
    TistepA = 0;
    for jj = 1:length(Sa)
        TistepR = TistepR + (ckR(jj)*cos((w(jj)*ti(mm))+Phase(jj)));
        TistepA = TistepA + (ckA(jj)*cos((w(jj)*ti(mm))+Phase(jj)));
    end
    TimeHR(mm) = TistepR*1000;  %Displ. for time step [mm]
    TimeHA(mm) = TistepA;       %Acceleration for time step [m/s^2]
end

%% PLOTTING OF PARAMETERS %%
if Plott == 1
    figure
    plot(w,ckR,'linewidth',2), grid, title('Amplitude Parameter c_{k}')
    xlabel('Frequency \omega [rad/s]'), ylabel('c_{k,r}')
    suptitle(MShape), saveas(gcf,'Camp','jpeg')
    figure
    subplot(2,1,1), plot(ti,TimeHR), grid, title('Time Series Simulation of S_{r}')
    xlabel('Time [s]'), ylabel('Displacement [mm]')
    subplot(2,1,2), plot(ti,TimeHA), grid, title('Time Series Simulation of S_{a}')
    xlabel('Time [s]'), ylabel('Acceleration [m/s^2]')
    suptitle(MShape), saveas(gcf,TimeSi,'jpeg')
end
```

StaticForce.m - Calculating Static Cross Sectional Forces

```
function[M,V] = StaticForce(rho,C_d,L1,x,Vm)

%% STATIC CROSS SECTIONAL FORCES %%

%Static transversal wind load [N/m]
qv = (rho*C_d*L1/2).*(Vm.^2);

%Integrating over the height by the rectangular rule
Mstep = 0;
Vstep = 0;
dx = x(2)-x(1);
for i = 1:length(x)
    Mstep = Mstep + (qv(i)*x(i));
    Vstep = Vstep + (qv(i));
end

M = Mstep*dx/1000;                  %BASE MOMENT [kNm]
V = Vstep*dx/1000;                  %BASE SHEAR FORCE [kN]
```

SigmaForce.m - Dynamic Parts of Cross Sectional Forces

```
function[SigmaM,SigmaV] =
SigmaForce(x,Vm,H,C_d,C_L,Cddot,Iv,Iu,L2,L1,rho,my,w_i,zeta,Jw_i,EI,F2,F3,fi,Plott,
M,V,MShape)

%% DYNAMIC CONTRIBUTIONS TO CROSS SECTIONAL FORCES %%

%% CALCULATING BACKGROUND PART OF CROSS SECTIONAL FORCES %%

%Defining integral length scale (eddy size), evaluated at the tower top
xfLu = (100/3)*(H/10)^0.3;
xfLv = (100/4)*(H/10)^0.3;

%Integrating by the Rectangular Rule
N = length(x);
FstepM = 0;
FstepV = 0;
for i = 1:length(x)
    A1 = (2*C_d*L1*Iu(i)/L2);
    B1 = (((Cddot*L1/L2)-C_L)*Iv(i));
    for j = 1:length(x)
        A2 = (2*C_d*L1*Iu(j)/L2);
        B2 = (((Cddot*L1/L2)-C_L)*Iv(j));
        dx = abs(x(i)-x(j));
        rhouu = exp(-dx/xfLu);
        rhovv = exp(-dx/xfLv);
        FstepM = FstepM +
(x(i)*x(j)*(Vm(i)^2)*(Vm(j)^2)*((A1*A2*rhouu)+(B1*B2*rhovv)));
        FstepV = FstepV + ((Vm(i)^2)*(Vm(j)^2)*((A1*A2*rhouu)+(B1*B2*rhovv)));
    end
end
FM = FstepM*((H/N)^2);
FV = FstepV*((H/N)^2);

%Calculating variances
VarMB = FM*(rho*L2/2)^2;
VarVB = FV*(rho*L2/2)^2;

%% CALCULATING RESONANT PART OF CROSS SECTIONAL FORCES %%

%Defining aerodynamic damping ratio
zeta_ae = AeroDamp(H,fi,x,Vm,rho,C_d,L1,w_i,my);

%Integral of H(w) over frequ domain
FRFInt = (pi*w_i/(zeta-zeta_ae));

%Constant term included in variances
constant = (rho*L2*Jw_i/(4*my*(w_i^2)))^2;

VarMR = constant*FRFInt*(EI*F2)^2;
VarVR = constant*FRFInt*(EI*F3)^2;

%% CALCULATING STANDARD DEVIATION OF FORCES %%

%Defining background and resonant variances of base shear and moment
SigVR = sqrt(VarVR)/1000;
SigMR = sqrt(VarMR)/1000;
SigVB = sqrt(VarVB)/1000;
SigMB = sqrt(VarMB)/1000;

SigmaM = sqrt(VarMB+VarMR)/1000;     %Standard deviation of moment in [kNm]
SigmaV = sqrt(VarVB+VarVR)/1000;     %Standard deviation of shear force [kN]

%% PLOTTING OF PARAMETERS %%
```

```
if Plott == 1
    explode = [1 1 1];
    ChartM = [SigMB SigMR M];
    ChartV = [SigVB SigVR V];
    figure, title('Mode 1'),
    colormap winter
    subplot(1,2,1), pie(ChartV,explode), title('Shear Force V'),
    legend('Background Part','Resonant Part','Static Part')
    subplot(1,2,2), pie(ChartM,explode), title('Moment M'),
    suptitle(MShape)
end
```

AeroDamp.m - Calculation of the Aerodynamic Damping Contribution

```
function[zeta_ae] = AeroDamp(H,fi,x,Vm,rho,C_d,L1,w_i,my)

%% AERODYNAMIC PART OF DAMPING %%

%Integrating velocity and modal shapes over the structural height
intFI = 0;
intFIV = 0;
dx = H/length(x);
for i = 1:length(x)
    intFI =  intFI + fi(i)^2;
    intFIV = intFIV + (Vm(i)*fi(i)^2);
end

%Multiplying by step size
InFI = intFI*dx;
InFIV = intFIV*dx;

%Calculating the aerodynamic damping
zeta_ae = (-rho*C_d*L1/(2*w_i*my))*(InFIV/InFI);
```

Appendix 7:
MATLAB Output

In the following appendix, the MATLAB output data from FrequencyResponse.m is provided. In addition, static shear and moment diagrams for both directions and spectral densities for both modes are shown graphically.

Wind Against the Short Side - Mode 1 Excitation

Resonant standard deviation of base shear [kN]:

829.4973

Resonant standard deviation of base moment [kNm]:

2.9905e+04

Background standard deviation of base shear [kN]:

156.4712

Background standard deviation of base moment [kNm]:

6.6171e+03

Static reaction forces at base (M [kNm], V [kN]):

1.0e+04 *

1.9398 0.0445

Total Standard deviations of base reactions (M [kNm], V [kN])

1.0e+04 *

3.0628 0.0844

Total base moment [kNm]

1.2415e+05

Total base shear [kN]

3.3316e+03

Acceleration at tower top [m/s^2]

0.0698

Frequency Weighted Design Acceleration at tower top [m/s^2]

0.0344

Static displacement at tower top [mm]

0.4001

Standard deviation of displacement [mm]

1.8953

Displacement at tower top [mm]

6.8822

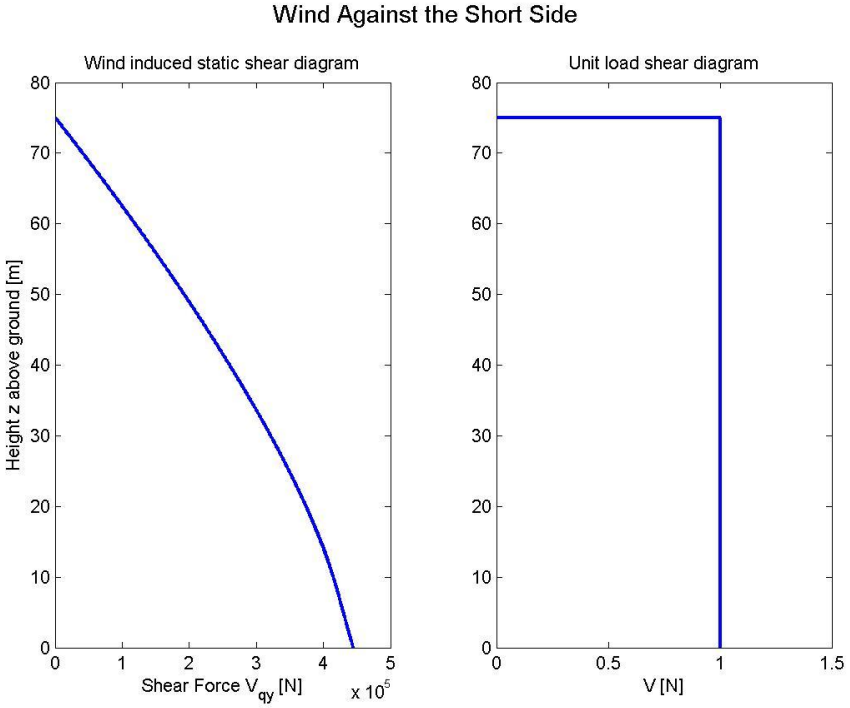

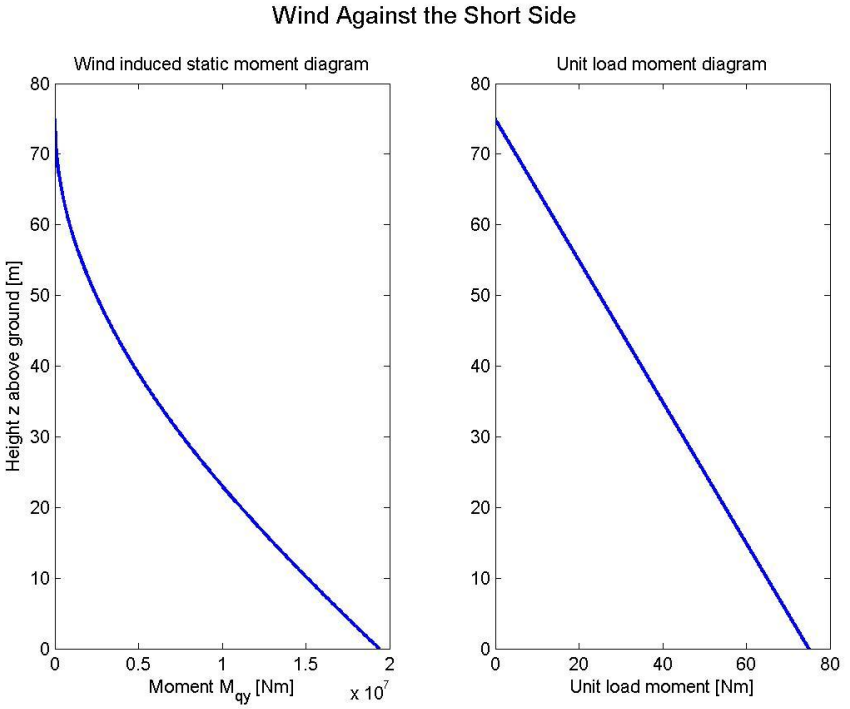

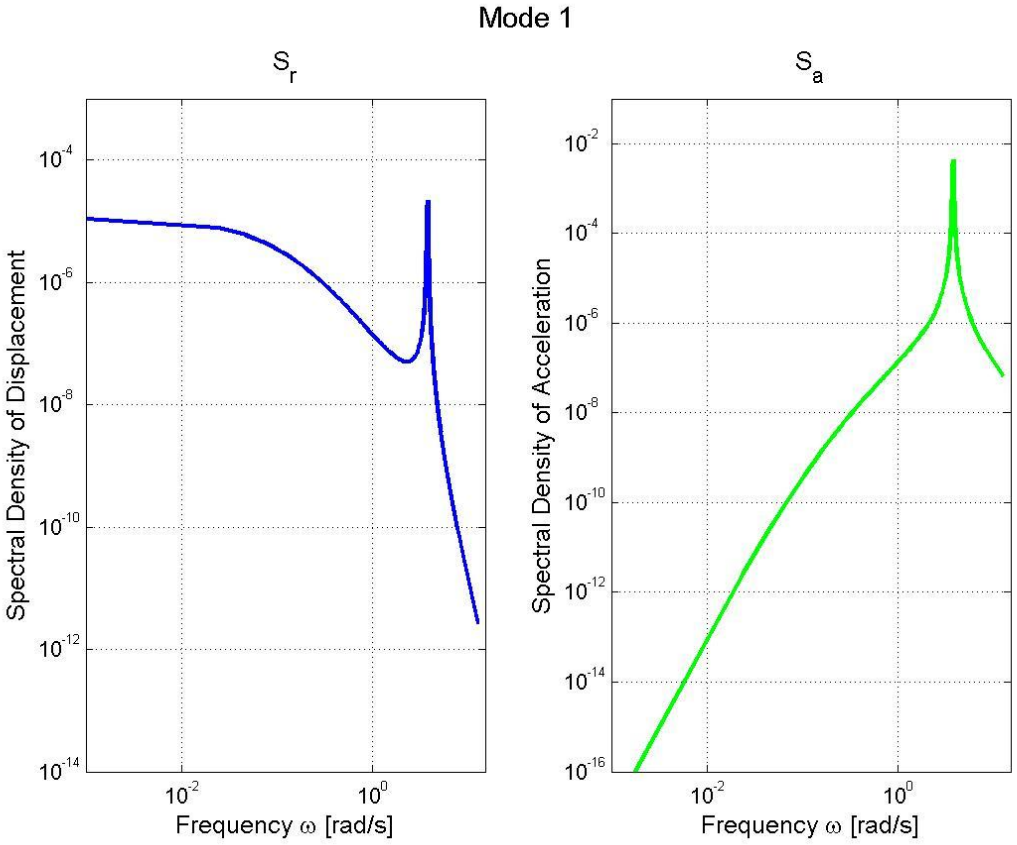
Mode 1
S_r
S_a
Spectral Density of Displacement
Spectral Density of Acceleration
Frequency ω [rad/s]
Frequency ω [rad/s]

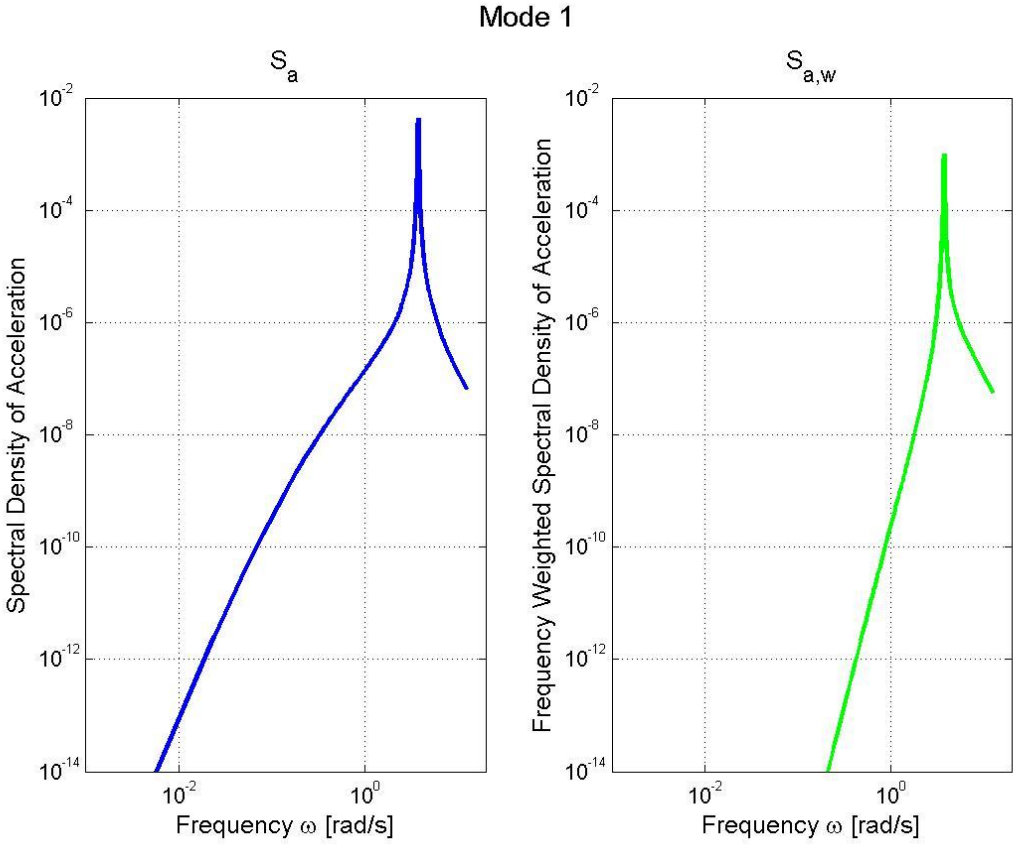
Mode 1
S_a
S_a,w
Spectral Density of Acceleration
Frequency Weighted Spectral Density of Acceleration
Frequency ω [rad/s]
Frequency ω [rad/s]

Wind Against the Long Side - Mode 2 Excitation

Resonant standard deviation of base shear [kN]:

897.7542

Resonant standard deviation of base moment [kNm]:

2.7028e+04

Resonant standard deviation of base shear [kN]:

704.1202

Background standard deviation of base moment [kNm]:

2.9777e+04

Static reaction forces at base (M [kNm], V [kN]):

1.0e+04 *

8.7293 0.2001

Standard deviations of base reactions (M [kNm], V [kN])

1.0e+04 *

4.0214 0.1141

Total base moment [kNm]

2.2080e+05

Total base shear [kN]

5.7892e+03

Acceleration at tower top [m/s^2]

0.1599

Frequency Weighted Design Acceleration at tower top [m/s^2]

0.1372

Static displacement at tower top [mm]

5.5650

Standard deviation of displacement [mm]

2.0205

Displacement at tower top [mm]

12.2730

Wind Against the Long Side

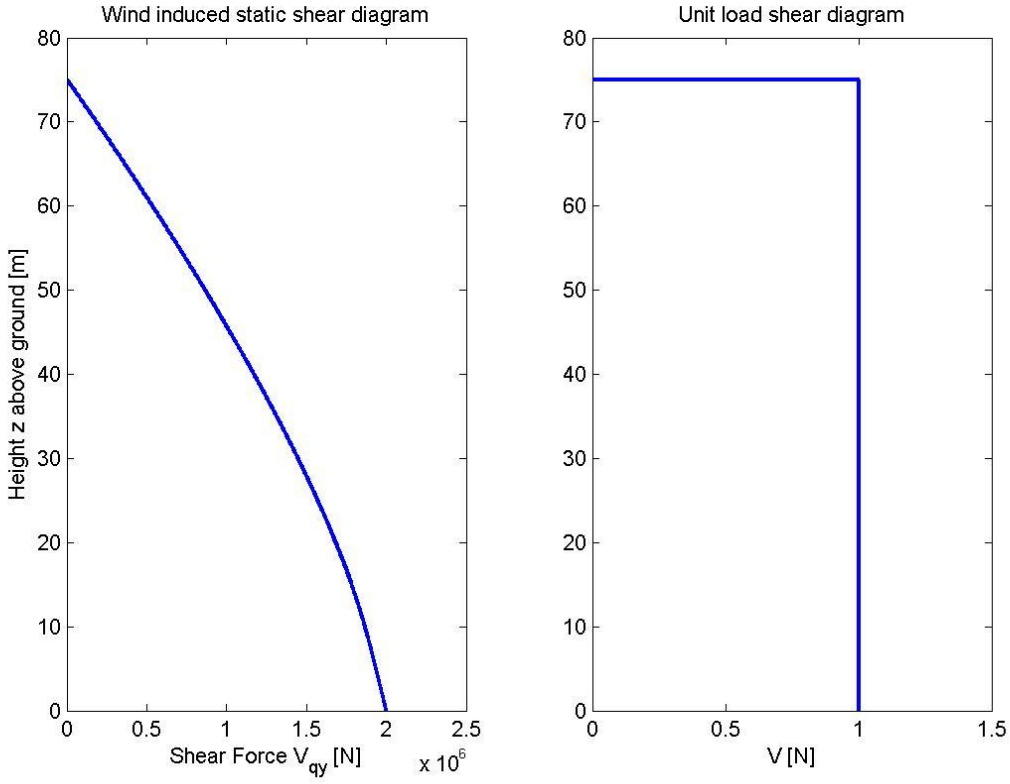

Wind Against the Long Side

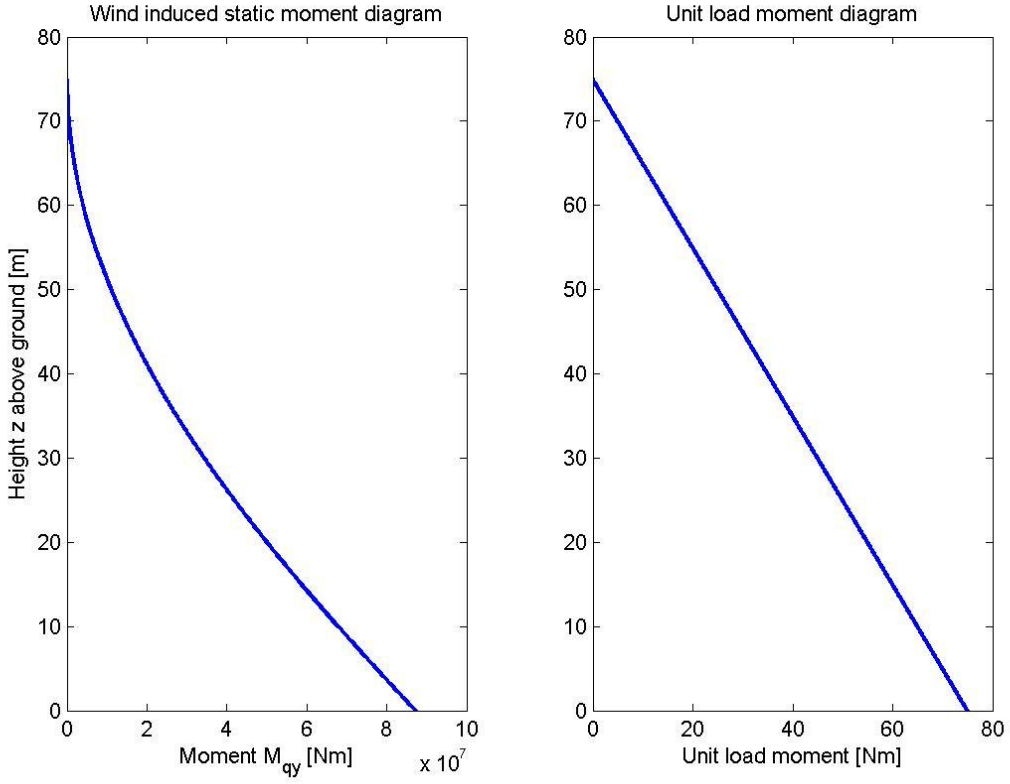

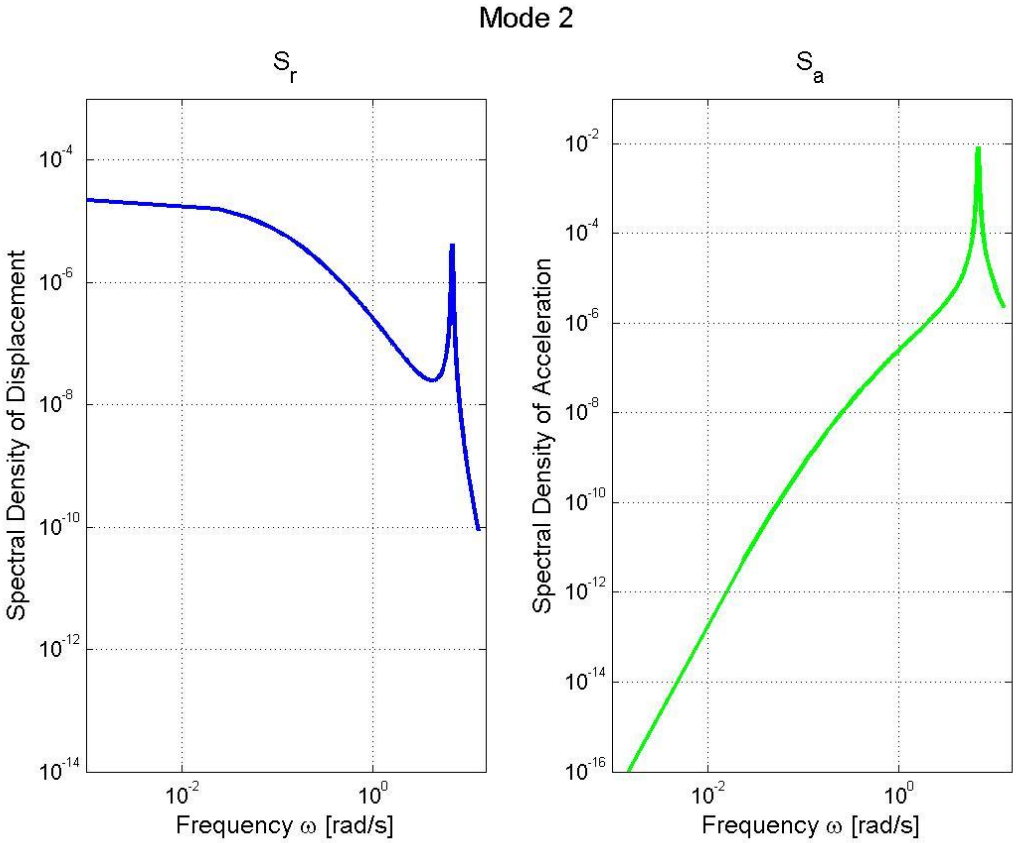
Mode 2
S_r
S_a
Spectral Density of Displacement
Spectral Density of Acceleration
Frequency ω [rad/s]
Frequency ω [rad/s]

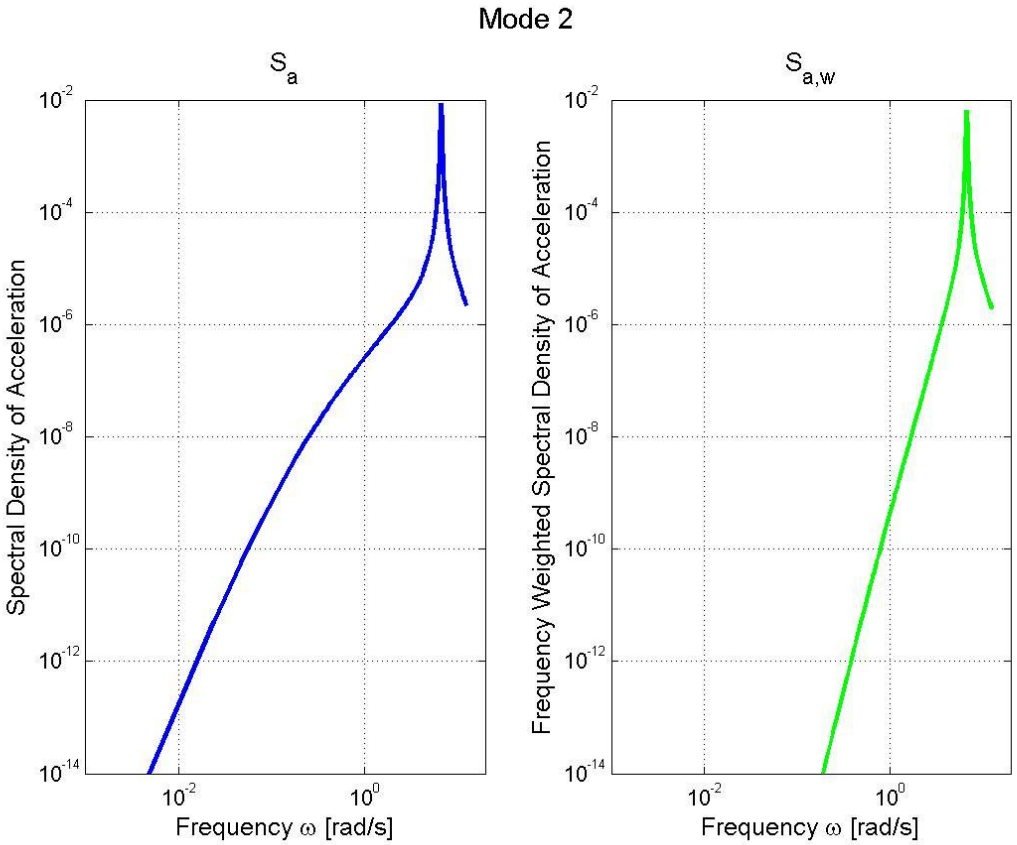
Mode 2
S_a
S_a,w
Spectral Density of Acceleration
Frequency Weighted Spectral Density of Acceleration
Frequency ω [rad/s]
Frequency ω [rad/s]

APPENDIX 8:
Blueprint, Lerkendal Hotel (Norconsult)

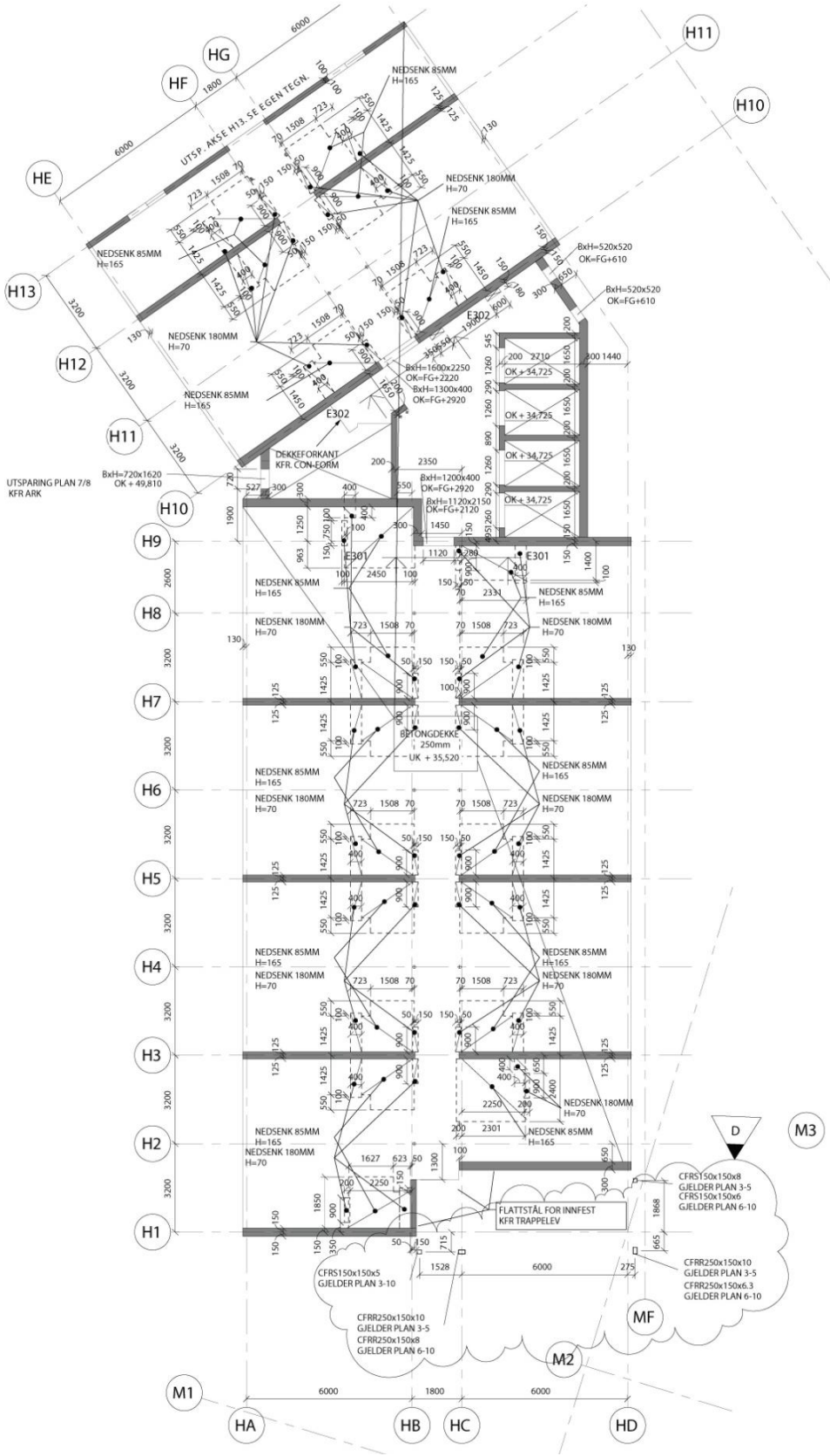

APPENDIX 9:
Floor Plan, Lerkendal Hotel